Reducation of Hazardous Waste Through
Advanced Coating Technology

Final Report

Contract Number MDA972-93-C-0022
Project Number 01-0623-03-4486-000
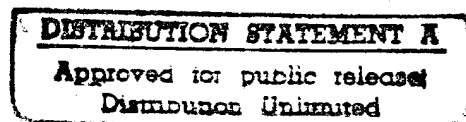Report Number SAIC-96/1073

May 1, 1996

SAIC®

Science Applications International Corporation
An Employee-Owned Company

19960508 136

Reducation of Hazardous Waste Through Advanced Coating Technology

Final Report

Contract Number MDA972-93-C-0022
Project Number 01-0623-03-4486-000
Report Number SAIC-96/1073

May 1, 1996

Submitted to:

DARPA

Submitted by:

Science Applications International Corporation
Applied Physics Operation
1710 Goodridge Drive
McLean, Virginia 22102

REPORT DOCUMENTATION PAGE

Public reporting burden for this collection of information is estimated to average 1 hour per response, including the time for reviewing instructions, searching existing data sources, gathering and maintaining the data needed, and completing and reviewing the collection of information. Send comments regarding this burden estimate or any other aspect of this collection of information, including suggestions for reducing this burden, to Washington Headquarters Services, Directorate for Information Operations and Reports, 1215 Jefferson Davis Highway, Suite 1204, Arlington, VA 22202-4302, and to the Office of Management and Budget, Paperwork Reduction Project (0704-0188), Washington, DC 20503.

1. AGENCY USE ONLY (Leave blank)	2. REPORT DATE 1 MAY 1996	3. REPORT TYPE AND DATES COVERED Final Report 1 Apr 1993– 31 Jan 1996

4. TITLE AND SUBTITLE	5. FUNDING NUMBERS
Reduction of Hazardous Waste Through Advanced Coating Technology	C: MDA972-93-C-0022

6. AUTHOR(S)

D.A. Kirkpatrick, Principal Investigator

7. PERFORMING ORGANIZATION NAME(S) AND ADDRESS(ES) Science Applications International Corporation 1710 Goodridge Drive MS 2-3-1 McLean, VA 22102	8. PERFORMING ORGANIZATION REPORT NUMBER

9. SPONSORING/MONITORING AGENCY NAME(S) AND ADDRESS(ES) ARPA/DSO	10. SPONSORING/MONITORING AGENCY REPORT NUMBER

11. SUPPLEMENTARY NOTES

12a. DISTRIBUTION/AVAILABILITY STATEMENT Distribution unlimited ~~with exception of Appendix A, which contains Armstrong Proprietary Information and is not for public release.~~	12b. DISTRIBUTION CODE

13. ABSTRACT (Maximum 200 words)

This project looked at applying an Ion-Beam Assisted Deposition (IBAD) alumina coating process to problems of DOD interest. The motivation for this effort was the potential of the IBAD alumina process as a "green manufacturing" and performance improvement alternative to existing coating processes. This project demonstrated the compatibility of the process with a wide array of substrates, including metals, composites, and plastics. Through manipulation of the process parameters and surface modification of the substrate materials, alumina or aluminum-oxynitride coatings have been successfully applied to virtually any substrate that has been attempted. The resultant coatings are very hard, highly transparent, chemically resistant, and relatively flexible.

A principal conclusion is that achieving a wider range of multi-requirement performance with a single coating layer of uniform composition is not likely. The compatibility of the IBAD process with a wide range of materials may offer a potential solution by dividing the functional responsibilities of a coating system structure across multiple layers. Each layer is the coating system addresses one or some of the above requirements while not compromising the performance of the other layers in the system.

The IBAD alumina coating has also been shown to be an effective diffusion barrier matieral and is being considered for use in long-life solar reflector materials.

14. SUBJECT TERMS Hard Coatings, Transparent Coatings, Green Manufacturing, Ion Beam Assisted Deposition, Ion Sources, Cost Modeling, Solar Reflectors			15. NUMBER OF PAGES 73
			16. PRICE CODE

17. SECURITY CLASSIFICATION OF REPORT Unclassified	18. SECURITY CLASSIFICATION OF THIS PAGE Unclassified	19. SECURITY CLASSIFICATION OF ABSTRACT Unclassified	20. LIMITATION OF ABSTRACT Unlimited

Table of Contents

List of Figures

List of Tables

Attachments

Attachment A: "Reduction of Hazardous Waste Through Advanced Coatings Technology," Final Report, Armstrong World Industries. J.S. Ross, J.F. Reuwer, and D.J. Kester, May 22, 1995. *NOT INCLUDED* ARMSTRONG WORLD INDUSTRIES PROPRIETARY, NOT FOR PUBLIC RELEASE

Attachment B: "Cost and Performance Analysis of Reducing DoD Hazardous Wastes Through Advanced Coating," Final Report, Massachusetts Institute of Technology. J.A. Isaacs. September 22, 1995.

Attachment C: "Tribological characterization of durable, environmentally friendly coatings," Final Report, Naval Research Laboratory Code 6176. I.L. Singer and L.E. Seitzman, August, 1995.

Attachment D: "Deposition of aluminum oxynitride films by magnetron sputtering: Effect of bombardment and substrate heating on structural and mechanical properties," Russell V. Smilgys, Eric Takamura, Irwin L. Singer, Steven W. Robey, and Douglas A. Kirkpatrick, Materials Research Society Proceedings, Vol. 388, 311 (1995).

Attachment E: "Effect of plasma pretreatment on adhesion of alumina coating to polycarbonate and poly(methyl methacrylate)," R.V. Smilgys, T. Long, D.A. Kirkpatrick, J.J. Hickman, J. Ross, D. Kester, J. Fu, I. Singer, to be submitted to the Journal of Adhesion Science and Technology, May 1996.

1. Executive Summary

This project was initiated to apply an Ion-Beam Assisted Deposition (IBAD) alumina coating process to problems of DOD interest. The motivation for this effort was the potential of the IBAD alumina process as a "green manufacturing" and performance improvement alternative to existing coating processes. The IBAD process under investigation in this project had been developed by Armstrong World Industries for application as a wear abatement coating process for flooring material. The limiting factor for the commerical scale up of this process was the availability of a suitably high power oxygen ion source. SAIC's advanced cathode technology held the promise for removing this roadblock to the scale-up of the process technology. Furthermore, SAIC's surface modification and adhesion promotion work offered the potential to extend the IBAD alumina coating process across a wider range of substrate materials— including most of the substrates of interest to the DOD. The IBAD alumina coatings were a strong performer in Armstrong's flooring application, and this project aimed to demonstrate its wider promise as an alternative to environmentally challenging wet polymer coating processes used for wear and abrasion abatement in the DOD.

The SAIC — Armstrong effort was augmented by the addition of the Naval Research Laboratory Tribology Section, and the Massachusetts Insitute of Technology Materials Systems Laborotory. SAIC, the prime contractor, was responsible for project management, substrate and application selection, advanced ion source development, coated substrate characterization, and substrate preprocessing and surface modification. Armstrong World Industries produced the coated coupons with their IBAD system located in Lancaster, Pennsylvania. NRL performed detailed tribological characterizations of the coating-substrate coupon systems. MIT performed cost and life-cycle analyses of the coating process both in the abstract and as applied to particular application process geometries.

During the course of this project, we have demonstrated the compatibility of the IBAD alumina process with a wide array of substrates, including metals, composites, and plastics. Through manipulation of the process parameters and surface modification of the substrate materials, alumina or aluminum-oxynitride coatings have been successfully applied to virtually any substrate that has been attempted. The typical coating parameters are

Thickness	1 – 4 µm (up to 8µm without cracking)	Flex to strain failure	~0.5% (depending on substrate)
Optical performance	transparent (>95%)	RF performance	transparent (>95%)
Micro-hardness	1 – 10 GPa (depending on substrate)	Chemical performance	resists attack from acids attacked by strong bases (pH > 10)
IR performance	transparent NIR, MIR (>90%) absorptive in the FIR (>8µm)	Production costs	<$1/ft^2 — $50/ft^2, depending on geometery and throughput volume

A particularly interesting aspect of the IBAD alumina coatings are their high degree of transparency. Transparent erosion-resistant coatings have many applications in the DOD, and the largest use of these coatings is on aircraft canopies. A "typical" canopy has several widely ranging requirements including protection from bird strike, rain erosion resistance, sand abrasion resistance, chemical and jet fuel resistance, night vision instrumentation compatibility, RCS performance, and protection from laser blinding. Furthermore, the tradeoffs among these requirements will vary significantly from aircraft to aircraft. Add in new requirements for advanced transparencies such as F-22, F-18, Comanche, and JAST, and current systems are forced to compromise some subset of performance parameters.

During the course of this project we were able to evaluate the application opportunity for the IBAD alumina coating process for several applications. These included not only canopies, but also plastic faceshields, radomes, leading edge systems, seeker heads, and aircraft sensor systems. In most cases, the intended application demanded both impact and abrasion resistance. Our investigations during this project demonstrated that while the alumina resisted abrasion under all but the most extreme conditions, the impact resistance of a simple alumina/substrate coating system could not meet the stated requirements. This is in constrast to most of the in-place polymeric coating systems that achieve the impact resistance requirement while sacrificing abrasion resistance.

One conclusion reached during the course of this effort is that achieving a wider breadth of multi-requirement performance with a single coating layer of uniform composition is not likely. In this context, the compatibility of the IBAD alumina coating process with a wide range of substrate materials opens another potential solution: to break the constrained performance parameter "box" by dividing the multifunction responsibilities of a coating system structure across multiple, mutually compatible layers, where each layer addresses one or some of the above requirements and does not compromise the performance of the other layers in the system.

The ion source development did not proceed as originally planned. Our initial plan called for a primary and one fall back approach. Neither of these approaches yielded the desired performance, but we did gain significant insight into what a successful source would require. We continued the development effort on SAIC IR&D funding and have developed two workable approaches. One of the approaches uses a slightly modified ion gun geometry and a modified gas mix that allows the ion source to operate for a signficant process duration (~48 hrs). The latter uses an extremely high power hollow cathode arc plasma source with a Ta_2N cathode. This latter source may also access other process opportunities. Both of these ion sources are sufficient to scale up the process to production level throughput (~500Å/sec deposition rate).

The direct application of the IBAD alumina technology to DOD applications was not achieved in this effort. A full mulitfunction coating system approach as discussed above will require further development. The oxygen plasma source technologies developed as a result of this and the supporting SAIC IR&D efforts have strong promise as an alternative cleaning process for oxygen system tubing and other parts cleaning operations. We are currently pursuing the application of this technology. Finally, the IBAD alumina coating process has been successfully demonstrated to provide a means for a cost effective, long-life solar reflector material for solar power systems. This application is funded by the National Renewable Energy Laboratory, and at a minimum will serve to maintain the availability of the technology for future DOD needs.

2. Introduction

2.1 Motivation

The purposes of this project were both to develop an advanced coating technology using ion beam assisted deposition (IBAD) of inorganic coatings and also to develop applications for this technology that might reduce the generation of hazardous waste. In such an application, an inorganic coating like alumina (Al_2O_3) would replace an organic paint or coating. An inorganic coating applied by IBAD evolves no problematic volatile organic compounds (VOCs) at any stage of its lifecycle. Furthermore, the high durability of inorganic coatings translates to long lifespan and low maintenance. Thus the significant amount of hazardous waste generated during the application, stripping, and replacement of organic coatings could be prevented by substitution of IBAD inorganic films.

2.2 Applications - Background

Surface coating operations release a significant fraction of stationary area source volatile organic compound (VOC) emissions. The VOCs of many of these sources cannot be reduced by add-on controls at a reasonable cost due to their small size and/or the difficulty of capturing emissions. Therefore, prevention technologies are the primary approach toward reduction of solvent emissions from DoD equipment and architectural coatings. These technologies include the replacement of VOCs with water or nonphotochemically reactive solvents, the use of high solids coatings, or improvement of the efficiency of transfer of coating material to coated surface. However, in current practice, reformulation with nonphotochemically reactive solvents may lead to other environmental problems, such as increased toxicity, greater stratospheric ozone depletion potential, and worsened multimedia effects [1].

Another key point is that lifecycle analysis must be used to evaluate the net environmental impact of any coating technology under consideration. The maintenance operations for a given coating, including washing and the stripping process required for recoating, will have associated environmental loads. For example, polymeric films are candidates for certain DoD applications requiring a protective transparent coating, as they can be applied with low VOC emissions. However, the lifetime of a polymeric coating is shortened by sunlight ultraviolet (UV) exposure that

is unavoidable in many DoD uses. The lifecycle total VOC burden of polymeric film use is raised when the VOC emission per treatment is multiplied by the number of treatments required over the equipment lifetime. UV inhibitors can be added to these coatings to increase lifetime in sunlight, but this will necessarily affect some material properties. Because many coating applications are multifunctional, i.e. have other roles besides protection, this use of inhibitors can interfere with other functions of the coating.

2.3 Applications – Findings

The alumina layer put down by the IBAD process is transparent and harder than any organic coating. It was found to improve dramatically the resistance of a soft plastic like polycarbonate to surface marring and scratching. However, testing also showed that particle impact, such as is present under rain erosion, leads to fracture in the coating. Resistance to rain erosion requires an energy-dissipating interlayer. We concluded that a simple coating system consisting of a hard coating on a soft substrate is not effective against rain erosion.

Consideration of military equipment such as canopies and radomes for IBAD coating applications has shown that even seemingly simple systems like these have multifunctional requirements that must be maintained. For example, the design requirements of a coating system for a canopy must extend beyond abrasion and rain erosion to include radar cross section, eye protection for the pilot against lasers, static electricity bleed off, and bird strike. In addition, all of these requirements must be attained with consideration of environmental impact. Thus application of an IBAD coating in this case must be integrable and non-interfering with all of these canopy design functions.

A multilayer coating system is necessary in order to be simultaneously abrasion _and_ impact resistant. The components of this system may be a alumina coating outermost for abrasion resistance, followed by an interlayer with high hardness initially to support the alumina coating against impact induced fracture. The hardness of the interlayer would need to be graded from hard to elastic with increasing depth in order to dissipate energy from particle impact.

Initial tests on the weathering of IBAD alumina coatings on polycarbonate have been performed at Texstar Inc., the manufacturer of the F-16 canopy. The results show

that an alumina coating may be an effective outer component for a multilayer coating stack on a canopy. The essential integrability of IBAD alumina coating technology into a multilayer coating stack was successfully demonstrated for solar reflector applications in related work for the National Renewable Energy Laboratory (NREL). As the lead government agency for solar energy generation, NREL tasked SAIC to develop an advanced solar reflective material (ASRM) utilizing the alumina coating technology. The multilayer coating stack developed consisted of (working out from the substrate) copper/silver/alumina on PET sheet, in which the outer alumina coating functioned as a barrier against atmospheric corrosion of the reflective silver layer. In accelerated testing the new ASRM has far exceeded NREL standards for durability and reflectivity. There is every indication that this application of the alumina coating technology will be a technical and commercial success.

2.4 IBAD Technology – Background

Prior to this project, the primary constraints limiting more widespread application of IBAD alumina coatings were cost issues related directly to the deposition rates available from IBAD source technology and the integrability of the alumina coating with various substrates. Therefore the IBAD source work in this project focused on 1) IBAD source technology enhancement, 2) characterization and testing of IBAD layer/substrate combinations, 3) examination of the chemistry and effects of various substrate surface preparations and modifications, and 4) analysis of the impact of source cost and throughput on the economics of a given application.

The IBAD process comprises an evaporative source of the material to be deposited and an ion beam source to impart energy to the depositing molecules as they arrange themselves on the substrate. Given that a certain level of ion energy per deposited evaporant molecule must be provided to achieve the desired film characteristics, a balance is required between the evaporation rate and the ion power delivered to the surface. In present IBAD technology, the deposition rate (and therefore the substrate coverage throughput rate) is limited by the output capacity of the ion source. Ion source technology in use at present limits rates for IBAD coating with alumina to ~ 6 nm/s.

2.5 Ion Source – Findings

The intent of this portion of the effort was to build a high-flux ion gun for IBAD. Our original design concepts used field emission cathodes fabricated from Si-TaSi$_2$ material. The course of the development of the advanced ion source led through three approaches, the first two of which were unsuccessful and the third of which worked beyond all expectations:

1. A retrofit of the same make and type of ion source as was already in use in the process chamber at Armstrong (Denton, CC-102), using the Si-TaSi$_2$ FEAs as the electron source.

2. A planar-cylindrical discharge PIG-type ion source using the Si-TaSi$_2$ FEAs as the electron source.

3. A hollow-cathode arc-source developed in collaboration with Commonwealth Scientific Corporation with SAIC IR&D funding, the design of which grew out of the PEFE discharge results but employed a true hollow cathode discharge geometry.

The results of these approaches can be summarized as follows:

1. The FEA approach in the Denton source did not work because a suitable pressure range could not be generated for the operation of the FEA cathodes in either their high pressure PEFE mode or their low pressure vacuum mode. The operating pressure of the Denton source must be in the range 10^{-3} — 10^{-4} Torr in order to balance the efficient generation of ions and their efficent escape into the ion beam extraction region. The high pressure PEFE (Plasma Enhanced Field Emission) mode of the FEAs has not been observed below a pressure of 0.5 Torr. The vacuum mode is not effective until the ambient pressure around the FEA is significantly below 10^{-5} Torr. Our attempts to modify the pressure distribution within the Denton source and thereby access either one of the FEA operating regimes were unsuccessful.

2. The planar-cylindrical discharge PIG type source could provide momentary large pulses of oxygen plasma, but stabilizing these discharges and obtaining long pulse or constant operation proved infeasible in this effort. Our opinion is that the ignition of the PEFE discharge resulted in a significant pressure variation in the dis-

charge volume, extinguishing the discharge and allowing only the initial pulse of plasma to seed the ion extraction region. We were successful in achieving a 1 Torr pressure in the discharge volume with a 10^{-4} Torr pressure in the extraction region, and we observed 5-10 A pulses of plasma current in the extraction volume from a 3 mm diameter Si-TaSi$_2$ cathode in the discharge volume. While we believe that it is possible to build an ion source in this configuration with a more robust design, we felt that a hollow discharge geometry would be less sensitive to the pressure variation from the ingnition of the device.

3. The hollow cathode arc source design was an outgrowth of our more mature understanding of the dynamics of the plasma ignition process. The discharge available with this source exceeds 50 A and can virtually fill a 20,000 lit. test chamber with plasma in seconds. The power available with this type of source exceeds all the requirements for any potential scale-up concepts for the IBAD process. The design is relatively simple and requires a low cost power supply for operation. This source was developed in concert with Commonwealth Scientific Corporation of Alexandria VA using the internal resources of SAIC and CSC (this effort was initiated after the funding set aside for ion source development in the ARPA effort was expended on the first two approaches). Following some engineering modifications this source should be available commercially through CSC.

The motivation for this advanced ion source development effort was that existing state of the art oxygen ion sources, with several sources ganged together in the most advantageous possible layout, could not support an IBAD process deposition rate greater than 15 nm/s. Hot cathode based ion sources could support an IBAD deposition rate of up to 60 nm/s, *but not with oxygen as the process gas*. Independent of the ion source development, a major achievement of this project was the discovery of a process gas for the IBAD alumina process that will allow the use of a hot cathode source for deposition rates up to 60 nm/s and process times of 12-24 hours.

Another development during the course of this project was the lowering of the ceiling on the maximum IBAD deposition rate for heat sensitive substrates. Earlier estimates of the maximum IBAD rate for thermal sensitive substrates had been as high as 300 nm/s. Subsequent calculations and measurements during this project have indicated that a more conservative value of 60 nm/s as a maximum IBAD deposition rate is appropriate for a substrate liuke a thn (few mils) PET plastic web moving on a

cooled drum. A thicker plastic substrate, such as the polycarbonate material of a canopy, is harder to cool from the back surface and requires an even lower rate limit.

The development of advanced O_2 ion source capabilities during this program has importance independent of its applicability to IBAD. Oxygen ion cleaning is viewed as a strong candidate to displace the use of ozone-depleting CFCs in a number of DoD applications, among them the cleaning of air supply lines in cockpit support systems. SAIC is a major supplier of Pollution Prevention planning, implementation, and technologies to the DoD and is well positioned to bring about timely application of ion source technology to this environmental problem.

2.6 Alumina/Substrate Interface Characterization and Modification – Findings

At a minimum, an alumina coating can not be effective unless it adheres to the substrate. The role for interface characterization and modification activities in this project was to assure adhesion. We found that alumina coatings deposited by the IBAD process adhere to most substrates, with some notable exceptions. This general success is attributable to the energetic nature of the IBAD process. Table 1 lists substrate materials for which adhesion to the alumina coating is sound.

Metallic:	**Inorganic:**
stainless steel	silicon
chrome plated steel	quartz
SAE 1010 low carbon steel	ceramic tile
nickel	glass
aluminum, grades 7075T6 and 2024T3	marble

Plastic and composites:	
polycarbonate: 'Lexan', 'Tuffak', 'Hyzod'	polyethylene terephthalate: PET
polymethyl methacrylate: 'Plexiglas'	polyethersulfone: PES
polyimide: 'Kapton'	polyetheretherketone: PEEK
polyvinyl chloride: PVC	polyester
polyurethane	fiberglass

Table 1. List of Substrate Materials Demonstrated to Adhere Alumina IBAD Coating.

As the list of substrates upon which adequate adhesion can be achieved is expanded, a wider area of problems can be considered for treatment by adding a protective alumina IBAD film. This general approach of expanding the substrate parameter space has implications beyond that of adding to the list of problem component surfaces which can be treated. It also means that multilayer, multifunctional approaches can be considered when designing a surface that must fulfill multiple requirements. An example would be advanced specialty canopy designs. In addition, the selection of materials and processes to meet environmental goals will be significantly expanded.

The example of an advanced specialty canopy design presents a representative spectrum of the multifunction characteristics that must be satisfied by an integrated coating-substructure system. The requirements include specifications for transparency in the visible spectrum, surface impredance at radar frequencies, sand abrasion resistance, rain erosion resistance, bird strike survival, laser blinding countermeasures, temperature variation tolerance, and possibly transmission characteristics in the IR an UV — just to list the most immediate. The layered coating/functionality approach spreads these requirements across many layers in the system. The outermost layer must meet the greatest range of functionalities: for instance providing the requisite sand abrasion resistance while transmitting all the remaining functionalities to the layers below without failing. The greater the diversity of substrates the outermost layer is compatible with, the larger the available parameter space there exists to find a solution. Our investigation of the applicability of this approach to the problem of specialty canopies for the F-16 has been met with interest from the Air Force, but there exist no immediate plans to carry this forward.

2.7 Economic Impact Analysis – Findings

As described above, the enhanced ion source technology explored under this program can produce the higher ion fluxes needed to achieve higher ion beam assisted deposition rates. Higher IBAD rates in turn allow higher throughput rates for coated material. The effect of higher throughput rates on the cost per unit product will vary with the particular application because of differences in production modes. The production modes for coating a web-type product or for coating an individual item like a canopy exemplify the difference between continuous roll processing and batch processing.

In a batch process, speeding up the deposition rate will not strongly affect the cost per unit output if the load/unload times are significant, i.e. that a relatively low total throughput of product area is involved. Another constraint in the particular batch process example of canopy coating is that the coating rate cannot be raised as high as the ion source technology would allow because of the substrate heat sensitivity and the fact that a batch item cannot be cooled with the techniques of web processes. However, a more efficient ion source of smaller size could reduce the capital costs of a coating system.

The economics of IBAD alumina coating on a continuous web process have been more fully explored for the treatment of rolls of the advanced solar reflective material (ASRM) under development by the National Renewable Energy Laboratory (NREL). This system is another example of a multilayer application. In this case, the enhanced process throughput available with advanced ion sources was shown to be essential in lowering the ASRM cost per area coated to economically attractive levels.

2.8 Report Organization

The full reporting of the program tasks is contained in the next section and is organized as follows. Following a short accounting of the program management and inter-task coordination, the surface preparation and characterization work applied to various DoD and non-DoD applications of IBAD alumina coatings is presented. Next is a subsection on the advanced ion source development design, modeling, and experiment task. The final part of the task report section contains the economic impact analysis of IBAD process systems. The report ends with a summary of conclusions and recommendations.

3. Tasks

3.1 Program Management and Inter-task Coordination

This project required the coordination of three technical efforts and almost continuous interaction with potential users of the technology in the DOD. The three technical task efforts were:

- *Surface preparation and characterization* - which involved the preparation, processing, and characterization of IBAD alumina coated coupons of a variety of substrate materials.
- *Advanced ion source development* - which involved the development of an advanced ion source suitable for the high-throughput scale-up of the IBAD process.
- *Impact analysis* - which involved the technical cost modelling of the IBAD process as is might be applied to specific systems of interest, and estimates of the life-cycle impact of the IBAD alumina process on these same systems and their surrounding environment.

These three technical efforts are described in detail later in this section.

Thoughout the project there was a high degree of coordination between the three technical tasks supported by input from the management task regarding specific requirements of potential users. Details of the process configuration and parameters had a strong effect on the cost structure of applying the IBAD alumina process to a given material or component. This encouraged close coordination between the surface preparation and characterization task and the impact analysis task. The potential capabilities of the ion source technology likewise affected both of these tasks in terms of viable system configurations and potential throughput rates. All of these inter-task communications, particularly those between different institutions that were part of our team, were carefully placed through the management task. This effectivly ensured that everybody was working from the same set of assumptions concurrently.

In addition to coordinating the technical tasks, a major challenge faced by the project was the exchange of information and needs with potential users in the DOD. Potential government users outside the DOD and even potential commercial users of the technology were also considered, in that they might provide a supporting path for the maturation of the technology.

The list of potential users of the technology that were given presentations or with whom we discussed the technology during the course of this effort is extensive. That list includes major offices from all three services, the Department of Energy, the Department of Transportation, and commercial industries in business areas of metals manufacturing, touch panel displays, electronics manufacturing and packaging, food packaging, and building products. The service interests included from the Air Force: the F-16 canopy, the F-16 radome, and F-16 specialty canopies (Texstar, Inc.), LO rotorblade treatments, and various seeker heads for missiles. The service interests in the Army included HUMVEE windscreen treatments, helicopter canopy treatments, LO rotorblade treatments, and CBW protective treatments. Interests from the Navy included the same set of canopy concerns as the Air Force, and treatments of shipboard windscreens.

Where possible, samples of the existing substrate material were obtained from the user and passed to the surface preparation and characterization task for IBAD alumina processing. By far the most accomodating collaborations in this regard came from the Corpus Christi Army Depot (Mr. Al Gonzales), the F-16 project office (Capt. Dan Bullock), and a supplier of the F-16 canopy - Texstar Inc. (Mr. Lance Teten). These individuals were very helpful in providing suggestions of what might work for their application and in working with us through the unavoidable initial missteps.

It should be noted that most offices were unapproachable from the standpoint of the environmental benefits offered by the IBAD alumina process. This continued to be true even when the performance benefits offered by the IBAD alumina process were presented at the same level of importance as the environmental benefits. Only when the environmental benefits were presented as a symbiotic, happenstance benefit were the majority of potential users attentive in anything more than a courteous manner.

The principal non-DOD applications under consideration were the building materials application at Armstrong World Industries and the application of the IBAD alumina coating as a low-cost protective process for solar reflectors with the National Renewable Energy Laboratory in Golden, CO. The building materials application was the basis for the initial development of the process by Armstrong, and most of the substrate materials of interest in those applications were similar in their chemical and physical configuration to substrate materials of interest to the DOD. After detailed consideration of the results from this project and their own internal efforts, Armstrong

concluded that the cost and throughput goals for the building materials market could not be met by any near term projected IBAD alumina capability.

The DOE/NREL application is focussed on the cost, transparency, and corrosion barrier performance of the IBAD alumina process as applied to solar reflectors for the generation of solar/thermal electric power. We are presently working a follow-on effort to our initial effort with NREL and the results to date have exceeded all expectations. In a 30::1 accelerated weathering chamber at NREL the solar reflector material described later (Sections 3.2.4.2 and 3.3) was processed in excess of 14 months with no measureable decline in its performance from ~94% reflectivity. The next phase of the NREL project will most likely consider the rate scale-up of the IBAD process, in preparation for integration of the IBAD process into a large-volume roll-coater in approximately a year's time. At the least, the continuing NREL/SAIC effort will assure the availability of the IBAD alumina technology for future DOD use.

3.2 Surface Preparation and Characterization

3.2.1 Introduction

The coating process described in this report was developed by Armstrong between 1987 and 1993. In the literature the process is known as ion beam assisted deposition (IBAD). IBAD originated in the early 1980s as a method to improve the properties of optical coatings. The principles of IBAD have been extensively reviewed [2,3,4]. The most basic system for IBAD consists of three components: a substrate, an evaporation source for coating material, and an ion source for film bombardment. Coatings have been deposited by evaporation for decades. The essential improvement offered by IBAD is the addition of ion bombardment during evaporation. Ion bombardment can have a wide range of effects, depending on the species, momentum, total flux, and, most importantly, the ion energy. As its energy increases, an ion is able to excite a wider range of physical effects in a material system. In this project the essential role for ion bombardment is to alter the coating microstructure.

Several years ago Movchan and Demchishin [5] described the microstructure of metal and oxide films deposited by evaporation. They identified three characteristic structure zones that occur according to the substrate temperature. The boundary temperatures between these zones, T_1 and T_2, occur at 0.22-0.26 T_m and 0.45-0.5 T_m for

oxides (where T_m is the material melting temperature). Each zone has a distinct microstructure (Figure 1).

Increasing substrate temperature during coating process

T_1 T_2

* Domed microstructure
* Amorphous
* Density below bulk
* No surface diffusion

* Columnar microstructure
* Polycrystalline
* Density near bulk
* Limited surface diffusion

* Equiaxed grains
* Monocrystalline
* Density equal to bulk
* Bulk diffusion
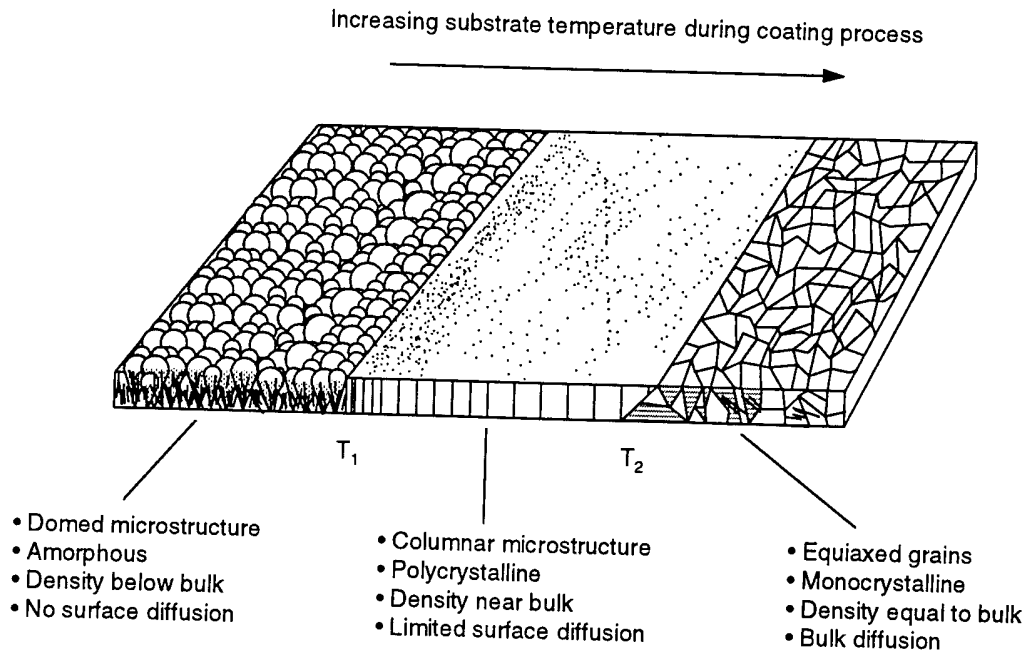
Figure 1. A graphical representaion of the three primary types of microstructure formed in a vapor deposited coating as a function of substrate temperature. The boundary temperatures T_1 and T_2 depend on the melting temperature of the bulk material.

The first zone is characterized by a domed structure in which the diameter of the domes increases with temperature. In this zone the structure is a consequence of inadequate adsorbate surface diffusion due to the relatively low substrate temperature. Adsorbates mostly remain where they strike initially, and shadow the next adsorbate. The surface is particularly prone to roughening and porous growth under conditions of oblique flux because high points receive more flux than low points. A film with this structure may be only 80-90% as dense as the bulk material. At T_1 there is a gradual transformation to the columnar structure characteristic of the second zone. In this zone well defined grain boundaries appear. The width of the columnar crystallites increases with temperature. The structures in this zone are dominated by adsorbate surface diffusion processes. An adsorbate has time to diffuse to vacant sites on a crystallite before being buried by incoming flux. Each initial grain continues to

grow as the film thickens. The third zone appears at higher temperatures in which bulk recrystallization occurs. The columnar grains recrystallize to form equiaxed grains. This structure is driven by the minimization of strain energy and grain surface free energy.

For alumina the boundary temperatures T_1 and T_2 occur at 350°C and 900°C. The low melting point of the transparent plastic substrates of interest in this project dictated that the coatings be deposited at substrate temperatures within the first zone.

The most important feature of ion bombardment is its ability to improve the microstructure of coatings deposited at temperatures in the first zone. Without ion bombardment, surface diffusion is inadequate to close voids and seal pores during deposition. Bombardment drives collision cascades that result in forward recoil and lateral displacement of atoms. These cause the lattice to collapse to a more densely packed configuration.

Another benefit of bombardment is the regulation of stress. Coatings deposited by vapor deposition have residual stress that can lead to cracking, delamination, or bending of a thin substrate. Stress can arise from a mismatch in thermal expansion coefficients between the coating and substrate if the coating is grown at an elevated temperature, then cooled to room temperature. A coating may also have stress if it is grown on a substrate subjected to mechanical stress, which is then relieved after growth. Even if these extrinsic sources of stress are removed, intrinsic stress often remains. Intrinsic stress can be caused by film impurities, the presence of defects, or the occurrence of solid state transformations. Ion bombardment can modify film stress through an atomic peening effect.

Coating quality on a plastic substrate is to a large extent determined by how well coating stress is regulated. The subcontractor report [6] from the Naval Research Laboratory includes a discussion of measurements of coating stress. Armstrong monitored coating stress by observing the bending of a thin Kapton substrate codeposited. Tensile stress drives the formation of 'mud' cracks on polycarbonate, for example, while excessive compressive stress leads to 'worm' tracks. This is a process whereby the coating delaminates along a furrow in order to relieve stress. Nonuniformity in ion bombardment can lead to the presence of mud cracks and worm tracks on the same coupon. These issues are addressed in more detail in Section 3.2.3.2 (canopies).

3.2.2 Advanced Coating Characterization

3.2.2.1 Abrasion Resistance

Polycarbonate (PC) is a relatively soft plastic subject to surface marring and scratching. One important property of the alumina coating is that it significantly increases the abrasion resistance of PC. A machine called a Taber Abrader is commonly used to quantify abrasion resistance. A coupon under test rotates beneath an abrasive wheel under a fixed load. After a certain number of revolutions the test is stopped. At this point a donut impression is evident where abrasion occurred.

PC coupons with an alumina coating were prepared in three runs (05/03/95, 05/05/95, and 05/19/95) with coating thicknesses of 0.7, 2.4, and 4.3 μm. Other than varying coating thickness the deposition conditions were identical (normal nitrogen ion assist). In order to compare the performance of alumina to a commercial hardcoating, we also tested a coupon prepared with a 'Silvue' coating. Silvue is an example of a polysiloxane loaded with colloidal silica. The particular coupon tested had a coating thickness of 3.7 μm.

The specific parameters for Taber measurements reported here were 500 revolutions under a 500 gram load, using a CS-10F wheel. The amount of abrasion was quantified in terms of a percentage loss in optical transmission. We also viewed surface damage using an SEM.

Table 2 and Figures 2-4 present the results of Taber tests. Without a protective coating PC appears badly abraded (Figure 2). Although the transmission does not drop to zero, only scattered light passes through the coupon. The coupon with a 0.7 μm alumina coating fared no better. On the other hand, the coupons with a 2.4 or 4.3 μm coating by eye appear hardly affected. **Figure 3** shows faint scratches on the 2.4 μm coating, but thickness measurements do not indicate any thinning of the coatings. This result indicates that for a given load on the Taber wheel, a minimum thickness is necessary to prevent abrasion; the 0.7 μm coating was too thin, broke up, and wore away. No advantage is conferred by a coating thickness greater than the minimum required for a given load.

Coupon #	Description	% Loss in Transmission at 400 nm
95-5-48	uncoated polycarbonate	69.8
95-5-50	0.7 µm alumina coating on polycarbonate	66.5
95-5-49	2.4 µm alumina coating on polycarbonate	3.0
95-5-46	4.3 µm alumina coating on polycarbonate	2.3
95-5-47	3.7 µm Silvue® coating on polycarbonate	34.4

Table 2. Results from Taber Abrasion Tests on Uncoated and Coated Polycarbonate.

5 µm
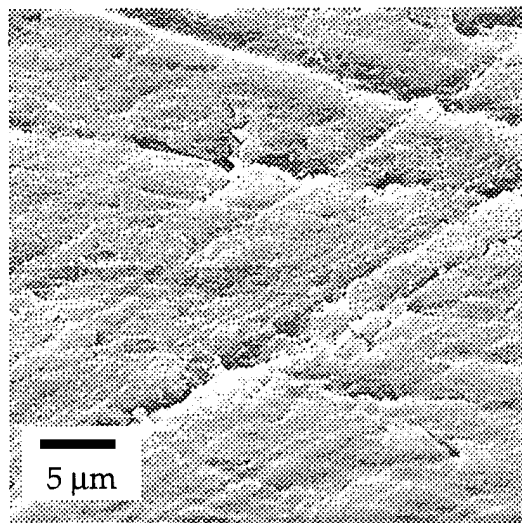
Figure 2. Surface view of uncoated polycarbonate sheet subjected to surface abrasion by Taber abrader (95-5-51). See text for details of test. Sheet was rendered opaque because of extensive abrastion damage.
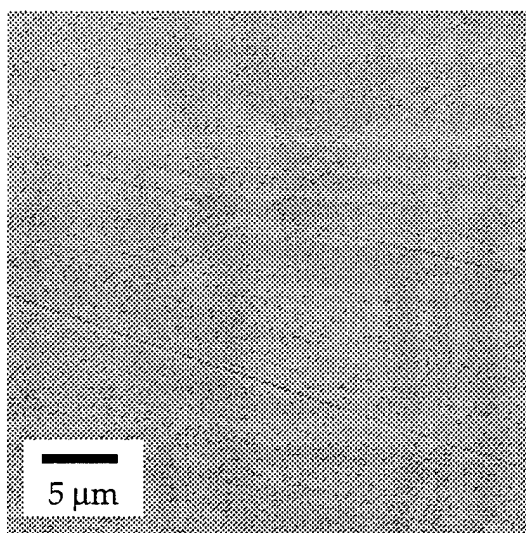
Figure 3. Same abrasion test peformed on poly-carbonate sheet protected with 2.4 μm thick alumina coating (95-5-49). Only minor scratching of coating occured with almost no effect on transparency or transmission.
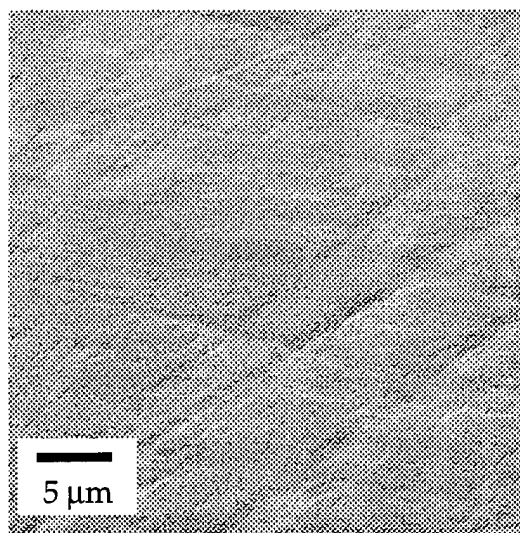
Figure 4. Same abrasion test performed on polycarbonate sheet protected with commercial hardcoating (Silvue®) 3.7 μm thick (95-5-47). More extensive abrasion occured leading to over 30% loss in transmission and a noticeable loss in transparency.

The coupon with a Silvue coating performed much better than uncoated PC. The transmission only dropped by 34%. However, Figure 4 shows that more extensive surface damage occurred than with even the 2.4 μm alumina coating. This shows that even a thinner alumina coating significantly outperforms the Silvue coating.

Overall, the Taber tests show that an alumina coating effectively protects against abrasion. The coating thickness required scales with the applied abrasion pressure. A coating only a few microns thick is enough to protect against a load over half a kilogram.

3.2.2.2 Chemical Attack Resistance

The alumina coatings were tested for their ability to protect plastic and metal substrates against chemical attack. In this role, not only must the coating be resistant, but it also must form an impenetrable barrier to prevent attack of the substrate. This is a more stringent standard than simply demanding that the coating itself be resistant to attack.

3.2.2.2.1 Polycarbonate Substrates

The only chemicals found to actually dissolve an alumina coating were hydro-fluoric acid (HF) and concentrated bases (e.g. KOH). Concentrated KOH can immediately dissolve a 4 μm thick coating, while immersion in a pH 12 solution requires about 8 hours. The reaction product is aluminum hydroxide. A 4.8% aqueous solution of HF clouded a coating in a matter of minutes.

The protective properties of an alumina coating on polycarbonate (PC) were determined by immersing coupons in a variety of solvents. The manufacturer advised that strong mineral acids, ketones, chlorinated hydrocarbons, and aromatics attack unprotected PC. Table 3 summarizes our observations.

Coupon Number 94-6-3 with 4.8 μm alumina coating.

chemical	visible effects after 10 minutes	visible effects after 17 hours
acetone	worm tracks originating at edges	substrate swelled, coating up-lifted and cracked, but adherent
toluene	extensive worm tracks originating mostly at edges, but also some in center	severe substrate swelling, coating uplifted and cracked
concentrated HCl	no effect	no effect
concentrated H3PO4	no effect	no effect
concentrated HNO3	no effect	substrate yellowed, no effect on coating
gasoline	no effect	no effect
concentrated H2SO4	no effect	coating flaked

Table 3. Solvent Immersion Effects on Polycarbonate.

The process of coating failure by acetone or toluene seems to begin by the solvent making contact with bare polycarbonate. This can happen either at an edge or through a pore, scratch, or crack in the coating. At this point the polycarbonate absorbs the solvent and swells. This causes cracking of the coating and further introduction of solvent. Eventually the surface of the substrate is coarsened by swelling and the coating is completely cracked. Toluene is a more powerful solvent for polycarbonate than acetone, so the process of crack expansion occurs faster.

The data show that for the most part mineral acids have little or no effect on the coating. The interesting exception is sulfuric acid, which causes flaking of the coating without obviously attacking either the substrate or the coating. The first small worm tracks appear in under 5 hours.

In summary, the alumina coating can effectively increases the resistance of PC to a wide range of solvents and acids. For example, unprotected PC is rendered opaque instantly in contact with toluene. Coated PC on the other hand requires several minutes of exposure before damage occurs.

3.2.2.2.2 Protection of metal substrates

Coated steel coupons were tested by immersion in an aqueous solution of 3.5% NaCl for 65 hours. Under these conditions unprotected steel becomes covered with rust. Table 4 lists results from these tests.

Depending on deposition conditions differences in performance are evident. The most effective protective coatings were 94-3-8 and 93-9-12. These coatings were deposited using oxygen ion beam assist. To prevent corrosion the coating must be free of pores or cracks that allow the solution to contact steel. Other deposition conditions may perform worse than standard oxygen assist because pores or microcracks are present.

Alumina coatings were also deposited onto aircraft grade aluminum (7075T6 and 2024T3). Figure 5 is a SEM images of coated aluminum (95-2-13). The aluminum had been polished only to a dull finish prior to deposition. The rough surface present shows that the coating conformed to polishing features. Corrosion protection was determined by applying concentrated HCl acid on the coating (95-2-15). HCl vigorously attacks unprotected aluminum with evolution of hydrogen. The result was that over the course of several minutes the acid attacked the underlying aluminum at pinpoint locations. Figure 6 shows one such pinpoint. It appears that acid reached the aluminum through a localized imperfection in the coating. Then the heat and gas that evolved cracked the coating and introduced additional acid to expand the attack. In this way a small point of attack expanded.

The initial roughness of the aluminum is a factor in creating imperfections. The evidence is that particularly deep scratches gave rise to a higher density of pinpoints. The reason may be that scratches have overhangs that remains uncoated.
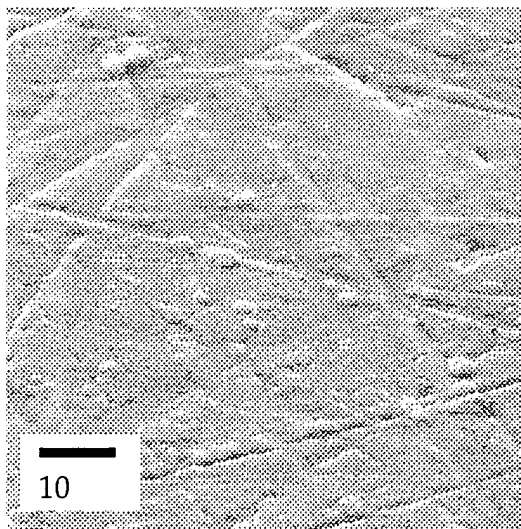
Figure 5. Alumina coating on aluminum substrate (95-2-13). The substrate was mechanically polished to a dull finish prior to deposition of the coating. Surface roughness arises because the vapor deposited coating conforms to the substrate scratches.
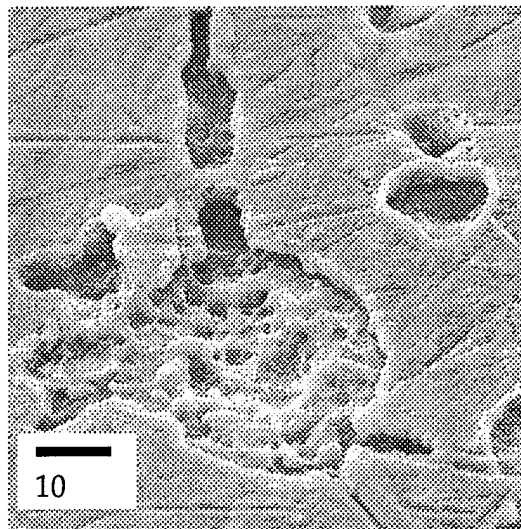
Figure 6. Alumina coating on aluminum substrate (95-2-15) after exposure to concentrated hydrochloric acid. Acid attacks the substrate through localized imperfections in the coating. Initial substrate roughness is a factor in creating coating imperfections.

Coupon #	Deposition conditions (IBAD type, alumina thickness)		Observations
93-9-18	no assist	5.5 μm	mirror finish, few pits
94-3-9	standard O_2	1.1 μm	50% corroded
94-3-8	standard O_2	2.1 μm	mirror finish
93-9-12	standard O_2	4.2 μm	mirror finish
93-9-24	high O_2	3.6 μm	mirror finish, many small pits
94-3-7	high O_2	3.8 μm	dull finish, many small pits
94-3-7	high O_2	4.0 μm	mirror finish, many small pits
94-3-15	slow O_2 dep	3.6 μm	roughened finish
94-3-11	standard N_2	2.0 μm	many large pits
94-3-14	high N_2	2.9 μm	mirror finish, high density tiny red pits
94-3-16	high N_2	5.0 μm	80% dull finish, 20% partially corroded

Table 4. Observations of the corrosion protection provided by the IBAD alumina coating on coupons of SAE 1010 low carbon steel polished to a mirror finish. Each coupon was immersed in an aqueous solution of 3.5% NaCl for 65 hours.

These attempts to prevent corrosion of metal substrates reveal limitations of the coating process. The coating is deposited from vapor by line of sight. No mobility is present on the surface to fill in macroscopic gaps. If a surface is rough it must be articulated during deposition to improve uniformity in coverage. Even then localized imperfections may exist.

Another factor is that the coating is hard and relatively brittle. Mechanical or thermal stress may cause the formation of cracks. At the base of a crack the substrate is not protected. If corrosion spreads laterally beneath the coating further cracking may be induced. For instance, if the corrosion product has lower density than the base metal, coating located over a corroded region would be uplifted. The resulting mechanical stress could lead to further cracking and corrosion.

In summary, the coating most effectively protects against corrosion on smooth substrates. It is important to adjust the deposition conditions to minimize cracks. If cracks do form, corrosion may still be limited if the corrosion is confined to the base of a crack.

3.2.3 DoD Applications

3.2.3.1 Fiberglass Radome

SAIC initiated a collaboration with Brunswick Mfg. Inc., the manufacturer of the F-16 radome, in order to investigate the application of the alumina coating technology to aircraft radomes. This collaboration was initiated with the assistance of Capt. Dan Bullock of the F-16 program office at Hill AFB. Capt. Bullock was associated with the radome and special coatings section and perceived that there might be an opportunity to improve the performance of the F-16 radome. The potential of the coating to assist in reducing sand abrasion wear of the radome coating material was raised in our proposal to ARPA in late 1992.

In September of 1993, Dr. Kirkpatrick of SAIC and Dr. Isaacs of MIT traveled to the Brunswick plant in Marion VA, toured the facility and discussed the opportunity of coating radome samples with the IBAD alumina process. Dr. Kirkpatrick returned with several samples of the flouropolymer coated fiberglass and bare fiberglass used in the F-16 radome. The possibility of directly coating the radome fiberglass was immediately discarded because of the need for an energy dissipative layer to absorb rain

droplet impact shock. The fluoropolymer rain erosion layer was extremely soft and applied at 10 mils thickness.

Our efforts to apply the IBAD alumina coating to the fluoropolymer coated fiberglass met with limited success. A total of 19 coupons were prepared during seven different batch runs, including both treatments of the bare fiberglass and elastomeric coated fiberglass materials. The IBAD alumina coating on top of the elastomeric layer was easily flaked off with a fingernail - we believe this flaking was due to the large mismatch in flexibility between the alumina and elastomeric layers. The radome fiberglass itself was straightforwardly coated, but this might present only a minimal advantage in the chemical protection of the underlying fiberglass during stripping operations for removal and replacement of the elastomeric layer. The value added that this would represent did not appear to merit the added cost burden of the IBAD processing.

These results and our interpretations were relayed to both Capt. Bullock at Hill AFB and the F-16 program manager at Brunswick. We subsequently discontinued examination of the F-16 radome application as a high priority transition opportunity for the IBAD alumina technology.

3.2.3.2 Polycarbonate and Specialty Coated Polycarbonate Canopies

SAIC initiated a collaboration with Texstar Inc., the manufacturer of the F-16 canopy, in order to investigate the application of the alumina coating technology to aircraft canopies. In October 1994, SAIC received from Texstar 14 panels of canopy material, each measuring 6" × 6" (152 mm × 152 mm). The panels consisted of 3/8" (9.5 mm) thick polycarbonate with either no coating (8 each) or an 'enhanced gold' coating (6 each). SAIC retained one of each type and transferred the remainder to Armstrong for coating.

Armstrong performed the first deposition onto Texstar panels in November using normal nitrogen assist. The thickness of the alumina coating was 5.3 μm. On an enhanced gold panel, the alumina coating showed extensive flaking and narrow coarse tracks extending several centimeters. However, on a bare PC panel the alumina coating adhered very well. Armstrong had problems with ion beam control during the run and thought this might be a factor in the poor performance on the enhanced gold panel. They performed a second run with improved ion assist control, but still

produced identical results. They believed flaking on the enhanced gold panel was caused by insufficient ion assist. For the third run they increased the level of ion assist by 10% to no beneficial effect. Adhesion of the alumina coating to bare panels was consistently excellent, but was poor to enhanced gold panels.

Visual inspection of panels coated at Armstrong by SAIC personnel identified the cause of the tracks on enhanced gold panels. During deposition Armstrong used grounded metal clips to mount the panels. The clips were in contact with the conductive front surface of the panels. During deposition the ion beam was not completely neutralized; this created a charge build-up on the surface of the coating. Tracks were formed in the coating as an electrical discharge of this build-up traveled to the grounded clips.

Armstrong performed a fourth deposition run in December in which the front surfaces of the panels were electrically isolated. Discharge tracks were eliminated, but the alumina coating still showed regions of flaking. Flaking may occur after cohesive failure in either the alumina or enhanced gold, or a bonding failure between the two materials. These possibilities were resolved by analyzing XPS spectra of the interface side of an alumina coating flake removed from an enhanced gold panel.

The first step was to characterize the enhanced gold coating without an alumina coating. Figure 7 is a montage of survey spectra acquired during a sputter depth profile. The spectrum closest to the front represents the outermost surface. The spectra reveal that the enhanced gold coating consists of gold sandwiched between layers of indium tin oxide (ITO).
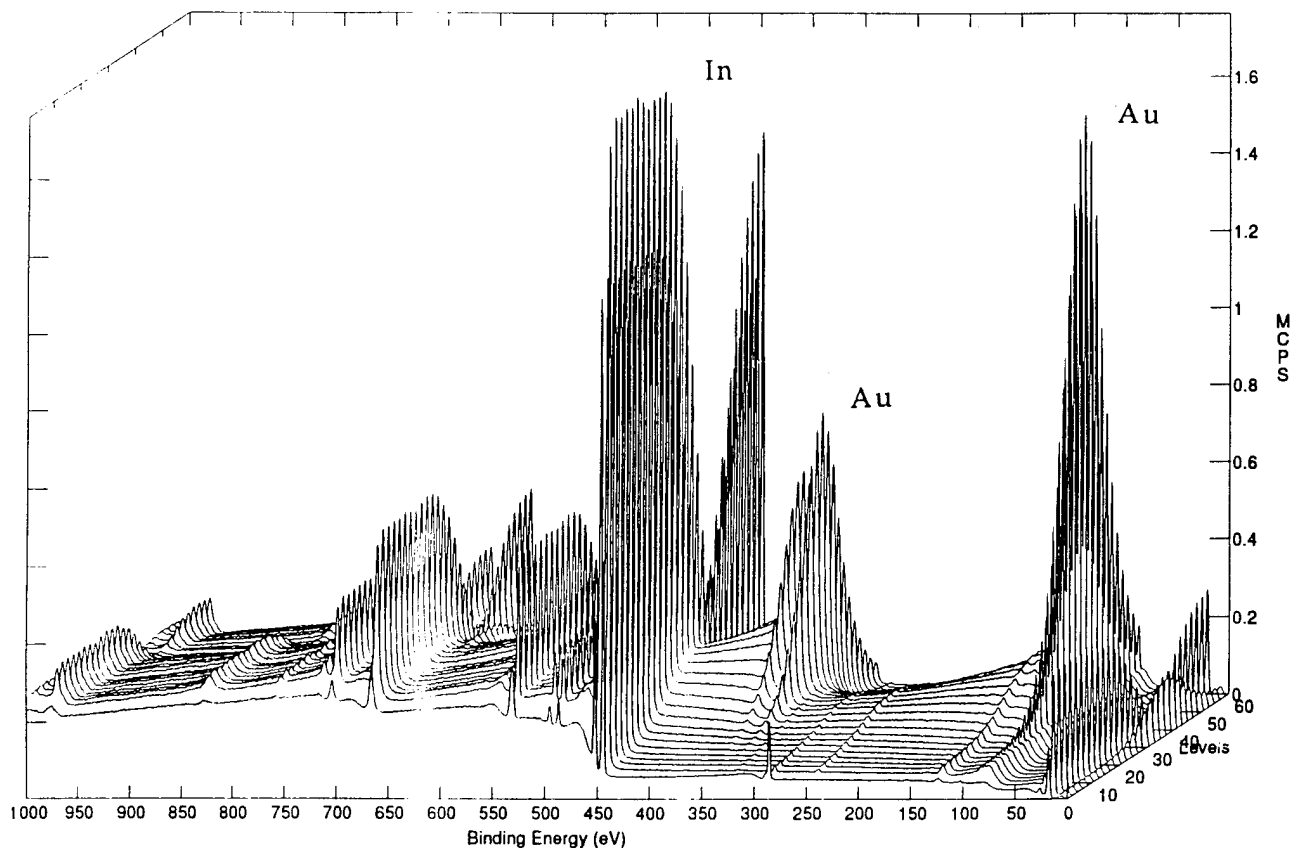
Figure 7. Multilayer structure of "enhanced gold" coating is revealed by x-ray photoelectron spectroscopy. Survey spectra are acquired sequentially while depth profiling using sputtering. The first level corresponds to the top surface of the coating. The structure consists of gold sandwiched between layers of indium tin oxide.

Figure 8 is a survey spectrum of the interface side of an alumina flake removed from a substrate with an ITO coating. The presence of indium, tin, and oxygen shows that a layer of ITO remained adhered to the flake. Therefore, alumina chemically bonds strongly to ITO and flaking of the alumina coating occurs because of cohesive failure in the ITO coating. It is stress developed in the alumina coating and transferred through the interface that causes this cohesive failure in the ITO.
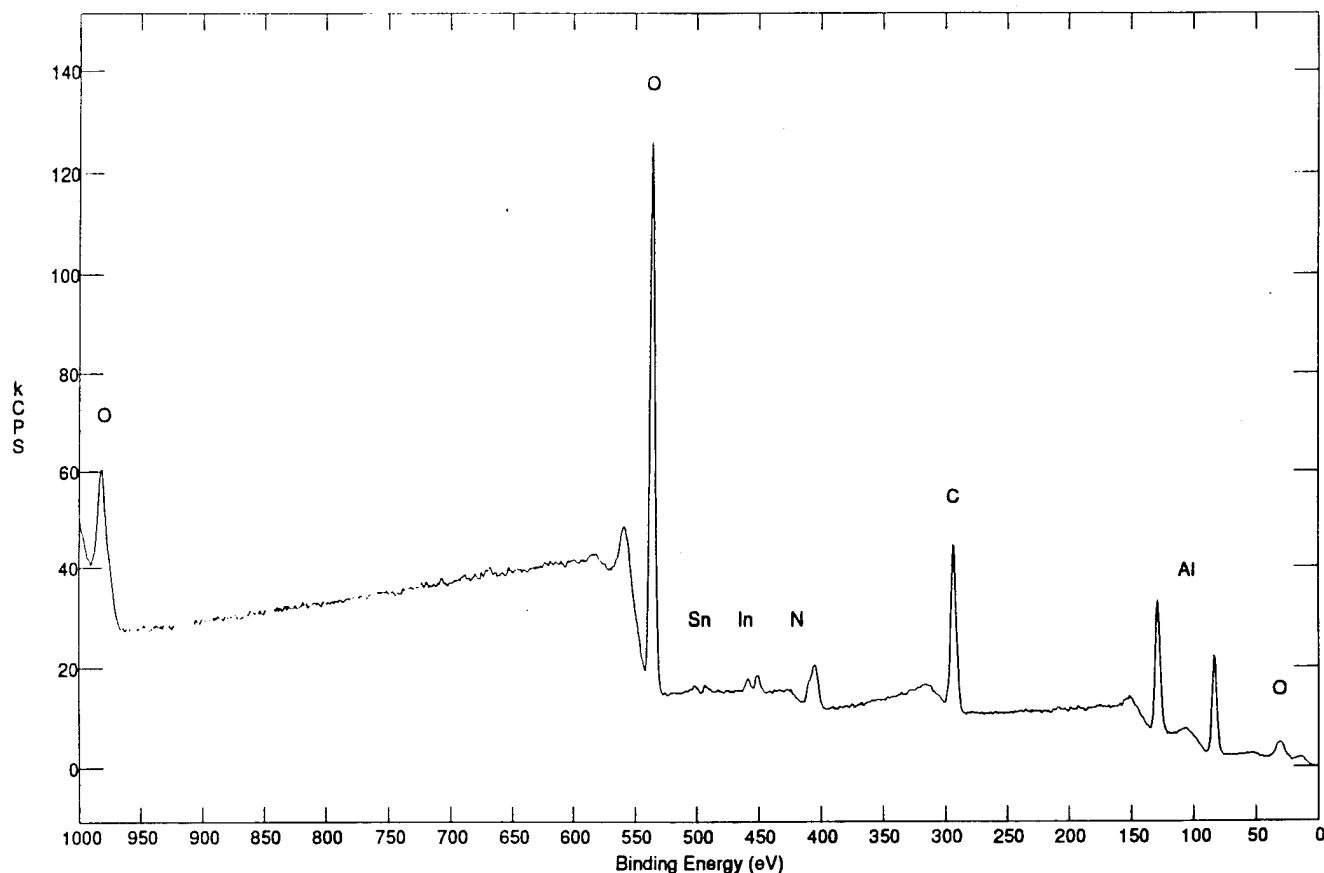
Figure 8. In some cases the alumina coating forms flakes on the ITO (indium tin oxide) surface of the enhanced gold structure. The interface side of a flak was analyzed by x-ray photoelectron spectroscopy. The survey spectrum shown above indentifies the elements present in the top most layer of ~4 nm. The presence of indium and tin shows that a surface layer of ITO is removed when the alumina coating forms flakes. This indicates that alumina adhesion fails because of cohesive failure in the ITO coating.

One approach to prevent adhesion failure is to reduce the level of stress in the alumina coating. The only means to regulate stress is ion flux. Nonuniformity in ion flux across a panel leads to nonuniformity in stress. We know from ion probe measurements that the ion beam flux is most intense in the center of a panel, and falls off towards the edges. On a single 6" × 6" panel this leads to a range of behavior. At the center of a panel, the coating flaked. Around a ring 25-50 mm from the center, the coating was adhered and crack-free, while around a ring 75 mm from the center the coating showed mud cracks. These observations indicate that the stress in the coating varied from tensile at the edges to compressive at the center. The coating was adhered and crack-free only in the intermediate region where the stress was neutral. This is

27

evidence that the Armstrong system lacked the process control to regulate stress across a single panel.

A solution would entail producing a more uniform ion flux. This could be achieved using multiple ion sources, for example. However, experimental work in this direction was beyond the scope of the existing program.

Another approach to prevent flaking is to deposit a thinner coating. The amount of compressive stress required to prevent tensile cracking in a coating scales with the coating thickness. A thinner coating requires less stress. We followed this approach and achieved a coating free of cracking and flaking only after decreasing the thickness to 1.2 μm (run 2/22/95). This is not an optimal approach because a thinner coating has significantly less abrasion resistance

The coupon with a 1.2 μm alumina coating (95-3-45) was shipped to Texstar for testing. The test involved heating to 55°C in high humidity. After accelerated exposure equivalent to 30 days, the coating flaked off. This was not totally unexpected since nonuniform stress was still present in the coating, and the mean stress was not necessarily optimal.

A second approach to prevent flaking is to insert an appropriate buffer layer between the alumina coating and ITO. One property of the buffer layer is that it must possess greater cohesive strength than ITO so as to withstand stress transferred by the alumina coating. Second, the layer can not transmit stress through to the underlying ITO. Two types of buffer layers were investigated: metal and polymer. The metal layer used was titanium. A film only 3 nm thick successfully adhered an alumina coating 2 μm thick on enhanced gold. This is nearly double the thickness possible without a buffer layer. Unfortunately, the adhesion was still only marginal, and the coating flaked when rubbed. A thicker film of titanium would be more effective, but optical transmission declines rapidly with increasing thickness.

The second buffer layer attempted was the Silvue hardcoating. Since no complete canopy panels remained for testing, only small samples could be tested. When applied to canopy samples, Silvue adhered well, but showed cracking. Due to a shortage of canopy samples, trial runs were performed on samples without an enhanced gold coating but only a Silvue coating. These runs showed that Armstrong lacked process control to consistently deposit the alumina coating onto a Silvue coating. Some

samples were adhered and crack-free while others showed worm tracks. No coupons were produced with the configuration alumina/Silvue/enhanced gold/PC.

3.2.3.3 Faceshield Lenses

The Corpus Christi Army Depot (CCAD) has primary responsibility within the DoD for overhaul and refurbishment of helicopters. This activity demands extensive amounts of sand blasting. While blasting, each worker protects his face with a plastic faceshield (referred to as a lens) that survives about 1½ days before being rendered opaque. CCAD uses over 1000 faceshields a year in this way. The manager who oversees sand blasting operations at CCAD contacted SAIC about the possibility of applying the alumina coating to faceshields in order to reduce the generation of waste faceshields.

We thought the high abrasion resistance qualities of the alumina coating might reduce sand blasting damage. We received from CCAD samples of faceshields in July 1994. Initial attempts at Armstrong to coat these faceshields were unsuccessful because the polyester used to fabricate the shields had a heat deformation temperature so low that the shields appeared optically distorted after the thermal loading of the IBAD coating process.

Two approaches were taken to solve this problem. First, shields were cut from polycarbonate (PC) sheet that could be coated using standard conditions. Second, Armstrong changed their process parameters to reduce the thermal load on the shields during deposition, mainly by reducing the deposition rate.

Four samples of alumina coated shields were shipped to CCAD in August 1994. These consisted of three samples of PC (94-8-41, 94-8-47, and 94-8-48) and one of polyester (94-8-17). All had alumina coatings about 4 µm thick. CCAD reported that in service the coated shields lasted a shorter time than uncoated ones. CCAD returned 94-8-48, 94-8-41, and an uncoated polyester shield to SAIC for inspection. 94-8-48 lasted for 7½ hours of blasting using plastic media, 94-8-41 lasted only 4 hours using sand media, and the uncoated shield 12 hours.

The coated shields were visibly frosted. The uncoated shield seemed more optically distorted. Under the SEM these differences in appearance were distinguishable on a microscopic level. The main damage on uncoated polyester was roughening and scuffing (Figure 9). The two coated shields showed no abrasion, but instead had circu-

29

lar cracks and tiling with sharp edges (Figure 10). Adhesion of alumina to 94-8-41 was poorer, perhaps because a lower level of ion flux was used during deposition.
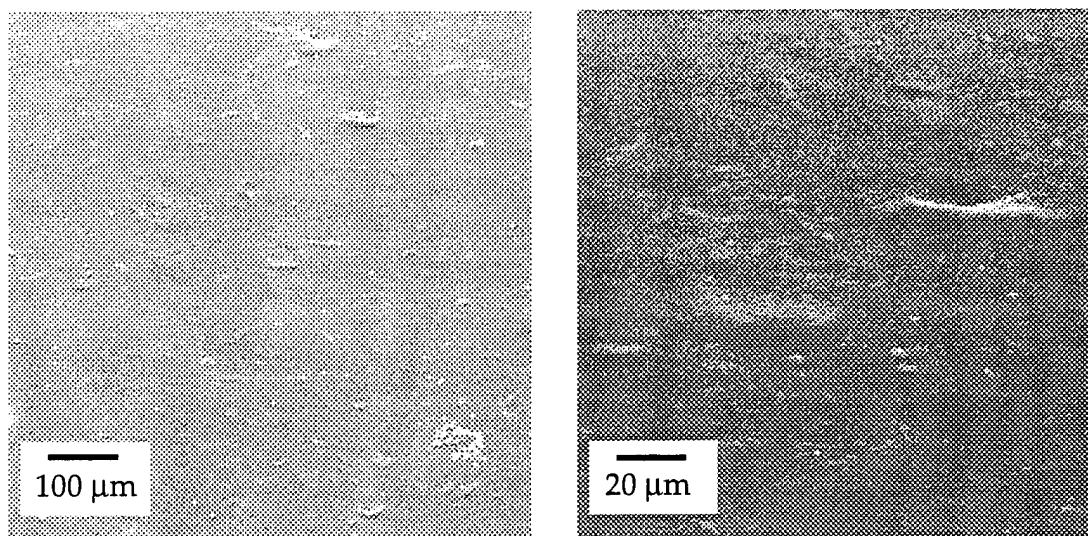
Figure 9. SEM images of polyester faceshield used to protect workers during beadblasting for 12 hours. The surface is torn and deformed by impacts, resulting in distorted vision for the worker.
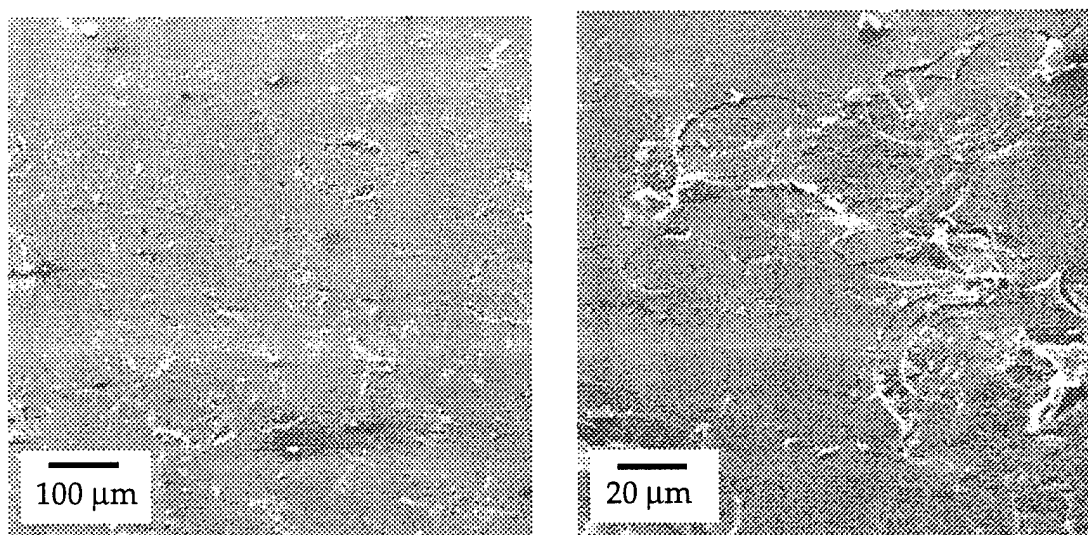
Figure 10. SEM images of polycarbonate faceshield with alumina coating (94-8-48). The shield was used to protect a worker for 7.5 hours. The alumina coating shows extensive cracking caused by bead impact. Sharp edges along cracks effectively scatter light and reduce worker vision.

We deduced that individual particles impact on the coating and are reflected. The energy of impact deflects the coating because the substrate is too soft for support.

When the impact deflection exceeds a critical amount, the coating cracks. Optical transparency is lost when light scatters from the sharp crack edges. When no coating is present, the plastic surface is abraded and roughened. These surface effects cause optical distortion in viewing, but less scattering.

In summary, coating sand blasting faceshields with alumina did not increase the life expectancy. An alumina coating on a plastic shield can protect against abrasion, but not without itself being fractured. Optical transparency is lost when light scatters from the sharp edges of a fracture.

3.2.4 Non-DoD Commercial Applications

3.2.4.1 Armstrong Industries

The coating process used in this project was developed by Armstrong Industries between 1987 and 1993. Their motivation was to put hard protective wear layers on floors, or on thin polymer sheeting that could be laminated to floors. Armstrong scientists determined that a 4 µm thick alumina coating effectively protected polymer surfaces against the types of wear a floor experiences.

Armstrong planned on commercial application of the process by using it to lower the cost of manufacturing flooring. In a web coating system, the deposition rate most strongly determines the cost per square foot of coated material. Armstrong projected that in order for the process to be cost effective a 300-fold scale-up in the deposition rate would be required. This would entail increasing the rate from about 1 nm/s to 300 nm/s. Commercially available evaporators are capable of this rate, but at the start of this project, no ion source was capable of matching the rate. If the process parameters are linearly scaled, the ion current required at the substrate would be 87 mA/cm^2, compared to 0.29 mA/cm^2 generated by the existing cold cathode source.

The current project grew from discussions between SAIC and Armstrong about the possibility of a 300-fold improvement in existing ion source technology using field emitter technology developed by SAIC. However, experience gained during the course of the project has indicated that insufficient ion current is not the only factor preventing a 300-fold scale-up. Another factor is heat load on the substrates. The sources of heat include radiation from molten alumina in the evaporator, the heat of condensation of the evaporant, and the ion beam assist. The relative contribution of

31

each source depends on the deposition rate. At high rates, the ion beam assist delivers the largest contribution.

The Armstrong system was designed for batch coating of substrates up to 8" (203 mm) in diameter. Even when the deposition rate was as low as 1.1 nm/s, deposition onto plastic substrates was limited to a 20% duty cycle in order to prevent thermal damage to the substrates. During the remainder of the cycle the substrates faced a shroud cooled by liquid nitrogen. In spite of this measure, the substrate temperature still exceeded 100°C during deposition.

Web coating systems can be designed with more effective cooling. A common method is to hold the web under tension against a cooled drum in the deposition zone. In order to prevent the web from melting, heat deposited onto the front surface must be in balance with heat removed from the back surface. Since plastic is a poor conductor of heat, the web must be thin to maximize the deposition rate without melting the top surface. Scaling formulas exist to determine the maximum power sustainable without melting [7]. For a 3 mil (76 μm) PET web, the maximum power is about 5 W/cm². This corresponds to a deposition rate of 60 nm/s using a typical level of ion assist (60 eV/atom). The maximum power allowed for a canopy would be much lower because it is much thicker.

In summary, deposition of a 4 μm thick alumina coating onto a plastic web was not cost effective for Armstrong. The limiting factor is that a plastic web can not withstand the high heat load mandated by a high deposition rate. Armstrong stopped IBAD work in May 1995 and has since sold all of the associated equipment.

3.2.4.2 National Renewable Energy Laboratory

The National Renewable Energy Laboratory (NREL) is the lead government organization for the development of optical reflector materials suitable for solar thermal concentrating systems. NREL awarded a contract entitled "A Cost Effective Process for High Volume Production of Enhanced Lifetime Solar Reflective Materials" to the Applied Physics Operation of SAIC in December 1994. The primary goal of this contract was to establish whether the alumina coating technology developed by SAIC and Armstrong could have application in an Advanced Solar Reflective Material (ASRM). ASRMs must meet the performance goal of maintaining at least 90% specular reflectance for longer than 5 years in service.

The reflector material developed under the contract was Structure 1 defined below (not to scale):

Top Protective Layer
Reflective Layer (Ag)
Metal Protective Layer (Cu)
Substrate (PET)
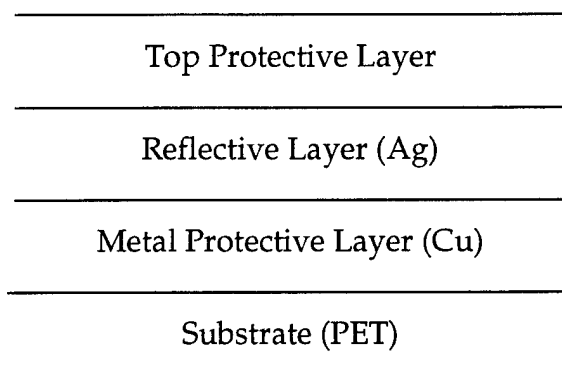
Structure 1 is a front surface reflector on a polymer substrate. This basic design was recognized as desirable early on, but it was difficult to find a durable top protective layer. For example, the 3M Company manufactures a reflector material (ECP305) with an organic protective layer. Unfortunately the material is prone to a form of failure called 'tunneling' whereby the organic layer delaminates. Also there is concern that an organic material will have a relatively short lifespan in the field.

The limitations of an organic protective layer can be overcome by using an inorganic protective layer instead. The alumina coating technology has proven to be highly effective in this application. Samples of Structure 1 with an alumina top coating have been subjected to accelerated weathering at NREL. Without a chemical barrier to atmospheric exposure, silver rapidly tarnishes and loses reflectivity. Figure 11 shows that after over six months of accelerated weathering, equivalent to over a decade in the field, there is no loss in reflectivity for samples protected by an alumina coating as thin as 0.5 µm. This performance exceeds the NREL standard for an ASRM. Based on these results, it appears that Structure 1 employing an alumina protective coating may be an ideal ASRM.

The cost to manufacture Structure 1 is equally as important as its technical performance. NREL has set a cost benchmark for ASRMs to be below $1/sq. ft ($11/m^2). A cost analysis was performed as part of the contract. The deposition rate of the alumina coating was found to be an important cost parameter. The cost is below $11/m^2 for deposition rates above 30 nm/s. This rate is achievable using existing deposition technology. Some details of the cost analysis are presented in Section 3.3.
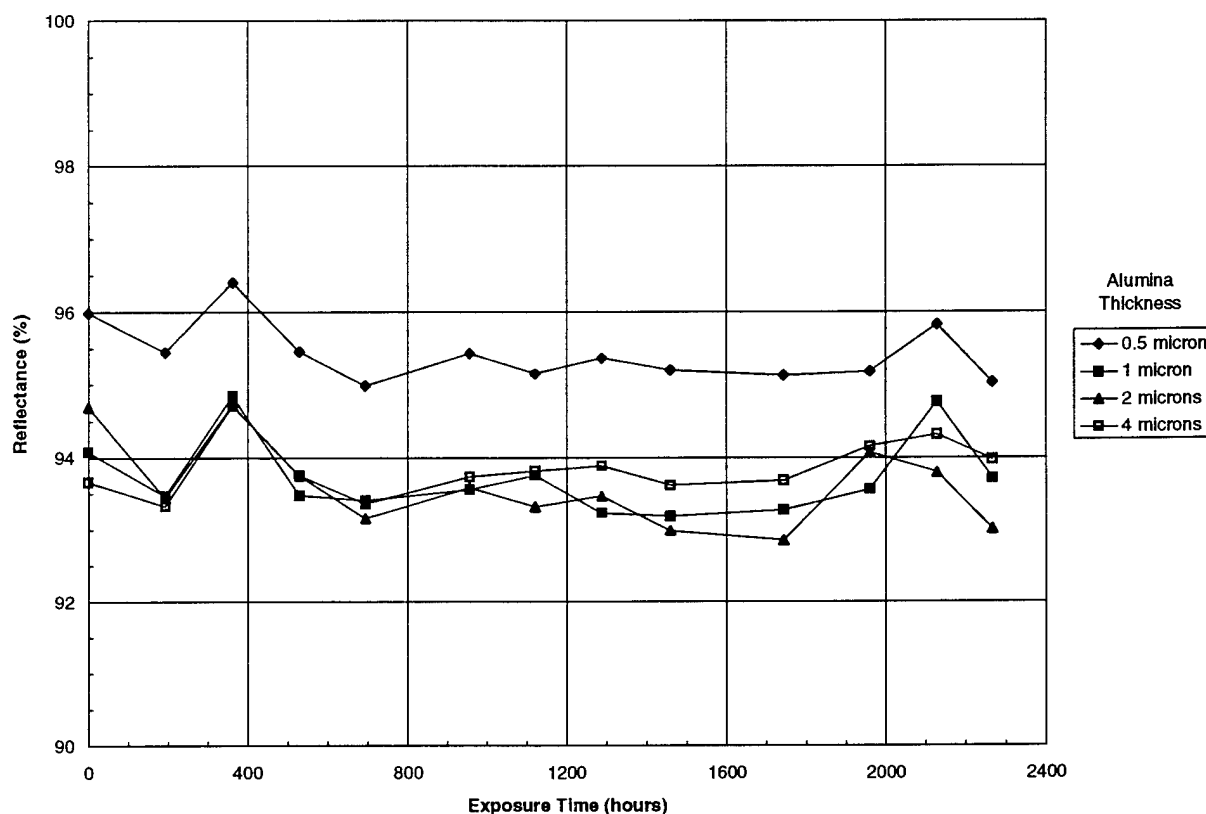
Figure 11. Reflectance vs Exposure Time for Alumina-protected Surfaces.

As this report is being written, work continues on developing Structure 1 as an ASRM. The ultimate plan is to manufacture upwards of 20 million sq. ft. (1.9 km²) of Structure 1 using web coating techniques. The next steps on this path are to demonstrate reflector performance on stainless steel and to meet mechanical tests required for field installation.

3.2.5 Conclusions on Advanced Coating Capability

The essential achievement of the Armstrong process is the deposition of thick alumina coatings on plastic substrates. The fact that alumina is hard and transparent led us to focus on its application as a protective coating for transparent plastics such as polycarbonate (PC) and polymethyl methacrylate (PMMA). During the course of the project, the conditions needed to deposit crack-free coatings on these plastics were determined. PC is widely used as a canopy material in the DoD. Although PC has excellent impact resistance, it is subject to surface abrasion in the canopy application. One finding from this project is that an alumina coating only a few microns thick effectively protects PC against abrasion.

Canopies have multifunction design requirements. Besides abrasion resistance there is rain erosion, radar cross section, protection for pilot and sensors against lasers, static electricity bleed off, and bird strike. With the exception of bird strike, these design requirements demand an approach employing integrated and non-interfering multilayers. Radar cross section and static bleed off requirements are currently been met by transparent conductive coatings, such as 'enhanced gold'. These coatings are soft and prone to erosion if left unprotected. Attempts were made in this project to coat 'enhanced gold' with alumina. Unfortunately this particular coating system has a very narrow process window in terms of acceptable coating stress. Across a single coupon, nonuniformity in ion bombardment led to coating variations from tensile cracking to compression induced flaking. To eliminate cracking and flaking in this coating system, further improvements in ion bombardment uniformity are necessary. Another approach is insertion of an interlayer beneath the alumina coating in order to distribute stress.

A similar issue of stress dissipation is raised when considering rain erosion. Rain erosion is a process whereby shock waves generated by particle impact erode a material. A simple system consisting of a hard coating on a soft substrate is not effective against particle impact. When the pressure of impact exceeds the strain to fracture point (0.6%) of an alumina coating, cracks will form. This failure mechanism was observed with faceshields subjected to bead blasting.

A multilayer coating system is necessary in order to be simultaneously abrasion and impact resistant. The components of this system could be an alumina coating outermost for abrasion resistance, followed by an elastomeric interlayer to absorb shock. The interlayer would need high hardness at the interface to support the alumina coating against impact induced fracture.

The emergence of high power laser threats has made laser protection a new requirement for canopies. A laser can blind a pilot or essential sensors from a great distance. The IBAD process is able to deposit a broad band reflective filter by modulating the coating index of refraction to achieve a multilayer structure such as a rugate filter. This has already been demonstrated by depositing alternating layers of aluminum nitride and aluminum oxide [8].

A multilayer coating system incorporating these diverse canopy design requirements can be achieved by an IBAD system in concert with other coating tech-

nologies. For example, elastomeric layers are probably best applied by wet chemical techniques. Testing at Texstar Inc. suggests that alumina can be used for abrasion resistance. However, a great deal of work remains before a multifunction canopy based on a multilayer coating system can be produced.

The path to eventual success in this effort is shown by work for the National Renewable Energy Laboratory (NREL), the lead government agency for solar energy generation. Since last December SAIC and Armstrong have developed an advanced solar reflective material (ASRM) utilizing the alumina coating technology. This required the integration of the alumina coating with a metal coating stack. The multilayer coating stack developed consisted of (working out from the substrate) copper/silver/alumina on PET sheet, in which the outer alumina coating functioned as a barrier against atmospheric corrosion of the reflective silver layer. In accelerated testing the new ASRM has far exceeded NREL standards for durability and reflectivity. There is every indication that this application of the alumina coating technology will be a technical and commercial success.

3.3 Advanced Ion Source Development

3.3.1 Introduction

Prior to this project, one of the primary constraints limiting more widespread application of IBAD alumina coatings was cost issues related directly to the deposition rates available from IBAD source technology. The IBAD process comprises an evaporative source of the material to be deposited and an ion beam source to impart energy to the depositing molecules as they arrange themselves on the substrate. Given that a certain level of ion energy per deposited evaporant molecule must be provided to achieve the desired film characteristics, a balance is required between the evaporation rate and the ion power delivered to the surface. Prior to the accomplishments of this project, the output capacity of the ion source was the limiting factor for the IBAD process deposition rate and therefore the substrate coverage throughput rate. The existing ion source technology at the start of this project limited rates for IBAD coating with alumina to ~ 6 nm/s.

3.3.2 Source Trade-offs

The Armstrong process uses IBAD of Al_2O_3, and their present device is limited to a deposition rate of 2 nm/s by the available ion (O^+) flux of 30 mA/cm^2 at the ap-

erture of their source. This source aperture current density produces 50 $\mu A/cm^2$ at the target substrate. To increase throughput by 100-fold requires deposition rates of 200 nm/s, which implies a requirement for 5 mA/cm^2 at the substrate. In a production process, the ion source will be a slit (or perhaps a linear array of circular sources) so that a wide strip of substrate material can be treated as it is moved under the source. Since the ion beam from a circular source expands in both transverse dimensions while the beam from a linear source expands in only one transverse dimension, a single circular source will require higher current density at the source aperture to produce a given current density at the substrate than is required from a slit source at the same stand-off distance. A 100-fold increase in throughput, therefore, may require only 10-100 fold increase in current density at a slit aperture. By this reasoning, a design goal for the ion source current density at the aperture was set to nominally 1.0†A/cm^2.

The optimum extraction voltage for the process is not known, but is believed to lie between approximately 30 V and 500 V. One role of the ions in the process is to hold the coating near the surface while surface chemistry takes place. Below 30 V, the ion energy is insufficient to reflect coating molecules back to the surface. Above 500 V, the ion energy is large enough to cause appreciable sputter.

The ion source development effort progressed through three concepts for producing significantly increased ion source current density. The first concept consisted of retrofitting the Denton Mfg. CC-102R cold cathode ion source that was already in place on the Armstrong deposition system. While we recognized that retrofitting the Denton source was unlikely to give us the 1.0 A/cm^2 source current density mentioned above, we held out some expectation that we could significantly improve the in-place source capability at Armstrong. This would in turn allow deposition tests at higher incident current densities and validate some scalability of the IBAD process to higher deposition rates. Unfortunately, the gas pressure distribution in the CC-102R ion source could not be modified enough to allow operation of the FEA cathodes in either their high or low pressure regimes.

The second concept built on the results of these efforts and split the oxygen plasma generation and oxygen ion extraction functions of the ion source into two separate chambers. This concept is well established and is more commonly referred to as a Plasma Injection Gun or PIG. The intrinsic geometry of the FEA cathodes favored

a planar plasma discharge, while the PIG geometry favored a cylindrical geometry, and this design sought to combine the two.

The third and final concept built on the lessons learned from both previous efforts. This concept employed a hollow cathode geometry driven discharge in a two-stage PIG configuration. The hollow cathode geometry avoided the effects of the pressure variation during the ignition of the plasma arc. This final geometry was successful in providing the necessary plasma current to populate a gun extraction chamber sufficient to allow 1 A/cm^2 extracted ion current densities.

Also important to this development effort was the discovery that the web structure to be coated in the IBAD process could not survive deposition rates in excess of 60 nm/s. This reduced, by a factor of five, the targeted maximum current density for the advanced ion source.

We first discuss our measurements and results with the Denton ion source, followed by those with the planar/cylindrical discharge PIG source. We close with discussions of the hollow cathode PIG source and the theoretical limitations on current extraction.

3.3.3 Denton Source

Part of the development effort for a high current oxygen ion beam source suitable for scale-up of the IBAD process focused on the characterization of a commercial ion source and the investigation of a retrofit with a Si-TaSi$_2$ eutectic field emitter (FE) electron source. This effort consisted of: (a) construction of a testing chamber and installation of a commercial ion source, (b) characterization of the ion source, (c) modification of the ion source for FE retrofit, (d) testing the FE retrofit design, (e) performing surface analysis post test (SEM, XPS), and (f) evaluating FE ion source performance for application to a subsequent ion gun design. The commercial ion source used was a CC-102R Cold Cathode Ion Source System from Denton Vacuum, Inc.

The commercial source was characterized by recording values for the Drive Voltage and Current, Beam Current, Bias Voltage, Neutralizer Current control settings, and the extracted ion current for argon and oxygen gas flows at a set chamber pressure. Data sets were taken at fixed chamber pressures for each of three interchangeable extraction grid apertures supplied by Denton:

- Aperture "A" is a flat flange with 1¼ inch (31.75 mm) diameter opening and is recommended for achieving a high density, self neutralizing beam of high uniformity.

- Aperture "B" assembly is a domed wire cloth with 20 × 20 mesh attached between two rings with a 3¾ inch (95.25 mm) diameter opening and is used to achieve a high density, divergent ion beam.

- Aperture "C" grid assembly is a flat cloth wire with a 20 × 20 mesh attached to a flange with 2 inch (50.8 mm) diameter opening and is used to achieve a narrow ion beam at a low chamber pressure.

The initial data analysis consisted of plots taken of voltage versus source current and voltage versus extracted ion density for each aperture under both argon and oxygen flow at a set chamber pressure. The extracted ion density was calculated from the undiscriminating current striking the masked and isolated aluminum collecting plate at a distance of 30.5 mm from the ion source. The exposed area of the plate is approximately 116†cm^2 and is isolated on ceramic stand-offs. The plots were then made for each aperture under characterization and their performance evaluated. This characterization of the CC-102R Cold Cathode Ion Source resulted in a set of base point data to compare the original source configuration and the FE cathode material retrofit. The results of the characterization for the standard commercial ion source configuration for each extraction aperture under oxygen gas flow are presented with the experimental data of the FE retrofit.

The modification of CC-102R Ion Cold Cathode Ion Source to incorporate FE cathode material was undertaken with a redesign of the gun cathode region. The positioning design for placement of the FE cathode was chosen to demonstrate improved cold cathode ion source performance in the form of higher ion current densities with longer operational lifetime. In this advanced ion gun design, a number of Si-TaSi$_2$ wafers, nominally 5/8 inch (15.9 mm) in diameter, were placed in an array as to lie just inside of the anode of the ion source. The FE cathode wafers were slightly recessed in the holder exposing roughly 80% of each surface. A 5 mil (127 µm) thick nickel disk was used behind each cathode, and an aluminum gasket foil was applied to the backside to ensure electrical, mechanical, and thermal contact.

A total of nineteen experiments and one control were conducted using the modified ion source configuration. In all cases extensive SEM analysis was performed on all FE cathode material to document its condition at vital steps in the preparation for retrofit and after test insertion. Under all test conditions, the final performance was compared to the original data taken during the ion source characterization. High resolution XPS analysis was performed after the several of the experimental cases. Details of this entire experimental effort are available in a separate report [9].

The performance goals for an advanced oxygen ion beam source in this context were defined as follows: (1) ion current densities of $0.3 \, A/cm^2$ at the output of the source; (2) operational time > 500 hours at this current density; (3) ion beam energy spread of 50 eV or less for a mean energy of 400 eV; (4) ion beam divergence angle of less than 20°; (5) tunable mean ion energy in the range of 100 eV to 2000 eV; (6) wall plug efficiency of > 5%; (7) total available ion current of 0.6 A for a source model suitable for retrofit onto the existing IBAD test bed; and (8) scaleable to a total available ion current of 15 A in a single unit. Presently the Denton CC-102R Cold Cathode ion source system, depending on which extraction aperture used, is capable of a producing the following: source voltage range of 300-1600 V; beam exaction of 7-20%; maximum beam current of 70-200 mA; maximum beam energy of 100-1000 eV; maximum beam density of $55-150 \, A/cm^2$; beam uniformity of > 0.76-0.95; and a minimum operational chamber pressure in the range of 5×10^{-5} to 1×10^{-4}†torr. These are typical performance values for a 44-inch (1.12 m) box coater with a pumping speed of 2500 l/s as summarized from the users' manual.

The Denton ion source as modified under this project falls into the category of single aperture sources employing magnetic fields. Of the sources based on this architecture for electron-gas interaction and/or ion extraction, the Denton gun is considered one of the best examples of a widely dynamic, cost effective, and robust system. This system falls short of the minimum on-target ion density required for large scale production of advanced coatings by a factor of about 100. Additionally, when the aluminum surfaces used in this system is subjected to oxygen at the pressures and voltages required for the effective deposition of Al_2O_3 coatings, the aluminum surfaces become oxidized, and a higher voltage is required to sustain the discharge current. Thus the ion intensity falls off over some hours of operation. When this condition starts to occur, the source then can be reconditioned by operation in argon at 800-1000 V, 100-200 mA for approximately a half hour, effectively reversing the oxidation

process by sputtering the inner surfaces with energetic argon ions. This procedure can be repeated until it is no longer effective. Then the source must be removed and disassembled for cleaning.

The objectives of the first key demonstration experiments were to investigate the enhancement of these capabilities by the replacement of some of the aluminum surfaces in the CC-102R source with a high density field emissive (FE) material. Predicted performance of the initial retrofit of the source with gold-coated Si-TaSi$_2$ FE cathode material was modest and based upon the areal comparisons. One order of magnitude improvement in total ion density and a significant increase in the operation of the modified ion source at that output were expected. The expected success of the retrofitted source employing Si-TaSi$_2$ field emitters as the primary electron source was based on their performance in other tested systems. With a record of: a) operation in a background of oxygen; b) producing electron currents of 75 A/cm^2 in vacuum (10^{-5} torr and below); and c) lifetimes exceeding 400 hours of continuous operation in similar discharge environments, the addition of eutectic field emitters was a valid modification to the Denton cold cathode ion source system.

The initial analysis of the FE performance did show some improved operation in an oxygen environment in the standard CC-102R ion source configuration until rapid surface contamination degraded its performance. Although a factor of ten improvement in ion flux performance was expected, the CC-102R FE cathode retrofit experiments did not produce on-target ion densities of that order. The most favorable data produced only a factor of two increase, and that data could not be reproduced. An explanation for the inability to achieve the expected result of an increased on-target ion density with extended lifetime follows.

The mechanism for producing field emission from Si-TaSi$_2$ composite material requires electric fields of the order of around 50-200 kV/cm depending mainly of the surface conditions of FE cathode. Initial "turn on" field strengths are usually higher than the "conditioned" FE cathodes which after several hours of operation maintain the same level of electron output at lower electric field strengths. In experiments conducted at SAIC, these FE surface conditions have been studied at length for optimum specification. Thus the procedures for processing the FE material are performed to produce single crystal material of the proper tip height with surface and tip uniformity. Though there are many steps in the production process from growing the raw

material to processing it for use, at crucial points the material is examined for integrity.

To change the power balance and make effective use of the FE material in the ion source would require that the field strengths 50-200 kV/cm be achieved at the surface. For this operational condition to exist in the CC-102R ion source, a phenomenon called plasma enhanced field emission (PEFE) must take place. Typically, Si-TaSi$_2$ cathode PEFE operation has been observed in vacuum pressures of argon or oxygen of 1-10 torr. PEFE has several requirements: 1) a positive sheath plasma boundary must form near the surface of the cathode; 2) the potential at the sheath boundary must be at least 1 V; and 3) the Debye length at the sheath boundary must be of order 10 μm. In the present modified CC-102R ion source configuration, this is not accomplished. A positive plasma sheath forms for discharges in most gas compositions due to the higher mobility of the electrons compared to the ions. However, we were unable to create pressures of 1-10 torr in the vicinity of the FE cathodes, and therefore the scale size of the sheath formation and the Debye length were unsatisfactory for obtaining the PEFE operation.

3.3.4 Cylindrical/Planar Discharge PIG

The cylindrical/planar discharge PIG was an attempt to achieve the necessary pressure range in the vicinity of the FE cathode to obtain a PEFE discharge, while at the same time achieving a pressure of ~10^{-4} torr in the ion extraction regime for efficient ion source operation. This four-order-of-magnitude pressure differential is achieved by separating the discharge and extraction volumes by a fine aperture, as shown in Figure 12. The upper chamber is designed to maintain a pressure in the range of 1-10 torr, and the FE cathode element drives the plasma discharge in the upper chamber via the PEFE mode of operation. Large amounts of plasma escape from the upper volume through the aperture to the lower volume, where the ambient pressure is in the range of ~10^{-4} torr. Typical gas flow speeds into the upper chamber are ~30 SCCM, while the pumping speed in the vacuum chamber is ~500 l/s.

Two elements of this design are critical to exciting a sustained PEFE discharge in the upper chamber. First, the distance from the FE cathode element to the aperture disk must be appropriately set. This spacing must be large enough that the necessary sheaths and boundary layers can form around the cathode and aperture disk without interfering with one another, yet at the same time be small enough that the initial

voltage spike required to break down the upper cavity and initiated the discharge does not damage the cathode. Second, the size of the aperture in the aperture disk must appropriately balance the need for the pressure differential against the efficient transfer of the PEFE plasma to the extraction chamber. Both of these conditions must be met to drive any substantial plasma into the extraction chamber.

Our measurements indicated that a cathode to aperture disk spacing of 3-10 mm could yield a PEFE discharge, with a spacing of approximately 5-7 mm appearing most optimal. The optimal aperture size was found to be 1-2 mm for a 1 mm thick aperture disk.

GAS INLET

V_1

FEA CATHODE

APERTURE

V_2

EXTRACTION GRID

VACUUM VOLUME
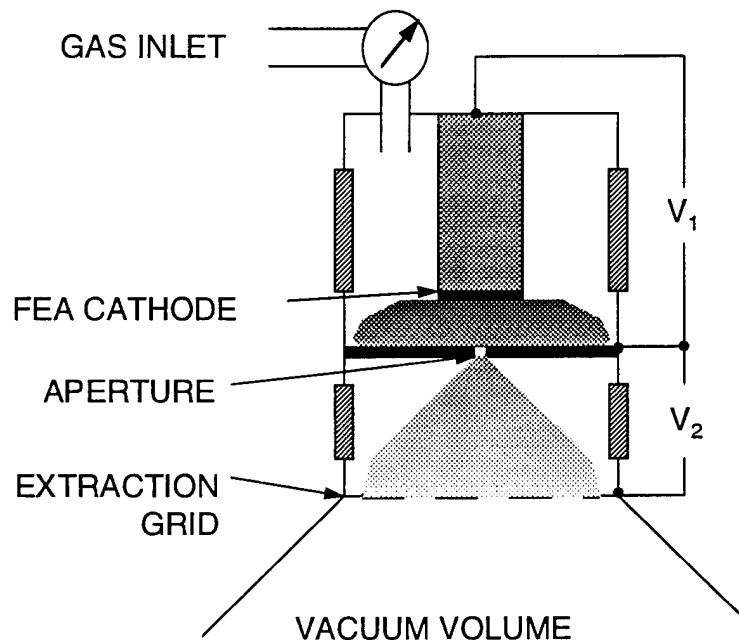
Figure 12. The layout of the cylindrical/planar discharge PIG.

Our measurments also included characterizations of a geometry similar to that shown in Figure 12 but where the aperture disk was formed from two separate elements. The geometric aperture affecting the gas flow was fabricated from an insulator. A second, metal, aperture disk with a larger aperture was placed behind the ceramic aperture disk, away from the FE cathode. This arrangement reduced the amount of current collected by the aperture disk relative to the current flowing into the plasma through the cathode.

While we were able to repeatedly show plasma discharge pulses with peak currents larger than 5 A from a 3 mm diameter cathode, we were unable to ingite and sustain a discharge for any substantial time. A fast pressure gauge was added to monitor the upper chamber and it was discovered that the pressure in the upper chamber was falling by as much as an order of magnitude as a result of each strong discharge. This large a pressure drop would certainly have the effect of extinguishing the PEFE discharge before there was any opportunity for operation to stabilize. The modification of this design geometry to compensate for this effect resulted in our third approach, described next.

3.3.5 Hollow Cathode Arc Source

The hollow cathode arc source is extremely similar to cylindrical/planar PIG source shown in Figure 12, with the exception that the cathode element is the interior and end areas of a hollow tube which also serves as the gas feed for the upper stage (see Figure 13). A striker electrode is brought into proximate contact with the cathode to initiate the arc, and then removed. The impedance of the striker electrode is large to prevent the arc current from seeking that circuit path to ground. The alternate ground path available to the arc is to transit to a lower pressure volume below the cathode. The cathode tube is long and thin; the end aperture of the cathode provides the same function as the aperture in the cylindrical/planar PIG described above: the gas flow through the tube is sufficient to raise the pressure inside the tube to ~1 torr, while the pressure in the volume below the cathode is ~10^{-4} torr. As the arc is initiated, however, the pressure variation only extends a small distance inside the tube due to the large flow impedance of the narrow tube.

The setup shown in Figure 13 was successfully used to generate ~60-90V, >50 Amp discharge pulses lasting up to several seconds. The limiting factor in the duration of the discharge was found to be a minor fault in the design of the striker circuit. This fault resulted in the discharge dumping through the striker circuit when some of the generated plasma drifted to the aperture through the shield cylinder for the striker electrode. A small circuit modification is planned to fix this problem.
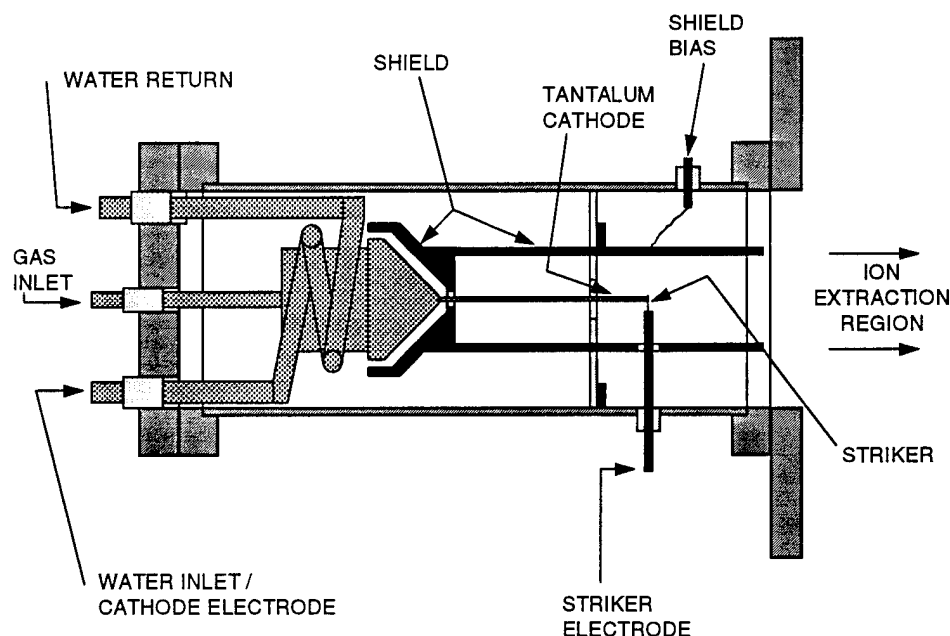
Figure 13. The hollow cathode arc source geometry, showing the various electrode contacts and gas feeds. The tantalum cathode is a long narrow tube; for pressures in the ion extraction region of ~10⁻⁴ torr, the pressure just inside the tantulum tube aperture is ~1 torr.

The >50 Amp discharge current available with this geometry is more than sufficient to drive commercial second stage ion sources to saturation. This includes ion sources working with an oxygen plasma feedstream to form an oxygen ion beam. The work on this last design was performed in collaboration with Commonwealth Scientific Corporation, and was wholly supported by the internal funding resources of SAIC and CSC.

3.3.6 Design and Modeling

The modeling effort was intended to identify and study design options for a process ion source. The computer code used in this analysis is SNOW, a widely-used dense ion-beam model that includes the plasma expansion cup, the ion acceleration region, and a neutralizing drift space in a two-dimensional configuration (either axisymmetric or with planar symmetry). It models the steady-state ion flow using an iterative procedure in which the trajectories of representative ions are computed through the device. These are then used as sources in Poisson's equation to determine

the potentials. The model allows a Boltzmann distribution of electrons in Poisson's equation.

The duopigatron-type source design was chosen for modeling to study the scaling of the extracted current density without neutralization with aperture size for both circular and slit aperture geometries. This particular source design has the advantages that: a) it has operated in an O_2 environment [10]; b) its geometry is compatible with a modular design approach in the process environment; and c) it provides a natural configuration for isolating the electron emitters from damaging ion bombardment. The basic duopigatron configuration consists of a high pressure plasma source that feeds a lower pressure discharge chamber where electrons injected from a filament are trapped electrostatically and produce copious ions. The ions are extracted through the electrode that traps the electrons, typically using an accel-decel column to control and focus the extracted beam. The major disadvantage of the duopigatron is that it requires the extraction of an ion beam, and therefore faces the issue of space-charge-limited extraction. Ion current densities of 0.3 A/cm² have been reported in the literature at an extraction voltage of 50 kV. While the accel-decel configuration allows the extraction voltage to be higher than is allowed at the substrate, it is not practical to extract at 50 kV and decelerate to < 500 V, even using an externally neutralized beam transport region to control space charge.

At low extraction voltage the current is limited by Child's Law, which is given by

$$J_{ion} = 0.17 \frac{V_{kV}^{3/2}}{d_{mm}^2} \left(\frac{m_p}{M} \right)^{1/2} \times \left\{ Geometry\, Factor \right\} \frac{A}{cm^2}$$

where m_p is the proton mass, M is the ion mass, V_{kV} is the extraction voltage in kilovolts, and d_{mm} is the extraction gap in millimeters. The "Geometry Factor" is a correction for non-planar electrodes, which can be ignored for the purposes of scaling.

If the extraction gap is decreased at fixed voltage, the electric field strength at the electrode will increase and eventually lead to breakdown. Decreasing the gap width and the extraction voltage in parallel, so that the field strength at the electrode is approximately constant leads to the interesting scaling law,

$$J_{ion} \sim d_{mm}^{-1/2} \quad for \quad V/d = constant \tag{2}$$

which shows that the required current density can be obtained (in a planar extractor) without breakdown if d is made sufficiently small. In fact, $d = 0.12$ mm is required for $J_{ion} = 1$ A/cm^2 at $V = 500$ V.

To actually extract this current, of course, requires an aperture in the electrode. The accepted rule of thumb in ion source design is that the diameter of the aperture be approximately equal to the gap width. Simulations with this configuration yield current densities in excess of 1 A/cm^2, but the total extracted current is very small (because of the small aperture). A series of runs has been made with SNOW to examine the effect of enlarging the aperture, with the result that the current density falls off very rapidly as the aperture is decreased.

Since the process source will have a slit-aperture geometry, instead of a circular aperture, a second series of simulations has been carried out with SNOW to examine the effect of this change in geometry. Again, the results indicate a rapid decrease in extracted current density as the aperture dimensions are increased. These results indicate that this source will only operate successfully with space-charge neutralization. In fact, neutralization must be provided not only in the extraction region, but throughout the transport from the source aperture to the substrate. Otherwise, space charge forces will cause the ions to reflect back to the source (i.e., the electrostatic potential will form a "virtual cathode"). The extractor region is particularly difficult to neutralize because it contains large electric fields that are drawing the ions toward the cathode. Injecting electrons at the cathode, making a bipolar diode, provides a small enhancement in the ion current density due to space charge neutralization, but causes a major loss of efficiency. Highly mobile electrons rapidly traverse the extraction gap, drawing power from the extractor power supply. The ratio of ion to electron current density in this configuration is given by the root of the mass ratio,

$$J_{ion}/J_{electron} = \left(m_e/M\right)^{1/2} \tag{3}$$

where m_e is the electron mass.

The electrons can be prevented from traversing the gap by imposing a transverse magnetic field on the gap, creating a "magnetically insulated" extractor. The

magnetic field strength can be selected so that the ion trajectories in the gap are unaffected while the electron trajectories are strongly deflected. This crossed-field configuration is similar to a magnetron geometry, which is a potentially viable ion extraction configuration for the duopigatron.

3.4 Impact Analysis

3.4.1 Cost Modeling

This task concentrated on the economic modeling and life cyclen analysis of the IBAD alumina deposition process. In particular we focussed on two applications of IBAD processing: i) coating polycarbonate aircraft canopies, which would reduce landfill volumes in the future and ii) solar reflector materials, which would enhance the use of renewable energy. Models of materials production technologies have proven to be powerful tools for evaluating alternative materials, processes and manufacturing technologies. This economic analysis consists of the construction and use of the a process based cost estimation model. The modeling approach breaks out the processing steps into unit operations where necessary, and separates the various cost elements for each operation. Data used to construct the model is obtained via collaboration with other team participants of this program, as well as through information from industry experts. Hence the model represents an accurate picture of the expected production scenario, and can be utilized in various ways. Sensitivity analyses aid in understanding the prime contributors to coating costs and provide approaches to cost reduction.

Process based cost models are useful tools for estimating the operating and overall product costs of these manufacturing deposition systems. The cost models are designed to reflect manufacturing intricacies by breaking out the processing steps into small, manageable steps, or unit operations. In the model various cost elements can be separated out for each unit operation. The estimation employs clearly defined and verifiable economic and accounting principles, and is based on engineering principles and the physics of the manufacturing process.

The processing conditions, deposition rates, and film thicknesses are varied for deposition via an IBAD system using a technical cost model to determine the trade-offs in economic viability. This investigation is done in concert with the results of technical performance of various coated substrates, i.e., the manufacturing costs are calculated for the most promising of the aluminacoated samples. As a first approxi-

mation for economic viability, the equipment for the deposition system is postulated as an adaptation of that used for standard metallization in the roll coating industry. A batch coating process is modeled by specifying a short roll length, or possibly by specifying several smaller components assembled into the analog of a short roll length.
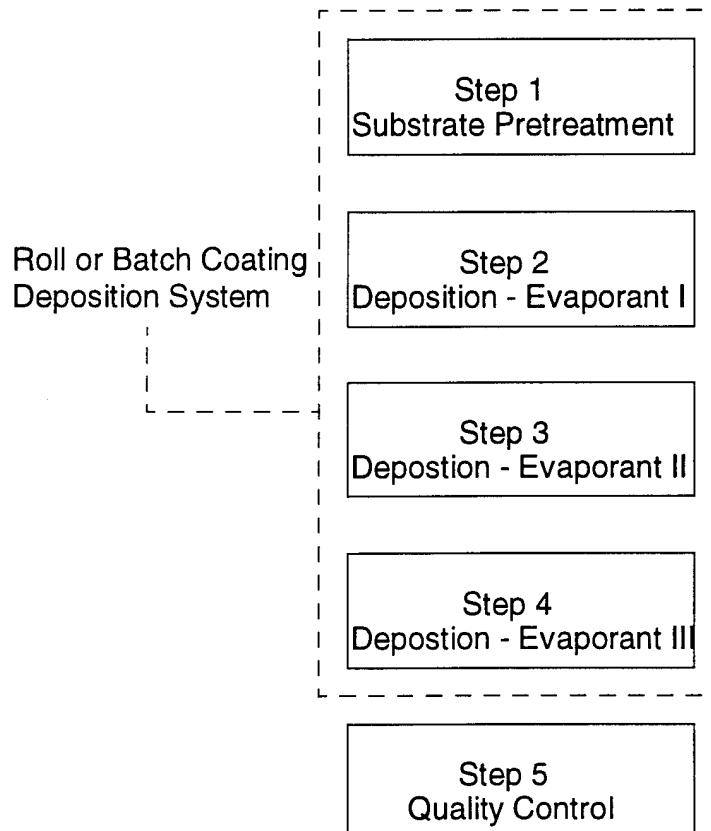
```
                          ┌ ─ ─ ─ ─ ─ ─ ─ ─ ─ ─ ─ ┐
                          │   ┌─────────────────────┐   │
                          │   │       Step 1        │   │
                          │   │ Substrate Pretreatment │   │
                          │   └─────────────────────┘   │
                          │                             │
                          │   ┌─────────────────────┐   │
   Roll or Batch Coating  │   │       Step 2        │   │
   Deposition System      │   │ Deposition - Evaporant I │   │
                          │   └─────────────────────┘   │
                          │                             │
                   └ ─ ─ ─ ┤   ┌─────────────────────┐   │
                          │   │       Step 3        │   │
                          │   │ Depostion - Evaporant II │   │
                          │   └─────────────────────┘   │
                          │                             │
                          │   ┌─────────────────────┐   │
                          │   │       Step 4        │   │
                          │   │ Depostion - Evaporant III │   │
                          │   └─────────────────────┘   │
                          └ ─ ─ ─ ─ ─ ─ ─ ─ ─ ─ ─ ┘

                              ┌─────────────────────┐
                              │       Step 5        │
                              │   Quality Control   │
                              └─────────────────────┘
```

Figure 14. Process Steps for Multi-Layer IBAD Process.

Figure 14 shows the generalized process unit steps for coating the substrates under consideration. In Step 1, the substrate surface is cleaned or prepared prior to deposition. Initially, several techniques for preparation were under consideration, including: 1) argon ion bombardment; 2) oxygen ion bombardment; 3) wet chemical treatment and 4) plasma radical treatment. However, after further experimentation and testing of coated samples, it was determined that only the argon ion bombardment is required for adequate surface preparation. Other pretreatment techniques are not considered in the cost analysis.

Steps 2, 3 and 4 represent the actual deposition steps. While some coating applications require only a layer of ceramic material, other coatings require deposition of

metallic interlayers as well as a ceramic coating. Incorporation of Steps 1 through 4 into a single piece of equipment allows diversification for a variety of potential applications without breaking system vacuum. A specific quality control step has not been implemented in this model.

In the cost analysis, the unit operations which are separated out for final cost analysis include only Steps 2, 3 and 4. Step 1, while included in processing, is not isolated as a processing step because it is highly incorporated into the deposition steps. The cost analysis includes the materials, energy, labor, and equipment costs for manufacture of the coated substrate. Cost is not included for cutting, installation or maintenance of the coated substrate. Waste disposal of replaced canopies or reflector materials is not included in this analysis. Cost savings from longer use over the product lifetime are also not included in the cost model analysis.

Each of the three deposition unit operations discussed above are broken down into the cost elements described below- either as variable or as fixed costs. The sum of these costs for a given unit operation provides an estimate of the total cost for a given unit operation. Breakdown and representation of the costs in this way allows developers to understand where the greatest cost burdens lies in each unit operation.

3.4.1.1 Variable Costs

Variable costs are the contributions to the manufacturing product cost, which are independent of the quantity of materials coated. The variable costs appropriate for this deposition process are: cost of materials, cost of direct labor, cost of energy.

Cost of Materials Material costs account for the transaction price of the substrate and each coating for each unit operation. Coating thicknesses and product rejection rates also affect the materials costs.

Cost of Direct Labor The cost of direct labor is a function of the wages paid, the time required for each operation, the number of laborers associated with the operation, and the productivity of this labor. Labor wages include the cost of benefits to the laborer. The costs for supervisors, janitors and support staff in general are accounted for separately in overhead labor costs.

Cost of Energy The major energy consumed for this process is generated from electric power. The total energy consumed in each unit operation is calculated from equip-

ment power requirements and anticipated power requirements for deposition equipment.

3.4.1.2 Fixed Costs

In contrast to variable costs, fixed costs are those which are dependent on the quantity of product fabricated. Each of these costs are divided equally among the number of part or square feet produced. As the production volume increases, the cost per piece attributed from fixed cost elements decreases, although the fixed cost itself remains constant. The fixed costs for this deposition manufacturing scheme include: equipment purchase and amortization, auxiliary equipment costs, equipment installation costs, maintenance of equipment, fixed overhead labor and building cost.

Equipment Cost Equipment cost refers to the cost of the capital equipment for each unit operation. For the rollcoating equipment, the cost is estimated via price quotes for various coating equipment dimensions, and is dependent on the anticipated deposition rate. The equipment investment is maintained as low as possible without underestimating the expected cost. To consistently distribute the equipment costs over the annual production volume, the total investment is amortized over a fixed period of years using an appropriate interest rate. The annual cost is then divided by the production volume to obtain the cost per unit.

In estimating the total investment, the fraction of utilization or "dedication" of the equipment must be considered to accurately attribute costs to a given product line. For the cost analysis in these deposition system, the deposition equipment is assumed to be fully dedicated to each product.

Auxiliary Equipment Cost The procedure for estimating the auxiliary equipment cost assumes that the ratio of the auxiliary equipment cost to the capital equipment cost is a constant. Because this assumption has been verified for other modeled systems in the MIT Materials Systems Lab, it is used for the equipment in this deposition system, because there are no other means for validation for projected new technologies.

Installation Cost The installation cost refers to the initial cost of installing the primary and auxiliary equipment. It is typically a percentage of the primary and auxiliary equipment costs and is amortized in the same way as for the equipment costs.

Fixed Overhead Labor Cost Overhead labor costs differ from direct labor costs as noted previously, since they are not directly associated with the manufacturing process, but are required nonetheless. This labor cost includes salaries for supervisors, managers, building maintenance and support staff etc.

Maintenance Cost Since maintenance is often unscheduled and is done in response to situations as they develop, an accurate estimation of the cost of maintaining capital equipment would require a prediction or forecasting of these problems. Subsequently, maintenance costs are treated as a fraction of the capital equipment cost as a reasonable estimate.

Amortization This is the interest portion the annual payment on the primary and auxiliary equipment and installation. The annual payments are calculated as an annuity, using an appropriate interest rate and time period.

Building Cost The cost of the building space is estimated by the amount of space required and its price per square foot. This contribution is not included in this cost analysis.

This summarizes the various cost elements of fixed and variable costs involved in the complete estimation of deposition cost per unit of product. To estimate these cost elements, the manufacturing process and production parameters must be specified. In particular, the annual production volume, the deposition rate and the coating thickness are all important for determining the number of lines of equipment that must operated to achieve the required production. The specific information utilized in this cost analysis is further clarified below.

A technical cost model spreadsheet was developed using Lotus 1-2-3 software and is shown schematically in Table 5. The model is set up in such a way that a user should be able understand how to generate manufacturing cost results. The spreadsheet cells that require input information are highlighted in the spreadsheet, and are located in the input data section and exogenous cost factor section. The input area of the cost model contains a host of input parameters for each unit operation which must be provided for accurate cost determinants. The cost calculation sections for each unit operation are programmed to reflect the various input specifications. The cost summary section provides a breakdown of production cost by factor and unit operation.

3.4.1.3 Input Data

The technical information necessary for calculation is entered by the user in this region of the spreadsheet. These include materials, process and labor parameters, cycle times and equipment costs for each process step.

Table 5. General Spreadsheet Layout of Technical Cost Model.

Input Data	Exogenous Cost Factors	Deposition Unit Steps Cost Calculations	Cost Summary
Product Geometry	Plant Operations	Variable Costs:	Variable Costs:
Equipment Parameters	Materials Prices	Materials	Materials
Processing Cycle Times	Wage Rates	Labor	Labor
Materials Parameters	Energy Prices	Energy	Energy
IBAD Processing Parameters		Fixed Costs:	Fixed Costs:
Technical Specifications		Equipment	Equipment
		Auxiliary Equipment	Auxiliary Equipment
		Installation	Installation
		Maintenance	Maintenance
		Fixed Overhead	Fixed Overhead
		Amortization Costs	Amortization Costs
			Process Based Cost Breakdown

The first information that a user must enter includes component or product specifications, such as substrate area, coating thickness and deposition and substrate materials. There are various choices available for substrate and deposition materials. After the substrate or deposition reference numbers are selected and input, the material price, atomic weight, and specific gravity automatically appear.

3.4.1.4 Equipment Assumptions

The deposition equipment costs must be specified, depending on the substrate dimensions and the choice of a roll or batch coating process. The deposition equipment for high volume manufacture has not actually been built to accommodate high volume manufacturing, but potential equipment designs have been explored for technical and economic viability. The equipment follows the design of a standard evaporation roll coater, where a large cylindrical roll of substrate (the web) is

threaded through a series of rollers. The web travels through the rollers to expose an area of the substrate to metal or ceramic evaporant at a rate (web speed) which allows the required coating thickness to accumulate.
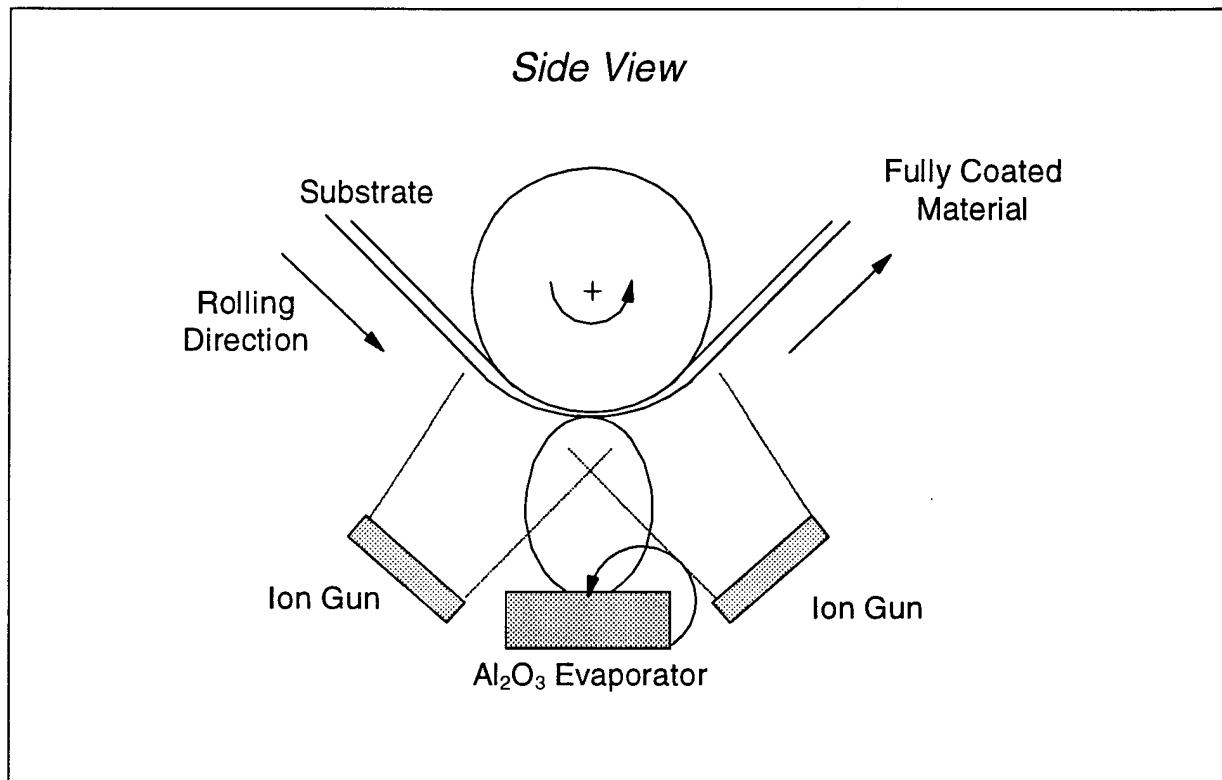

Figure 15. Schematic Sideview of Roll Coating System - Region with IBAD Configuration.

The process is much the same for a batch coating system set up to coat a large substrate by moving the substrate through a deposition zone. Such is the case, for instance, with the canopy application considered in this work. Most of the equipment factors for the batch coating of a canopy structure have almost direct analogs to the roll coating equipment necessary for solar reflectors or decorative building products.

The important process parameter which controls and limits the web speed is the deposition rate for the various coatings. The aluminum oxide coating requires enhancement via IBAD processing which includes the addition of the oxygen ion sources acting in concert with the evaporators to achieve adequate coating properties. Without improved oxygen ion sources, the aluminum oxide deposition rate would remain too low for high volume production . The development by SAIC of improved ion sources, if implemented, would increase production rates and throughputs. These

modifications to standard roll coater equipment costs are included in the input to the cost model.

Sideview and topview schematic diagrams for the roll coater process IBAD equipment are shown in Figure 13 and Figure 14, respectively. The sideview shows a detail of the roll coating equipment in the region of IBAD processing as the web passes through a 20 cm deposition zone, lying along the direction of web travel. The web travels past the evaporator and two ion-assist sources to complete the aluminum oxide deposition process. To accommodate homogeneous coating thickness across the web width (fixed at 1.067 meters (3.5 ft) in this configuration), a bank of nine evaporators with a bank of nine ion-assist sources is evenly spaced along the web width. Figure 14 additionally shows the initial bank of nine ion sources used to bombard the web to clean and prepare the surface prior to deposition. This processing configuration for the IBAD equipment is used throughout this study to generate the various cost results.
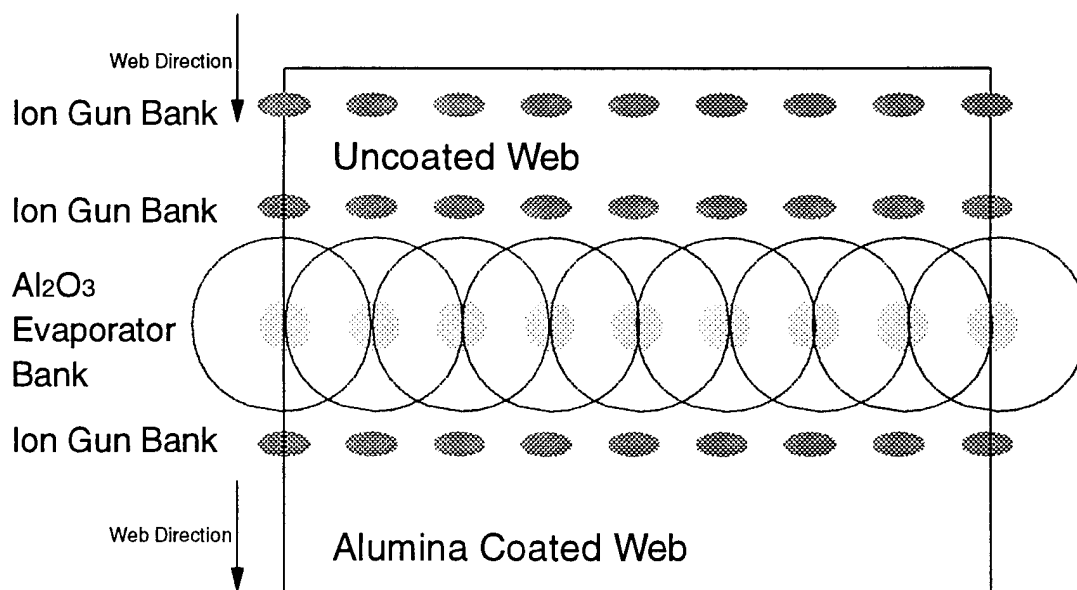

Figure 16. Schematic Topview of Roll Coating System – Region with IBAD Configuration

For Single Stage Deposition:	Quantity	Cost/Unit	Equipment Cost
Evaporator/Controller	9	$25,000	$225,000
Deposition Arc Cathode Ion Source/Controller	18	$30,000	$540,000
Bombard Arc Cathode Ion Source/Controller	9	$30,000	$270,000
Deposition Chamber	1	$50,000	$50,000
Instrumentation	1	$100,000	$100,000
Water Cooling	1	$50,000	$50,000
Cold Trap Diffusion Vacuum Pumps	6	$64,000	$384,000
Roots Roughing Pump	1	$40,300	$40,300
TOTAL			$1,659,300
For Double Stage Deposition:	Quantity	Cost/Unit	Equipment Cost
Evaporator/Controller	9	$25,000	$225,000
Deposition Arc Cathode Ion Source/Controller	18	$30,000	$540,000
Bombard Arc Cathode Ion Source/Controller	9	$30,000	$270,000
Additional Deposition Chamber Size	1	$50,000	$50,000
TOTAL			$1,085,000
TOTAL FOR BOTH STAGES USED:			$2,744,300

Table 6. Canopy Processing Equipment - Breakdown of Parts with Estimated Price List.

In addition to this configuration, a two-stage deposition system was investigated to determine the trade-offs of increased capital equipment cost versus shorter processing throughput time. The decrease in deposition cycle time may offset the increased initial investment. The equipment cost assumptions are shown in Table 6 for single and double stage deposition systems. For solar reflector materials, additional metallization equipment costs are added to this list to generate capital equipment costs for that deposition system. Similar costs might need to be added in the case of canopies if special purpose coatings were to be integrated into the IBAD process to meet multifunction performance requirements.

3.4.1.5 Processing Cycle Time Parameters

The next input area in the spreadsheet addresses the total amount of time for batch processing deposition of the substrate. There are four general phases required

to complete one batch of coated material. These include pre-coating, deposition, after-coating and re-charging. Each of these times are input to determine the total cycle time. The pre-coating period requires time for a number of start-up activities which include time to evacuate the pressure chamber, cool the coating drum, accelerate the web to processing speed, and begin deposition. The actual time for deposition is calculated using other parameter specified by the user of the model, or it can be over-ridden with another input. After deposition has finished, the evaporants are deactivated, the winding mechanisms are stopped, the coating drum is reheated to ambient temperature and the chamber is vented to atmosphere. During the re-charging period, the chamber is opened and the coated roll is removed. The chamber is cleaned and checked during routine maintenance before a new roll is loaded, and finally the chamber is closed. The total time between the end of deposition processing and the restart of deposition is input in the model as approximately one hour. This is only a small fraction of the time required for deposition, which depends on the length of the roll, the input deposition rate and the coating thickness.

3.4.1.6 Materials Parameters

The materials required for the desired layered structure are initially specified by the user. For the aircraft canopy application, only the aluminum oxide coating material is needed with an assumed commodity price of about $50 per pound. For the solar reflector application, copper (at $2.50 per pound) and silver (at $200 per pound) metallic layers are specified in addition to the aluminum oxide. The total materials costs are calculated according to the thickness and density of each coating, as well as the specified production volume, including a percentage of scrap.

The other materials utilized for this process include various gases . The ion sources require argon gas at $2.62 per cubic meter for the bombardment during surface, and the ion-assist sources require oxygen at $1.38 per cubic meter. The volume of gas used during processing, and hence the cost, is calculated depending on the specified gas flow rate and on the specified annual production volume. The recirculating water and other incidental materials, e.g., pump oil, have not been included, and are considered incidental to changes in the manufacturing cost.

The substrate materials cost for the polycarbonate canopy is not included in this analysis, and therefore the cost of reworking, scrapping or destroying the high value canopy substrate through IBAD processing is not accounted for. The cost

analysis is meant only to suggest the additional coat of the coating. In the case of the solar reflector materials, the PET substrate cost, although minimal at $0.03 per square foot, is included in the manufacturing cost.

The variable and calculated operating parameters for the evaporators and ion sources used for deposition processing are displayed in Table 7. The IBAD deposition rate can be changed here to explore its impact on product cost. The variable input parameters, shown in bold, are used to calculate the total ion current and total ion power at the film surface, as well as to determine the total actual power used by each ion gun. These calculated values are shown in the table below for the variable input and the equipment design shown in Figure 13 and Figure 14, using a single stage deposition operation. The only operating parameter required for the evaporator is its transfer efficiency, which is a measure of the percentage of material that is transferred from the evaporator melt to the substrate surface. The 25% transfer efficiency implies that 75% of the evaporant material is ineffectively deposited elsewhere in the chamber. The transfer efficiency is included as an input variable, although a value could be calculated. The power requirements for the equipment must also be specified in the model to allow calculation of total energy requirements for the deposition process.

The labor required for operation of each line of deposition equipment is set in this model at two hourly workers, each spending 50% of their time on line during the processing cycle. The manpower could be reduced if it is possible to utilize one worker to monitor more than one line of equipment during the lengthy deposition period, but this is not assumed in this analysis.

IBAD Process Parameter	Value	Units
IBAD Deposition Rate of Al_2O_3	60	nm/s
Ion Energy Flux at Film Surface	60	eV / atom in film
Ion Energy at Film Surface	500	eV / ion
Ion Acceleration Voltage Energy	500	Volts
Ion Gun Exposure Factor	1.4	(dimensionless)
Density of Film	70%	of theoretical
Expected Density of Film	2.73	g/cm^3
Molecular Weight of Coating	102	g/mole
Number Atoms/ unit time - unit area	4.834×10^{-17}	$atoms/s\text{-}cm^2$
Ion Current Density at Substrate	9.281×10^{-3}	$Amps/cm^2$
Total Required Ion Current	42.25	Amps
Total Required Ion Power (at surfaces)	21,124.06	Watts
Ion Source Electrical Efficiency	20%	
Arc Cathode Beam Current/Gun	2.35	Amps
Arc Cathode Source Current/Gun	9.39	Amps
Total Power Used by Each Ion Gun	5867.8	Watts
Ion Cathode Energy Used per Bomb Gun	3.26	kWhr/Bomb Gun
Ion Cathode Energy Used per Depo Gun	3.26	kWhr/Depo Gun
Evaporator Transfer Efficiency	25%	

Table 7. IBAD Processing Parameters for One-Stage Deposition with Equipment.

Exogenous cost factors used in the IBAD deposition processing model are displayed in Table 8. All manufacturing cost estimates are based on a standard working period of 260 days, with two shifts of eight hours each. It is assumed that the loan for equipment costs is amortized at 15% over a period of five years. Installation costs are assumed to be 15% of the total equipment investment, and maintenance costs are as-

sumed as 5% of the total equipment investment. The wage rate is set at $35 per hour and the price of electric power is assumed to be $0.10 per kilowatt-hour. The fixed overhead is assumed at 35% of the total investment (including maintenance costs) per year. Each of these input factors can be changed by the user.

Input	Value	Units or Base
Operating Days Per Year	260	days/year
Shifts per Day	2	shifts/day
Hours per Shift	8	hr/shift
Capital Recovery Rate	15%	per year
Capital Recovery Period	5	years
Direct Labor Wage	$35.00	per hour
Electricity Price	$0.10	per kilowatt-hour
Unscheduled Downtime	0%	
Variable Overhead Cost	0%	
Auxiliary Equipment Cost	5%	of Capital Equipment
Installation Cost of All Equipment	15%	of Capital & Auxiliary
Maintenance Cost	5%	of Capital & Auxiliary
Fixed Overhead Cost	35%	of Fixed Cost

Table 8. Exogenous Cost Factor Inputs Used in the IBAD Deposition Processing Model.

3.4.2 Batch Coating Modeling Projection: IBAD Processing of Canopies

The total cost associated with IBAD deposition is composed of material, capital, labor and energy costs. The factor based cost components were calculated for a one stage deposition process, assuming a production volume of 2674 coated canopies each with an assumed area of 9.75 m^2, with a Al$_2$O$_3$ ceramic coating thickness of 4 µm, at a deposition rate of 60 nm/sec. Again, the equipment design used in the model is based on roll coating applications, and is used as a first estimate of the manufacturing costs. Under these assumptions and using one line of equipment at full capacity with no downtime and no scraped substrates, the total cost for coating each canopy is $468 ($48/m^2 or $4.45/ft^2).
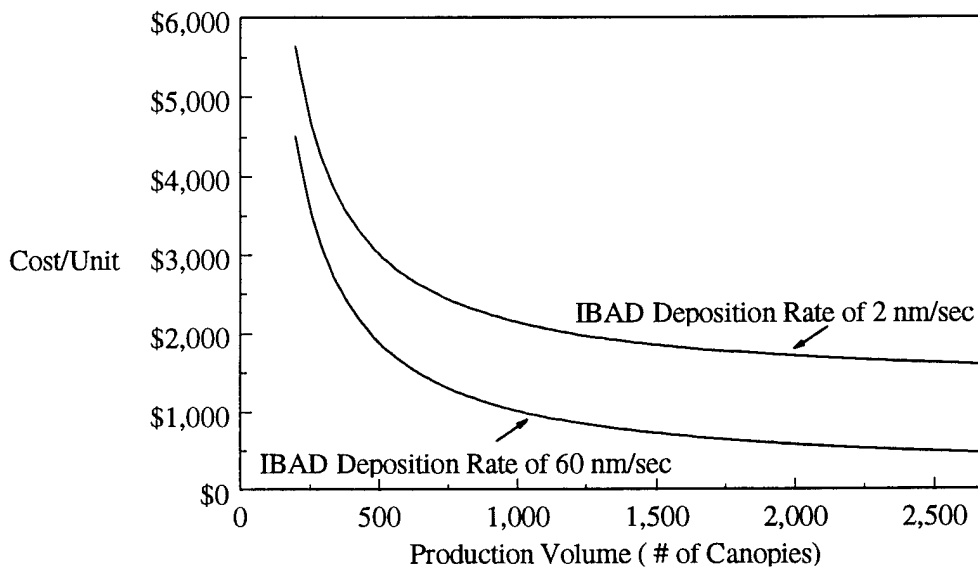
Figure 17. Economies of Scale for Coated Canopies at Different Deposition Rates.

The capital cost, which includes primary and auxiliary equipment, installation, maintenance, and fixed overhead, is the major contributor to the coated substrate costs, accounting for almost 70% of the total cost at maximum production volume. Since this process is so highly capital intensive, high utilization of the deposition line is essential to reduce cost per coated unit area. At an equipment utilization of 50%, producing 1337 canopies, the fixed cost accounts for 82% of the manufacturing cost. Larger production volumes achieve higher economies of scale by spreading the fixed costs over more manufactured goods. As the production volume increases, capital equipment costs per unit drop, and consequently the total cost for coating each canopy decreases as shown in Figure 15. The increase in costs for a slower IBAD deposition rate is also shown.

For the assumptions given, the cost of labor is substantial, accounting for 23.3% of the total cost, because essentially one technician is using all available work time to produce coatings and monitor the equipment. A fraction of that labor time would be required if automated equipment can be used to monitor the deposition process. The energy costs reflect the electric power used for the ion sources. At 5.9%, this contribution is not unexpected. The material cost for this deposition process is very low (1%) due to the small volumes of gases and minimal coating thickness, and it does not include the substrate cost.
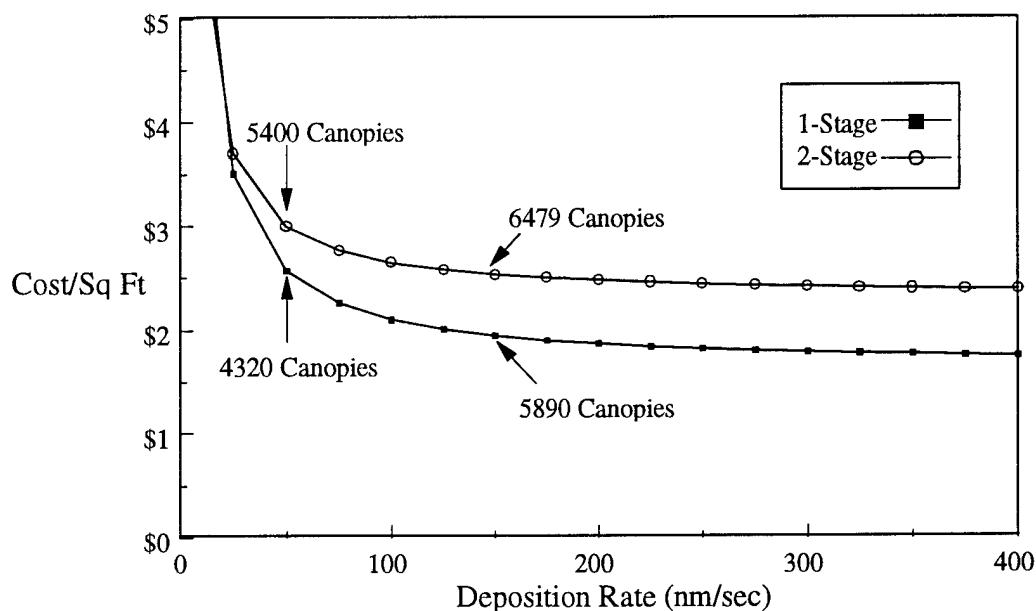
Figure 18. Effect of Equipment Design on Manufacturing Cost.

In addition to understanding the cost contributions for a specific set of processing conditions, other processing variables can be systematically changed while holding the other parameters constant to explore their effect on manufacturing costs. The IBAD deposition rate is a major contributor to costs, because slow deposition rates or cycles times give lower rates of throughput. In order to realize the equipment design factors affecting throughput, the single stage and double stage deposition designs are compared as a function of deposition rate in Figure 16.

As expected both curves show a decrease in cost per unit area with increasing deposition rates. These results assume a 4μm coating on polycarbonate canopies with area 9.75 m^2 (105 ft^2) using one line of equipment at maximum capacity with no downtime, and 100% yield. As the deposition rate increases, the production volume is not constant along each curve. The maximum number of coated canopies is given for deposition rates of 50 and 150 nm/s. As the cycle time increases, more substrates can be coated, which decreases the fixed costs per canopy by spreading them over the higher output. Comparison of single stage and double stage equipment curves shows that the double stage remains at a greater cost/ft^2 for the entire deposition range, although at very low deposition rates the double stage equipment is less expensive than

the single stage. This cross over occurs at about 20 nm/s. At 50 nm/s, the cost differential is about \$0.50/ft^2 due to increased capital costs of the two-stage equipment, but the production capacity of the two stage equipment is higher.
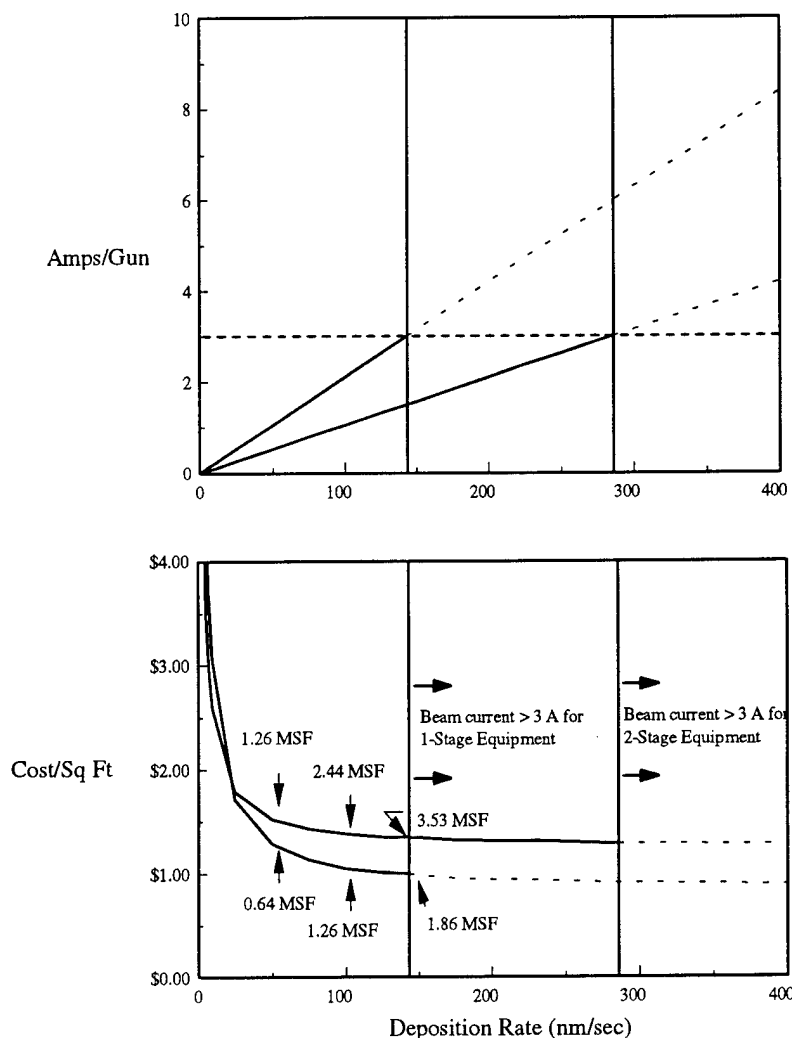

Figure 19. Current per Ion Gun and Cost per Area as a Function of Deposition Rate.

The deposition rate range explored in Figure 16 extends from currently achievable rates (below 10 nm/s) to rates that are beyond the capability of the new cathode technology. In Figure 17, the feasible regions of IBAD deposition rates for single and double stage equipment are shown graphically from ion gun current limitations. The upper portion of this graph indicates the increase in ion gun current with deposition rate for one and two stage equipment. Each cathode is limited to a current below 3 Amps, hence deposition rates where the current becomes greater than 3 Amps are

unachievable, as indicated by the dotted lines. The lower portion of Figure 19 is a reiteration of Figure 18 with the regions of feasible deposition rates indicated by solid curves. For deposition rates using single stage equipment, coating is infeasible above 143 nm/s and for double stage equipment, coating becomes infeasible above 286.3 nm/s.

A comparison of the economies of scale are shown for various deposition rates in Figure 20. Again, these results assume a 4μm coating on polycarbonate canopies with area 9.75 m^2 (105 ft^2) using one line of equipment at maximum capacity with no downtime, and 100% yield. For each of the four deposition rates 2, 6, 60 and 100 nm/sec, the two-stage equipment incurs a higher manufacturing cost for a given production volume. The maximum annual production capacities for the one-stage equipment are shown in the graph in MSF, and translate to 236, 634, 2674 and 3120 total canopies for deposition rates of 2, 6, 60 and 100 nm/sec, respectively.
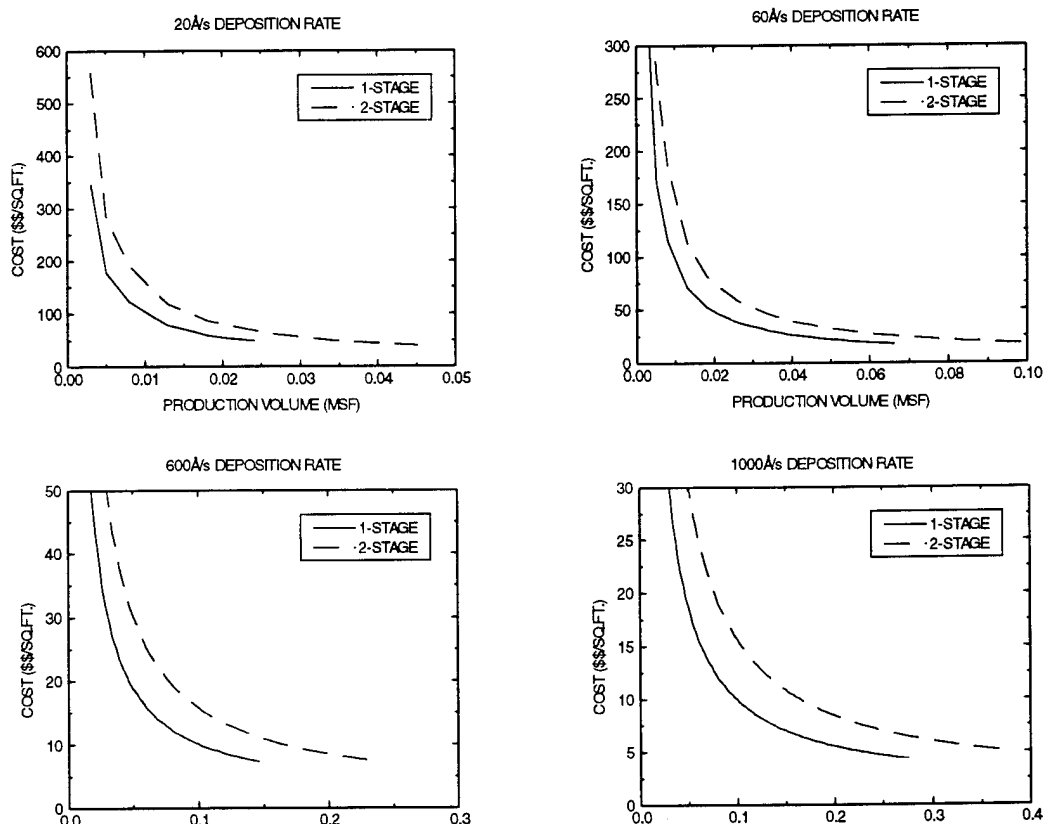

Figure 20. Economies of scale vs. deposition rate for canopies.

3.4.3 Economic Analysis for Coated Solar Reflector Materials

The same technical cost model is used to simulate the deposition costs for manufacturing solar reflector films which generally require a larger area product than the canopy. For this analysis, a web width of 1.07 meters (3.5 ft) is maintained, with a web length of about 730 m (2400 ft). With all other parameters and assumptions unaltered, this change has a major effect on the cycle time per batch. The simulation at this point does not include the metallic evaporant coating as part of the manufacturing cost.

Recall in Figure 19, the feasible regions of IBAD deposition rates for 1- and 2-stage equipment shown graphically from ion gun current limitations with the unachievable deposition rates shown by dotted lines. The two stage curve remains at a greater cost per area for the most of the deposition range, but at deposition rates less than 25 nm/sec, two stage is less expensive. This implies that the two stage equipment could be cost effective for higher production volumes for a critical substrate roll length at a given deposition rate. This occurs because the percentage of cycle time dedicated to actual coating is increased, rather than breaking chamber vacuum and recharging. Under single stage conditions, 5.9×10^4 m^2 (0.64 MSF) of coated material can be produced for less than \$13.75/m^2 (\$1.28/ft^2), if deposition rates of 50 nm/sec can be achieved.

As the deposition rate and concurrently the production volume increase, the cross over point becomes apparent in Figure 21. These results assume a 4-µm coating on a PET substrate with area 780 m^2 (8400 ft^2) using one line of equipment at maximum capacity with no downtime, and 100% yield. For three of the deposition rates 2, 6, and 60 nm/sec, the two-stage equipment incurs a higher manufacturing cost for a given production volume. However for the 100 nm/sec rate, two stage equipment becomes more cost effective. The maximum annual production capacities for the one-stage equipment in the graph although substantial in MSF, are rather limited in the number of webs processed. For the single stage deposition rates of 2, 6, 60 and 100 nm/sec, the number of webs coated is 3, 9, 91 and 150, respectively. If the number of shifts is increased to allow 24 hour production, the production volumes and the equipment utilization would increase, and the cost per unit area in turn would drop.

A modified version of this technical cost model is used to simulate the deposition costs for manufacturing solar reflector films with metallic layers as well as the

protective alumina coating, as shown in Figure 22. This configuration is represented in text form as Al2O3/Ag/Cu/ PET. The manufacturing cost per square foot is assessed for this scenario based on varying thicknesses of the aluminum oxide coating, and changes in the IBAD deposition rate. The substrate cost, though minimal is included in these assumptions.
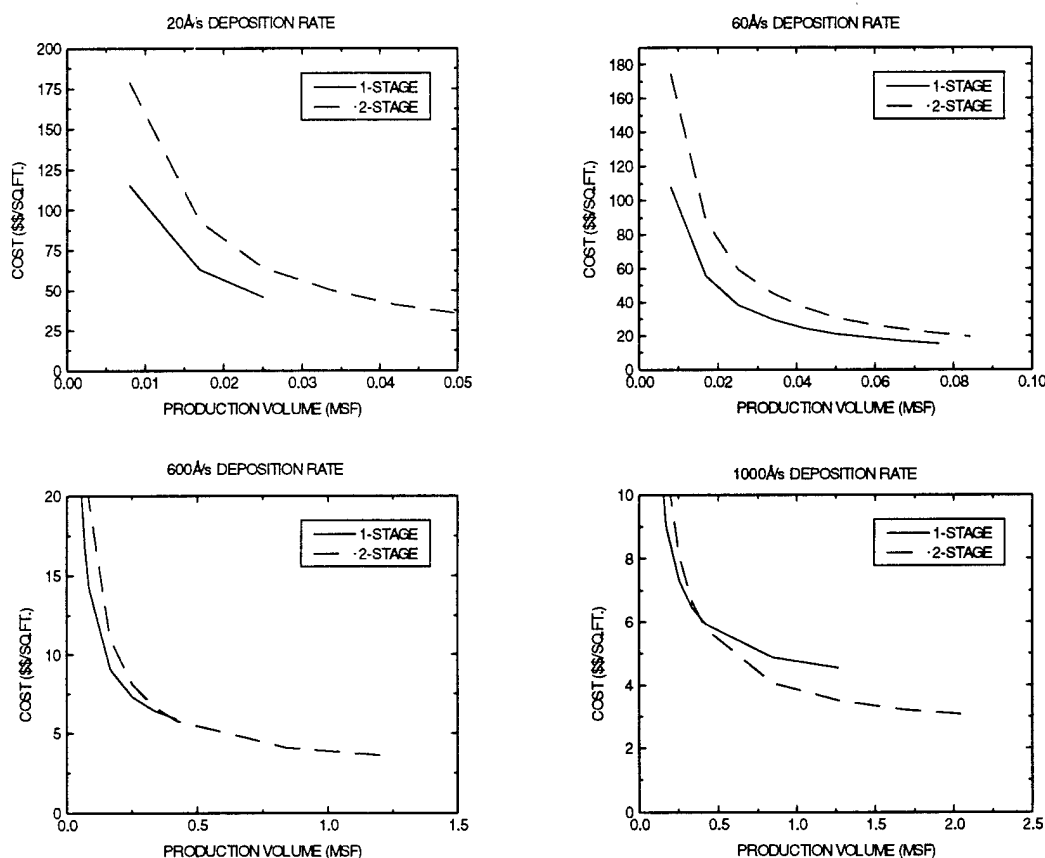

Figure 21. Economies of Scale versus Deposition Rate for Solar Reflectors.

The cost results in Figure 21 are generated for an annual production of approximately 1 MSF (9.3×10^4 m^2) of a solar reflector material, which consists of a PET substrate coated with 40 nm copper layer, then coated with 70 nm silver, followed by the protective alumina of varying thicknesses. One line of equipment is in use with single stage deposition at maximum capacity with no downtime, and 100% yield. As the alumina coating thickness decreases from 5 μm to 1 μm, the cost per unit area decreases as expected since a reduced amount of material is used. As each curve approaches lower deposition rates, it ends abruptly, indicating that further decreases to the deposition rates would require introduction of another line of equipment. At 5 μm

thickness, the rate must exceed 60 nm/sec to maintain a single line, while for a 1 μm coating, rates as low as 20 nm/sec can still accommodate a single line. A second phenomena occurs as each curve approaches lower deposition rates. The capacity utilized decreases with increasing deposition rates, since each curve represents a constant annual production of 9.3×10^4 m^2 (1 MSF). As the deposition rate increases, it requires less time to finish the production cycle, and the equipment lies idle. The cost of $9.60/m^2 ($0.89/ft^2) at a deposition rate of 60 nm/sec for 9.3×10^4 m^2 (1 MSF) of coated material with a 1 μm coating actually reflects the price of underutilization. If the maximum production capacity of the equipment is achieved, the increased production volume of 4.6×10^5 m^2 (5 MSF) reduces the cost to $3.75/m^2 ($0.35/ft^2).
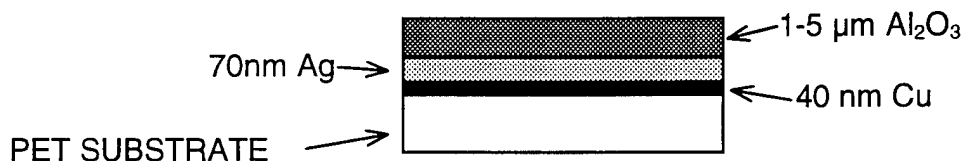

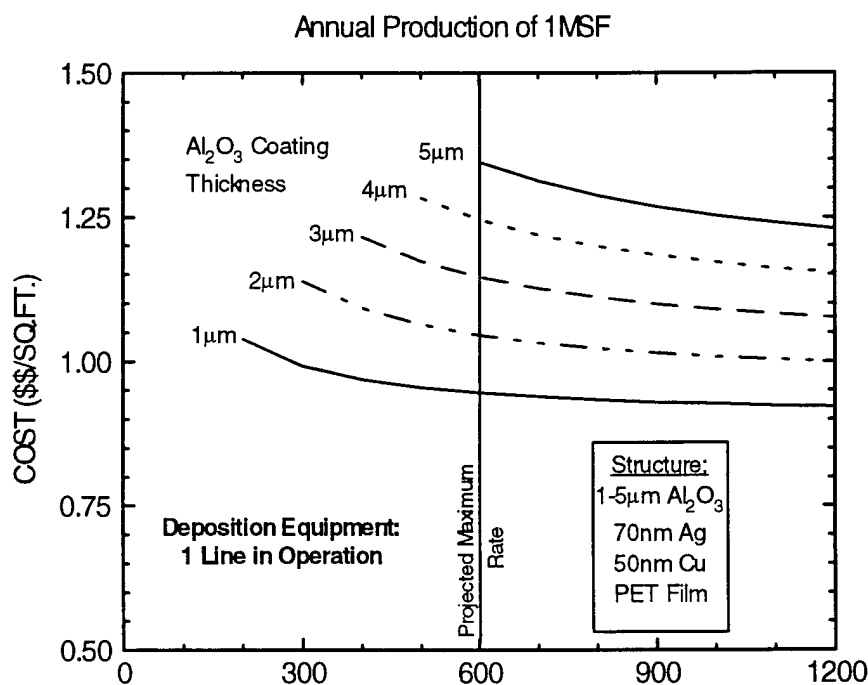*Figure 22. Solar Reflector Film Layer Structure.*

Figure 23. Cost per Area versus Deposition Rate for Solar Reflector Material (1 MSF).

When more than one line of equipment is available, higher production volumes can be achieved for this set of assumptions. The manufacturing cost per unit area now assessed for production volumes of 4.6×10^5 m^2 (5 MSF) based on varying thicknesses of the aluminum oxide coating, and changes in the IBAD deposition rate. One line of equipment is in use with single stage deposition at maximum capacity with no down-time, and 100% yield.

With reduced coating thickness, the manufacturing cost decreases, showing the same trend as found in Figure 23. The curves in Figure 24, however, show disconti-nuities, which increase the cost per unit area in small jumps as the deposition rate de-creases. These jumps in cost indicate that another line of equipment is required and is implemented by the model to achieve the desired production volume. The disconti-nuity shows the difference in cost between 100% utilization at the lower cost side of the jump versus a much lower initial utilization for an additional equipment line at a constant production volume.
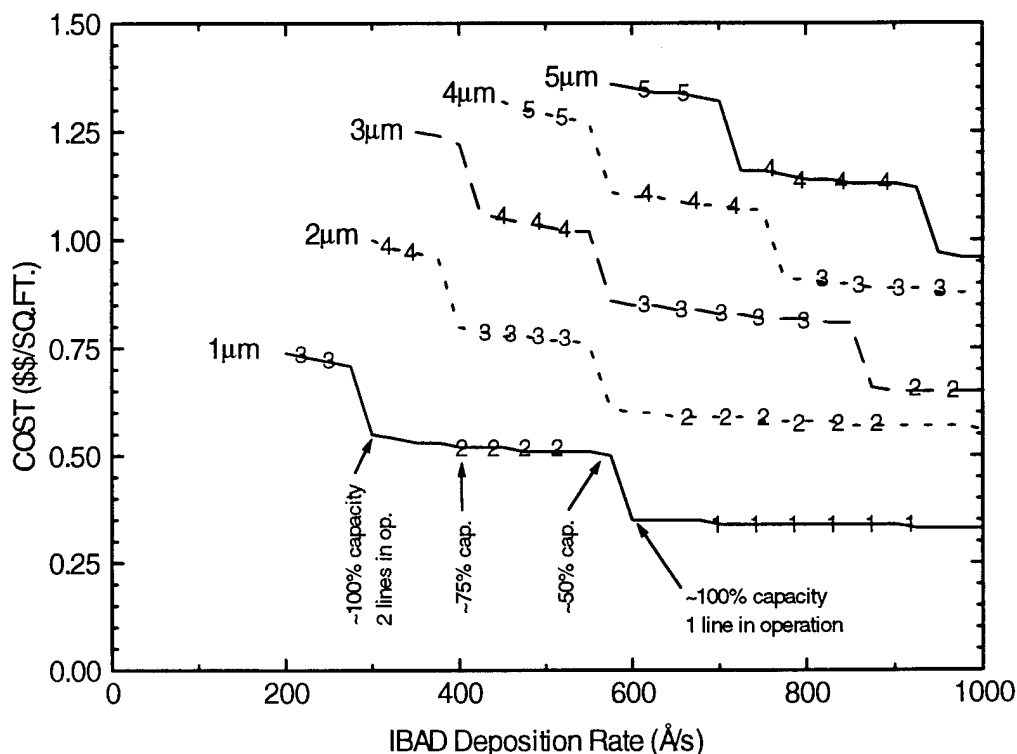

Figure 24. Cost per Area versus Deposition Rate for Solar Reflector Material (5 MSF).

The curve for 1 µm coating thickness requires only one line at high deposition rates (70-100 nm/sec), and at speeds lower than 60 nm/sec a second line is needed. For the 2 µm coating, two lines are necessary at high rates, and a third is needed below 60 nm/sec. The 3 and 4 µm coatings require three lines of equipment at high deposition rates, and the 5 µm coating uses four deposition lines at annual volumes of 4.6×10^5 m^2 (5 MSF).

3.4.4 Summary & Conclusions

A technical cost model has been developed to simulate the manufacturing costs for an IBAD deposition system, implemented with a new cathode technology. The deposition of aluminum oxide ceramic coating is explored for two equipment scenarios under various operating conditions. The important variables which particularly affect the cost of the coated products include the IBAD deposition rate, the thickness of the ceramic coating, and the desired annual production volume. The assumptions behind these cost analyses are meant to reflect expected processing conditions for high volume production scenarios. The ranges of production volumes are suggested from discussions with potential customers for the technology. The coating thicknesses and deposition rates addressed in the cost analysis are under direct investigation on the technical side. The economic information generated here will be used in concert with the scientific results of film properties to indicate the most promising layered configurations, which warrant further consideration for technological development.

Applications for both military and commercial end use are explored, specifically for coated polycarbonate aircraft canopies and ceramic coated solar reflector materials. The main objective in both economic analyses is to identify the processing conditions which minimize the manufacturing costs. The potential manufacturing process is based on adaptation of standard roll coating equipment. This allows calculation of a series of first order cost estimates for both applications under consideration.

A cost breakdown of materials, labor, energy, and capital indicates that based on the given assumptions this process is highly capital and labor intensive. High utilization of the equipment is essential to the economic viability of this technology. Feasible implementation may also require additional automation to reduce the labor costs. Single stage and double stage IBAD deposition equipment schemes show that for canopies, the single stage manufacturing costs are lower at most deposition rates,

while for solar reflector, double stage manufacturing could be economically feasible under certain conditions.

A cost analysis for canopies is presented where each canopy has an assumed area of 9.75 m^2 (105 ft^2), with a Al$_2$O$_3$ ceramic coating thickness of 4 nm, using one line of equipment at full capacity with no downtime, and no scrapped substrates. If the deposition rates are able to achieve 60 nm/sec, the cost to coat each of 500 canopies would be around $2000 per unit. For low deposition rates of 2 nm/sec, the cost rises to about $3000 per canopy. Since high production volumes of canopies are required to achieve lower cost however, this technology while perhaps technically superior, might not prove economically viable for aircraft canopy, due to low fleet demands and the high specificity of other coating requirements for different aircraft canopies. The question remains as to whether investors or government agencies are willing to pay an additional cost to coat aircraft canopies for enhanced performance and lifetime.

A cost analysis for solar reflector layered structures which include metallic interlayers of 40 nm copper and 70 nm silver on a PET substrate is presented for larger web areas of 780 m^2 (8400 ft^2). Using one line of single stage equipment at maximum capacity with no downtime and 100% yield, only the manufacturing cost of the 1 μm ceramic coating thickness falls below the desired $11/m^2 ($1/ft^2) goal at deposition rates greater than 60 nm/sec. At higher annual production volumes of 4.6×10^5 m^2 (5 MSF), the cost of 1 μm coated materials is reduced to $3.75/m^2 ($0.35/ft^2) for rates greater than 60 nm/sec. If the 1 μm and 2 μm coated reflector materials prove technically superior than its competition, the economic analysis indicates significant incentive for investment in the development of high volume production.

4. Summary of Conclusions and Recommendations

The IBAD alumina deposition process that was the focus of this project was successfully used to coat a variety of substrate materials and configurations. The IBAD coatings were demonstrated to be abrasion resistant, resistant to chemical attack, highly transparent, and well adhered to most every substrate that was attempted in the course of our two year effort. Unfortunately, the combination of requirements for impact resistance, rain erosion resistance, *and* abrasion resistance was found to be beyond the capabilities of the simple system of the IBAD alumina coating applied directly on polycarbonate. While the strain-to-failure ratio of the IBAD alumina coating at 0.5% is large, it was insufficient to prevent cracking under the large flexures of the relatively soft polycarbonate substrate. This issue of a hard coating on a too-soft substrate was exacerbated for the case of the IBAD alumina on the even softer fluoroelastomeric coating on an F-16 radome.

The IBAD alumina coating does present an opportunity for increasing the abrasion resistance of already moderately hard substrates, and this presents a possible solution path to the application of the IBAD alumina process on softer material substrates. When applied to the glass used for standard microscope slides, the IBAD alumina coating increased the surface hardness significantly — in some cases to within half that of single crystal sapphire. It was also noted that the critical load to failure for the on-glass samples was ten to fifteen times higher than that for the on-polycarbonate samples. This suggests the possible application of the IBAD alumina coatings to improving the abrasion performance of already tough substrates, such as glass windshield for automobiles. Moreover, it suggests that the application of the IBAD alumina coatings to softer substrate materials might be better achieved by gradually building up the hardness of the substrate in a vertically integrated, multi-layer "stack."

The necessary data for the scale up of the ion source performance was finally achieved in late 1995. Discovery during the coupon preparation and testing work had made some elements of the ion source development unnecessary: the maximum deposition rate target shifted from 3000 Å/s to 600 Å/s. The necessary ion assist energy to achieve good coating performance was noted to span the range of ~10-100 eV/atom depending on the substrate material, which also gave some lattitude to the ion source development effort. The ion source capability that is now latently avail-

able as a result of this project represents a several order of magnitude increase in the state of the art for oxygen plasma sources and oxygen ion sources. We are already engaged in other projects that may see the widespread use of oxygen plasma sources by themselves as efficient, effective cleaning agents with minimal environmental side effects.

The IBAD alumina coating technology has not successfully transitioned to a DOD project during the course of this effort. The technology has, however, found strong success in its application to the wear protection of solar reflectors for NREL and the DOE. The cost modelling efforts by SAIC and MIT, and accelerated lifetime measurements by NREL indicate that IBAD alumina treated solar reflector materials may be a solar power "Holy Grail": an effective solar reflector with greater than 30-year field life and a per-unit cost of less than $1/ft^2$. The development efforts planned by NREL should at the least ensure the continued development and maturation of this technology for future use by the DOD.

1. C. M. Northeim and E. J. Darden (compilers), *Proceedings: Pollution Prevention Conference on Low- and No-VOC Coating Technologies,* US Environmental Protection Agency, Office of Research and Development, EPA-600/R-94-022 (February 1994).

2. J. M. E. Harper, *et al.,*"Modification of thin film properties by ion bombardment during deposition," in *Ion Bombardment Modification of Surfaces: Fundamentals and Applications* (Elsevier, 1984).

3. F. A. Smidt, "Use of ion beam assisted deposition to modify the microstructure and properties of thin films," *International Materials Reviews,* **35,** 61 (1990).

4. U. J. Gibson, "Ion-beam processing of optical thin films," *Phys. Thin Films,* **13,** 109 (1987).

5. B. A. Movchan and A. V. Demchishin, "Study of the structure and properties of thick vacuum condensates of nickel, titanium, tungsten, aluminum oxide and zirconium dioxide," *Fiz. Metal Metalloved.,* **28,** 653 (1969).

6. I. L. Singer and L. E. Seitzman, "Tribological characterization of durable, environmentally friendly coatings," Final Report ARPA Order A680 (August 1995).

7. S. Schiller, M. Neumann, H. Morgner, N. Schiller, *38th Technical Conference of the Society of Vacuum Coaters* (April 1995).

8. C. K. Hwangbo, L. J. Lingg, J. P. Lehan, H. A. MacLeod, and F. Suits, "Reactive ion assisted deposition of aluminum oxynitride thin films," *Appl. Optics,* **28,** 2779 (1989).

9. M. Czarnaski, "The Characterization of the Denton CC-102R Ion Source/EFE Retrofit Experiments," Final Report, SAIC Project Number 01-0623-03-4486-003 (April 21, 1995).

10. M. R. Shubaly, R. G. Maggs, and A. E. Weeden, "A High Current Oxygen Ion Source," *IEEE Trans. Nucl. Sci.,* **NS-32,** 1751 (1985).

Attachment B

"Cost and Performance Analysis of Reducing DoD Hazardous Wastes Through Advanced Coating"

Cost and Performance Benefit Analysis of Reducing DoD Hazardous Wastes Through Advanced Coating

Subcontract

for

Science Applications International Corporation

for

ARPA Contract Number MDA972-93-C-0022

Reduction of Hazardous Waste through Advanced Coating Technology

Massachusetts Institute of Technology

Materials Systems Laboratory

Final Report

September 22, 1995

Table of Sections

List of Tables

List of Figures

Introduction

The potential exists to reduce the volume and toxicity of wastes generated by the DoD and the government at large through the use of advanced coatings. These coatings are more wear resistant, more easily cleaned and maintained, and hence less environmentally threatening than processes currently in use. One coating process under consideration, IBAD, is extremely energy efficient and has been shown to be capable of depositing a wide variety of thin-film materials on a wide variety of substrates.

A combined team proposal was accepted by ARPA from SAIC to demonstrate the viability of aluminum oxide films and the deposition process for large-scale applications to systems of DoD interest. The proof-of-concept demonstration for this work has been adapted from the application of a wear resistant, antistatic coating on the substrate of the F-16 aircraft radome, to that of a wear resistant optically clear coating on polycarbonate aircraft canopy substrates. In addition, commercial applications have been investigated, which show high potential for use in optically clear protective coatings for solar reflector materials.

The original intent of the proposed work at MIT was to study the economic and environmental issues associated with the manufacture, use and disposal of fluoro-elastomer coatings used to protect the F-16 radome. The focus of this task has been changed to modeling the economic and technical factors which affect the production of ceramic coated products for systems in an environmentally beneficial manner.

This project encompasses the economic modeling of various deposition systems under development by SAIC: coating a) polycarbonate aircraft canopies, which would reduce landfill volumes in the future, and b) solar reflector materials, which would enhance the use of renewable energy. Models of materials production technologies have proven to be powerful tools for evaluating alternative materials, processes and manufacturing technologies.

Revised Problem Statement

Investors and venture capitalists need to evaluate the economics of manufacturing before any new technology can be successfully brought to market. In areas of technological change, investors cannot afford to rely on cost estimation techniques which are set up for traditional accounting purposes. Furthermore, these techniques cannot be used effectively to assess cost implications of processing changes or changes in technology.

By understanding all of the costs involved in new and existing coating technologies, technology developers can more readily suggest means for reducing costs other than by simply decreasing materials costs. An understanding of the economic factors can help researchers and system developers optimize manufacturing conditions and work towards testing the performance of coatings and coating systems which seem most economically viable. This intersection of technical performance and economic performance is vital for the successful commercialization of new materials. While environmental compliance and coating performance are important factors in deciding which coating to choose, cost often remains the bottom line.

This report renders an economic analysis of an innovative SAIC coating technology via the construction and use of a process-based cost estimation model. The modeling approach divides the processing steps into unit operations where necessary, and separates the various cost elements for each operation. Data used to construct the model have been obtained through collaboration with other team participants in this program and from industry experts. This model therefore portrays an accurate picture of the expected production scenario, and can be utilized in various ways. Sensitivity analyses are included, which can aid in understanding the prime contributors to coating costs and which may suggest non-obvious approaches to cost reduction.

Process-Based Cost Estimation

Deposition systems for applying advanced coatings can be complex or simple operations, depending on the coating's intended use. Process-based cost models are useful tools for assessing operating and overall product costs of these deposition systems. The cost models are designed to represent manufacturing intricacies by dividing the process into small, manageable steps, or unit operations. In the model, various cost elements can be separated out for each unit operation. The cost model employs clearly defined and verifiable economic and accounting principles, and is based on engineering principles and the physics of the manufacturing process. This section describes the coating scenarios addressed in this project, and the modeling methodology that has been used to construct process-based cost models of these deposition systems. Two potential end uses of the deposition technology have been analyzed: coated polycarbonate aircraft canopies and coated solar reflector materials.

Coated Canopy Systems

The performance requirements of polycarbonate aircraft canopies in military applications are stringent and demanding. The flight conditions to which aircraft canopies are subjected can be severe, and thus may significantly decrease the lifetime of the canopy. By applying a ceramic coating to the polycarbonate canopy material, the useful lifetime of the canopy can be extended. There are, however, cost trade-offs between these two scenarios. While uncoated canopies cost less to manufacture than coated ones, they have a higher probability of a shorter lifespan and hence generate higher volumes of expended materials. The objective of this task is to model the processing conditions for ceramic deposition on the canopies, including the economics thereof, to allow a better understanding the cost trade-offs and thus suggest ways to minimize their manufacturing cost.

Solar Reflector Deposition System

Solar reflector materials are now manufactured commercially as layered structures with polymer film protective coatings. While this configuration is functional, the performance requirements for viable economic implementation of solar power demand longer reflector lifetimes than the polymer coating can now provide. Replacement of the polymer with a ceramic coating would allow longer operation for a given reflector, thereby decreasing the maintenance and overall costs

for solar power. Industry specialists note that it is imperative that the cost of any new reflector materials be less than currently available materials. Further, they suggest that a manufacturing cost below $1 per square foot is necessary for competitive implementation of solar power. The objective in this task is to identify processing conditions and methodologies for which the manufacturing costs meet these requirements.

Deposition Processing

The technological basis for the ceramic coating system under investigation is ion-beam-assisted deposition (IBAD). In this process, evaporators are used to volatilize the deposition material, and additional ion sources are used to assist in the deposition by bombarding the ceramic film as it deposits on the substrate. Utilization of the IBAD technique produces ceramic films with enhanced density and improved index of refraction - a benefit over films produced without the ion-assist. The new development in this IBAD technology is an improved cathode material for the ion sources which significantly increases the deposition rate and overall throughput. In this technical cost model, the processing conditions, deposition rates, and film thicknesses which describe deposition via an IBAD system are varied to determine the trade-offs in economic viability. This investigation is done in concert with technical performance test data for various coated substrates; i.e., the manufacturing costs have been calculated for the most promising of the ceramic coated samples. The ceramic coating which is under investigation for these applications is aluminum oxide, i.e., alumina.

As a first approximation for economic viability, the equipment for the deposition system is postulated as an adaptation of that used for standard metallization in the roll coating industry. Figure 1 shows the generalized process unit steps for coating the substrates under consideration. In Step 1, the substrate surface is cleaned or prepared prior to deposition. Initially, several techniques for preparation were under consideration, including: 1) argon-ion bombardment, 2) oxygen-ion bombardment, 3) wet chemical treatment and 4) plasma radical treatment. After further experimentation and testing of coated samples, it was found that only the argon ion bombardment is required for adequate surface preparation. Other pretreatment techniques will no longer be considered in the cost analysis.
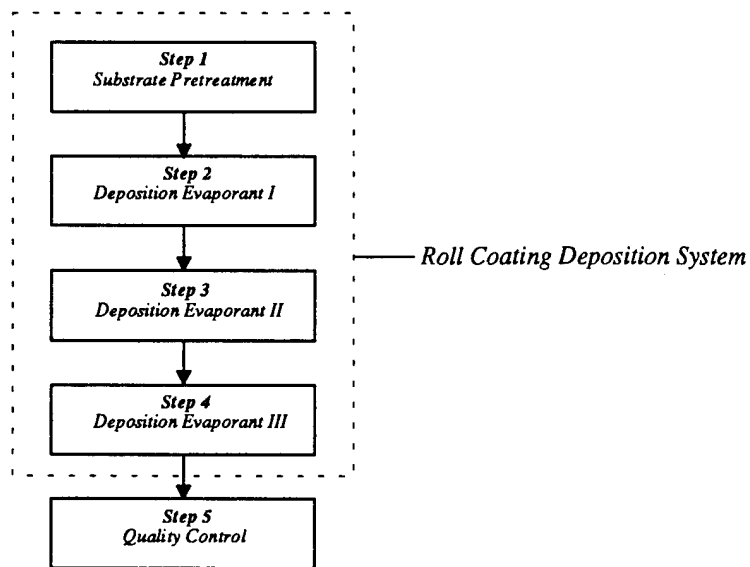
Figure 1: Process Steps for Ceramic Deposition

Steps 2, 3 and 4 represent the actual deposition steps. While some coating applications require only a layer of ceramic material, others require the deposition of metallic interlayers in addition to the ceramic coating. Incorporation of Steps 1 through 4 into a single piece of equipment provides versatility, allowing for a variety of potential applications without breaking system vacuum. Costs related to a specific quality control step have not been implemented in this model.

In the cost model, the unit operations which are separated out for final cost analysis include only Steps 2, 3 and 4. Step 1 is not isolated as a processing step because it is incorporated into the deposition equipment and is therefore included in the deposition processing step. The cost model includes the materials, energy, labor and equipment costs for manufacture of the coated substrate. Costs are not included for cutting, installation or maintenance of the coated substrate. Waste disposal costs of replaced canopies or reflector materials are not included in this analysis. Cost savings from longer product use over its lifetime are also not included. These last three costs may add significantly to the economic benefits of implementation of this technology.

Overview of the Cost Model

Each of the three deposition unit operations discussed above are broken down into the cost elements described below - either as variable or as fixed costs. The sum of these costs for a given unit operation provides an estimate of the total cost attributed to that unit operation. Breakdown and representation of the costs in this manner allows developers to understand where the greatest cost burdens lie in each unit operation.

Variable Costs

Variable costs are the contributions to the manufacturing product cost which are independent of the quantity of materials coated, on a per unit basis. The variable costs appropriate for this deposition process are: a) cost of materials, b) cost of direct labor and c) cost of energy.

Cost of Materials

Material cost represents the transaction price of the substrate and each coating for each unit operation. Coating thickness and product rejection rates also affect the materials cost.

Cost of Direct Labor

The cost of direct labor is a function of the wages paid, the time required for each operation, the quantity of labor associated with the operation, and the productivity of this labor. Labor wages include the cost of benefits to the laborer. The cost of supervisors, janitors and support staff in general are accounted for separately in overhead labor costs.

Cost of Energy

The majority of the energy consumed in this process is obtained from electric power. The total energy consumed in each unit operation is calculated from actual equipment power requirements, when known, and anticipated power requirements for new deposition equipment.

Fixed Costs

In contrast to variable costs, fixed costs are those which are dependent on the quantity of product fabricated, when calculated on a per unit basis. Each of these costs are divided equally among the number of parts or square feet of coated substrate produced. As the production volume increases, the cost per piece attributed to fixed cost elements decreases, although the fixed costs

themselves remain constant. The fixed costs for this deposition process include: equipment purchase and amortization, auxiliary equipment costs, equipment installation costs, maintenance of equipment, fixed overhead labor and building cost.

Equipment Cost

Equipment cost refers to the cost of the capital equipment for each unit operation. For the roll coating equipment, the cost has been estimated via price quotes for various coating equipment dimensions, and this cost is dependent on the anticipated deposition rate. The equipment investment has been maintained as low as possible without underestimating the expected cost. To consistently distribute the equipment costs over the annual production volume, the total investment is amortized over a fixed period of years using an appropriate interest rate. The annual cost is then divided by the production volume to obtain the cost per unit.

In estimating the total investment, the fraction of utilization or "dedication" of the equipment must be considered to accurately attribute costs to a given product line. For the cost analysis of these deposition systems, the deposition equipment is assumed to be fully dedicated to each product.

Auxiliary Equipment Cost

The procedure for estimating the auxiliary equipment cost is to assume the ratio of the auxiliary equipment cost to the capital equipment cost to be a constant. Since this assumption has been verified for other systems modeled by the MIT Materials Systems Lab, it will be used for the equipment in this deposition system because there is no other means of validation for projected new technologies.

Installation Cost

The installation cost refers to the initial cost of installing the primary and auxiliary equipment. It is typically a percentage of the primary and auxiliary equipment costs and is amortized in the same manner as are the equipment costs.

Fixed Overhead Labor Cost

Overhead labor costs differ from direct labor costs as noted previously, since they are not directly associated with the manufacturing process, but are required nonetheless. This labor cost includes salaries for supervisors, managers, building maintenance and support staff, etc.

Maintenance Cost

Since maintenance is often unscheduled and is performed in response to situations as they develop, an accurate estimate of the cost of maintaining capital equipment would require a prediction or forecasting of these problems. Consequently, maintenance costs have been estimated as a fraction of the capital equipment cost.

Amortization

This is the interest portion the annual payment on the primary and auxiliary equipment and installation. The annual payments are calculated as an annuity, using an appropriate interest rate and time period.

Building Cost

The cost of the building space is determined by the amount of floor space required and its price per square foot. This contribution is not included in this cost analysis.

This summarizes the various cost elements of fixed and variable costs involved in the complete estimation of deposition cost per unit of product. To calculate these cost elements, the manufacturing process and production parameters must be specified. In particular, the annual production volume, the deposition rate and the coating thickness are all important variables for determining the number of lines of equipment that must operated to achieve the required production. The specific information utilized in this cost analysis is described below.

The Deposition Cost Model

A technical cost model spreadsheet has been developed using Lotus 1-2-3® software and is shown schematically in Figure 2. The model is organized so that a user should be able to generate manufacturing cost results. The spreadsheet cells that require input information are highlighted in the spreadsheet, and are located in the "input data" and "exogenous cost factor" sections. The input area of the cost model contains a number of input parameters for each unit operation, which must be provided for accurate cost determination. The cost calculation sections for each unit operation are programmed to utilize the various input specifications. The cost summary section provides a breakdown of production cost by factor and unit operation.

Input Data

The technical information necessary for the calculations is entered by the user in this region of the spreadsheet. This includes materials, process and labor parameters, cycle times and equipment costs for each process step.

The first information that a user must enter encompasses component or product specifications, such as substrate area, coating thickness and deposition and substrate materials. There are various choices available for substrate and deposition materials. After the substrate or deposition material reference numbers are selected and input, the material price, atomic weight and specific gravity automatically appear.

Input Data	Exogenous Cost Factors	Deposition Unit Steps Cost Calculations	Cost Summary
Product Geometry	Plant Operations	Variable Costs:	Variable Costs:
Equipment Parameters	Materials Prices	Materials	Materials
Processing Cycle Times	Wage Rates	Labor	Labor
Materials Parameters	Energy Prices	Energy	Energy
IBAD Processing Parameters		Fixed Costs:	Fixed Costs:
Technical Specifications		Equipment	Equipment
		Auxiliary Equipment	Auxiliary Equipment
		Installation	Installation
		Maintenance	Maintenance
		Fixed Overhead	Fixed Overhead
		Amortization Costs	Amortization Costs
			Process Based Cost Breakdown

Figure 2: General Spreadsheet Layout of Technical Cost Model

Equipment Assumptions

The deposition equipment costs must be specified, and are dependent on the substrate dimensions. The deposition equipment has not actually been built to accommodate high volume manufacturing, but potential equipment designs have been explored for technical and economic viability. The equipment follows the design of a standard evaporation roll coater, where a large cylindrical roll of substrate (the web) is threaded through a series of rollers. The web travels

through the rollers to expose an area of the substrate to metal or ceramic evaporant at a rate (web speed) which allows the required coating thickness to accumulate.

The dominant process parameter which controls and limits the web speed is the deposition rate, [coating thickness/unit time], for the various coatings. The aluminum oxide coating requires
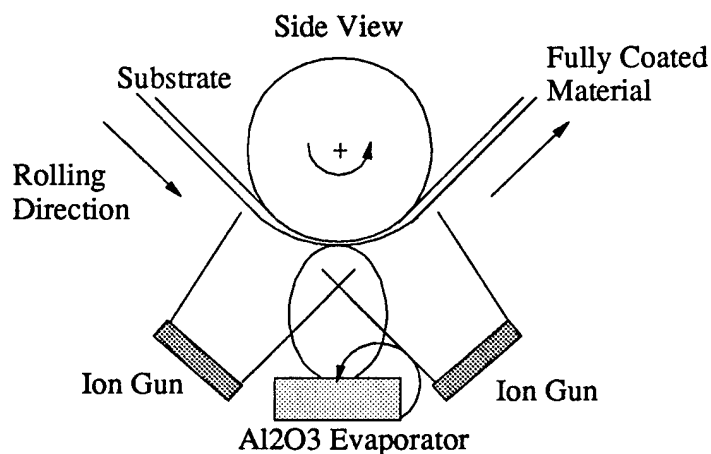

Figure 3: Schematic Side View of Roll Coating System - Region with IBAD Configuration
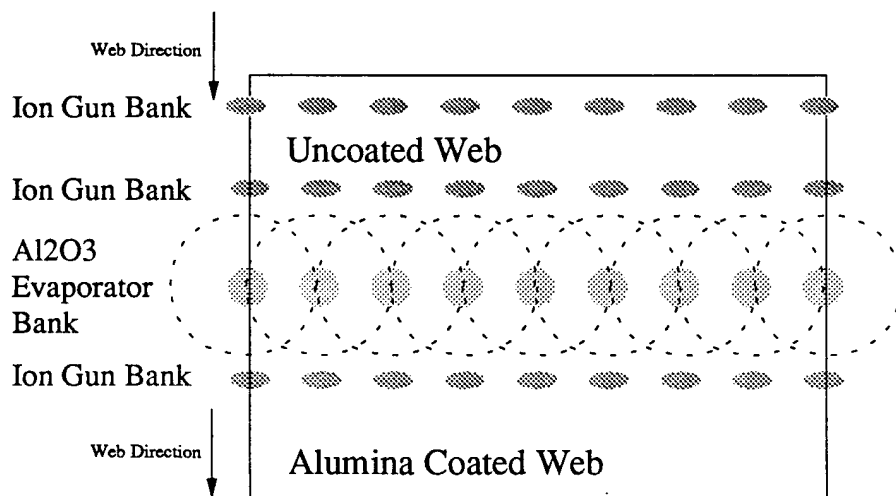

Figure 4: Schematic Top View of Roll Coating System - Region with IBAD Configuration

enhancement via IBAD processing, which includes the oxygen-ion bombardment sources acting in concert with the evaporators to achieve adequate coating properties. Without improved ion sources, the aluminum oxide deposition rate would remain too low for high volume production. The implementation of improved ion sources, developed by SAIC, would increase production rates and throughputs. The costs associated with modifications to standard roll coater equipment are included in the cost model.

Side view and top view schematic diagrams for the proposed IBAD equipment are shown in Figures 3 and 4, respectively. The side view shows a detail of the roll coating equipment in the region of IBAD processing as the web passes through a 30 cm deposition zone lying along the direction of web travel. The web travels past the evaporator and two ion-assist sources to complete the aluminum oxide deposition process. To achieve homogeneous coating thickness across the web width (fixed at 3.5 ft (1.067 m) in this configuration), a bank of nine evaporators and nine ion-assist sources is evenly spaced along the web width. Figure 4 also shows the bank of nine argon ion sources used to bombard the web to clean and prepare the surface prior to deposition. This configuration for the IBAD equipment is used throughout this study to generate the various cost results.

Although the actual deposition equipment necessary to manufacture canopies would differ significantly from that necessary to manufacture solar reflector materials, this IBAD configuration is used as a lower end cost estimate for the coating of aircraft canopy systems. With the addition of metallization evaporators, the roll coating equipment in this IBAD configuration is, however, more suitable for coating solar reflector materials.

In addition to the single stage configuration described and illustrated, a two-stage deposition system was investigated to determine the tradeoff of increased capital equipment cost versus shorter process throughput time. The decrease in deposition cycle time may offset the increased initial investment. The equipment cost assumptions are shown in Table 1 for single- and double-stage deposition systems. For solar reflector materials, additional metallization equipment costs must be added to this list to reflect accurate capital equipment costs for that deposition system.

Table 1: Canopy Processing Equipment -- Breakdown of Parts With Estimated Price List

For Single Stage Deposition:	Quantity	Cost/Unit	Equip. Cost
Evaporator/Controller	9	$25,000	$225,000
Deposition Arc Cathode Ion Source/Controller	18	$30,000	$540,000
Bombard Arc Cathode Ion Source/Controller	9	$30,000	$270,000
Deposition Chamber	1	$50,000	$50,000
Instrumentation	1	$100,000	$100,000
Water Cooling	1	$50,000	$50,000
Cold Trap Diffusion Vacuum Pumps	6	$64,000	$384,000
Roots Roughing Pump	1	$40,300	$40,300
TOTAL			$1,659,300
For Double Stage Deposition:	**Quantity**	**Cost/Unit**	**Equip. Cost**
Evaporator/Controller	9	$25,000	$225,000
Deposition Arc Cathode Ion Source/Controller	18	$30,000	$540,000
Bombard Arc Cathode Ion Source/Controller	9	$30,000	$270,000
Larger Capacity Deposition Chamber	1	$50,000	$50,000
TOTAL			$1,085,000
TOTAL IF BOTH STAGES USED:			$2,744,300

Processing Cycle Time Parameters

The next input area in the spreadsheet addresses the total amount of time needed to process a batch of the substrate. There are four general phases required to complete one batch of coated material. These are pre-coating, deposition, after-coating and recharging. Each of these times is summed to determine the total cycle time. The pre-coating period represents the time for a number of start-up activities which include time to evacuate the pressure chamber, cool the coating drum, and accelerate the web to processing speed to begin deposition. The actual time for deposition is calculated using other parameters specified by the user of the model, or it can be overridden with another input. After deposition has finished, the evaporators are deactivated, the winding mechanisms are stopped, the coating drum is heated to ambient temperature and the chamber is vented to atmosphere. During the recharging period, the chamber is opened and the coated roll is removed. The chamber is then cleaned and checked and routine maintenance is

performed before a new roll is loaded, and then the chamber is closed. The total time between the end of deposition processing and the restart of deposition is estimated as approximately one hour in the model. This is only a small fraction of the time required for deposition, which depends on the length of the roll, the deposition rate and the coating thickness.

Material Parameters

The materials required for the desired layered structure are initially specified by the user. For the aircraft canopy application, only the aluminum oxide coating material is needed, with an assumed commodity price of about $50 per pound. For the solar reflector application, copper (at $2.50 per pound) and silver (at $200 per pound) metallic layers are specified in addition to the aluminum oxide. The total materials costs are calculated according to the thickness and density of each coating, as well as the specified production volume, including a percentage for scrap.

Other materials used in this process include various gases. The ion sources require argon gas at $2.62 per cubic meter for the bombardment during surface preparation, and the ion-assist sources require oxygen at $1.38 per cubic meter. The volume of gas used during processing, and hence the cost, is calculated as a function of the specified gas flow rate and annual production volume. The recirculating water and other incidental materials (e.g., pump oil) have not been included, and are considered incidental with respect to their effects on the manufacturing cost.

The substrate material cost for the polycarbonate canopy is not included in this analysis, and therefore the cost of reworking, scrapping or destroying the high value canopy substrate through IBAD processing is not accounted for. The cost analysis is meant only to suggest the cost of the coating itself. In the case of the solar reflector materials, the PET substrate cost, although minimal at $0.03 per square foot, is included in the manufacturing cost.

Ion Beam Assisted Deposition Process Parameters

The variable and calculated operating parameters for the evaporators and ion sources used for deposition processing are displayed in Table 2. The IBAD deposition rate can be changed here to explore its impact on product cost. The variable input parameters, shown in bold, are used to calculate the total ion current and total ion power at the film surface, as well as to determine the total actual power used by each ion gun. These calculated values are shown in the table below for

the input variable and the equipment design shown in Figures 3 and 4, using a single-stage deposition operation. The only operating parameter required for the evaporator is its transfer efficiency, which is a measure of the percentage of material that is transferred from the evaporator melt to the substrate surface. The 25% transfer efficiency implies that 75% of the evaporant material is ineffectively deposited elsewhere in the chamber. The transfer efficiency is included as an input variable, although a value could be calculated.

The power requirements for the equipment must also be specified in the model to allow calculation of total energy requirements for the deposition process.

Table 2 - IBAD Processing Parameters for One-Stage Deposition

IBAD Deposition Rate of Al_2O_3	600	Angstrom / sec
Ion Energy Flux at Film Surface	60	eV / atom in film
Ion Energy at Film Surface	500	eV / ion
Ion Acceleration Voltage Energy	500	Volts
Ion Gun Exposure Factor	1.4	
Density of Coating	70	% of Theoretical
Expected Density of Coating	2.73	g / cm^3
Molecular Weight of Coating	102	g / mole
Number Atoms/ unit area- unit time	4.834×10^{-17}	atoms /s-cm^2
Ion Current Density at Substrate	9.281×10^{-3}	Amps / cm^2
Total Required Ion Current	42.25	Amps
Total Required Ion Power (at surfaces)	21124	Watts
Ion Source Electrical Efficiency	20	%
Arc Cathode Beam Current/Gun	2.35	Amps
Arc Cathode Source Current/Gun	9.39	Amps
Total Power Used by Each Ion Gun	5867	Watts
Ion Cathode Energy Used per Bomb. Gun	3.26	kWhr/Bomb. Gun
Ion Cathode Energy Used per Depo. Gun	3.26	kWhr/Depo. Gun
Evaporator Transfer Efficiency	25	%

Labor Parameters

The labor required for operating each line of deposition equipment is set in this model at two hourly workers, each devoting 50% of their time to monitor the processing cycle. The manpower requirement could be reduced if one worker could be used to monitor more than one line of equipment during the lengthy deposition period, but that is not assumed in this analysis.

Exogenous Cost Factors

Exogenous cost factors used in the IBAD deposition processing model are shown in Table 3. All manufacturing cost estimates are based on a standard working period of 260 days per year, with two shifts of eight hours each. It is assumed that the loan for equipment costs is amortized at 15% over a period of five years. Installation costs are assumed to be 15% of the total equipment investment, and annual maintenance costs are assumed as 5% of the total equipment investment. The wage rate is set at $35 per hour and the price of electric power is assumed to be $0.10 per kilowatt-hour. The fixed overhead is assumed at 35% of the total investment (including maintenance costs) per year. Each of these input factors can be changed by the user.

Table 3 - Exogenous Cost Factor Inputs Used in the IBAD Deposition Processing Model

Operating Days Per Year	260	days/year
Shifts per Day	2	shifts/day
Hours per Shift	8	hr/shift
Capital Recovery Rate	15	%
Capital Recovery Period	5	years
Direct Labor Wage	$35	/hr
Electricity Price	$0.10	/ kilowatt-hours
Unscheduled Downtime	0	%
Variable Overhead Cost	0	%
Auxiliary Equipment Cost	5	% of Capital Equip
Installation Cost of All Equip.	15	% of Capital & Auxiliary
Maintenance Cost	5	% of Capital & Auxiliary
Fixed Overhead Cost	35	% of Fixed Cost

Economic Analysis for Coated Aircraft Canopy Systems

The total cost associated with IBAD deposition is composed of material, capital, labor and energy costs. Figure 5 shows the factor-based cost components for a one-stage deposition process, assuming a production volume of 2674 coated canopies per year each with an assumed area of 105 square feet (9.75 m^2), and coated with a Al$_2$O$_3$ ceramic coating thickness of 4 μm at a deposition rate of 600 Å/sec. Again, the equipment design used in the model is based on roll coating applications, and is used as a first estimate of the manufacturing costs. Under these assumptions and with one line of equipment at full capacity, no downtime and no scrapped substrates, the total cost for coating each canopy is $468 (or $4.45 per square foot).
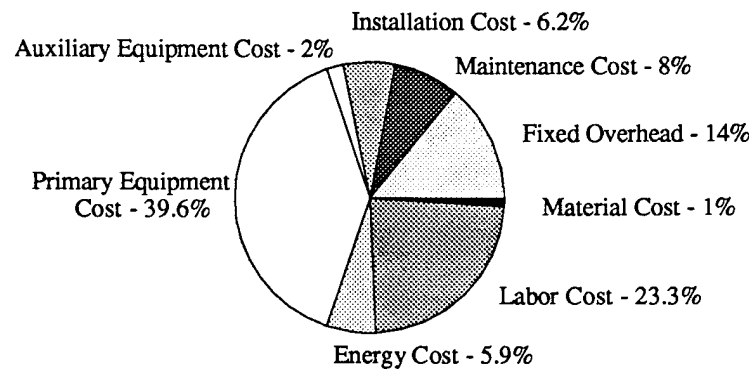

Figure 5: Factor Based Cost Components of IBAD Canopy Coating Process

The capital cost, which includes primary and auxiliary equipment, installation, maintenance and fixed overhead, is the major contributor to the coated substrate costs, as it accounts for almost 70% of the total cost at maximum production volume. Since this process is so highly capital intensive, high utilization of the deposition line is essential to reduce the cost per unit of coated area. At an equipment utilization of 50%, producing 1337 canopies per year, the fixed cost accounts for 82% of the manufacturing cost. Larger production volumes achieve greater economies of scale by spreading the fixed costs over more product. As the production volume increases, capital equipment cost per unit drops, and consequently the total cost for coating each canopy decreases, as shown in Figure 6. The increase in costs for a slower IBAD deposition rate is also shown.
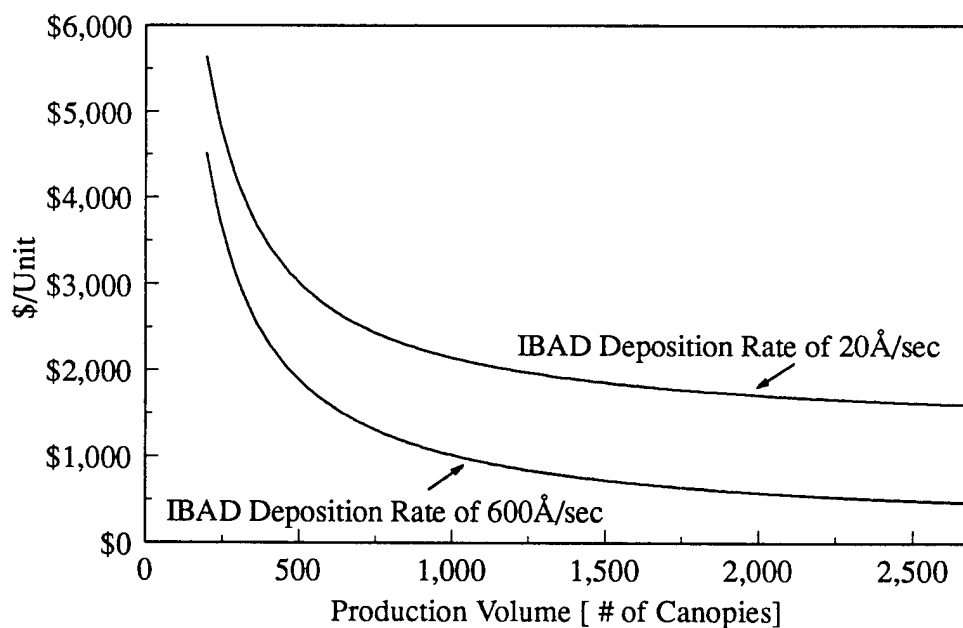
Figure 6: Economies of Scale for Coated Canopies at Different Deposition Rates

The pie chart in Figure 5 indicates that for the assumptions given, the cost of labor is substantial, accounting for 23.3% of the total cost, essentially because one technician is using all available work time to produce coatings and monitor the equipment. A fraction of that labor time would be required if automated equipment is used to monitor the deposition process. The energy costs reflect the electric power used for the ion sources. At 5.9%, this contribution is not unexpected. The material cost for this deposition process is very low (1%) due to the small volumes of gases and minimal coating thickness, and it does not include the substrate cost.

In addition to understanding the cost contributions for a specific set of processing conditions, other processing variables can be systematically changed while holding the other parameters constant to explore their effect on manufacturing costs. The IBAD deposition rate is a major contributor to costs, because slow deposition rates or long cycles times give lower rates of throughput. In order to compare the equipment design factors affecting throughput, the single- and double-stage deposition designs are compared as a function of deposition rate in Figure 7.

As expected both curves show a decrease in cost per ft^2 with increasing deposition rates. These results assume a 4 μm coating on polycarbonate canopies, each with area of 105 ft^2 (9.75 m^2), using one line of equipment at maximum capacity, with no downtime and 100% yield. As the
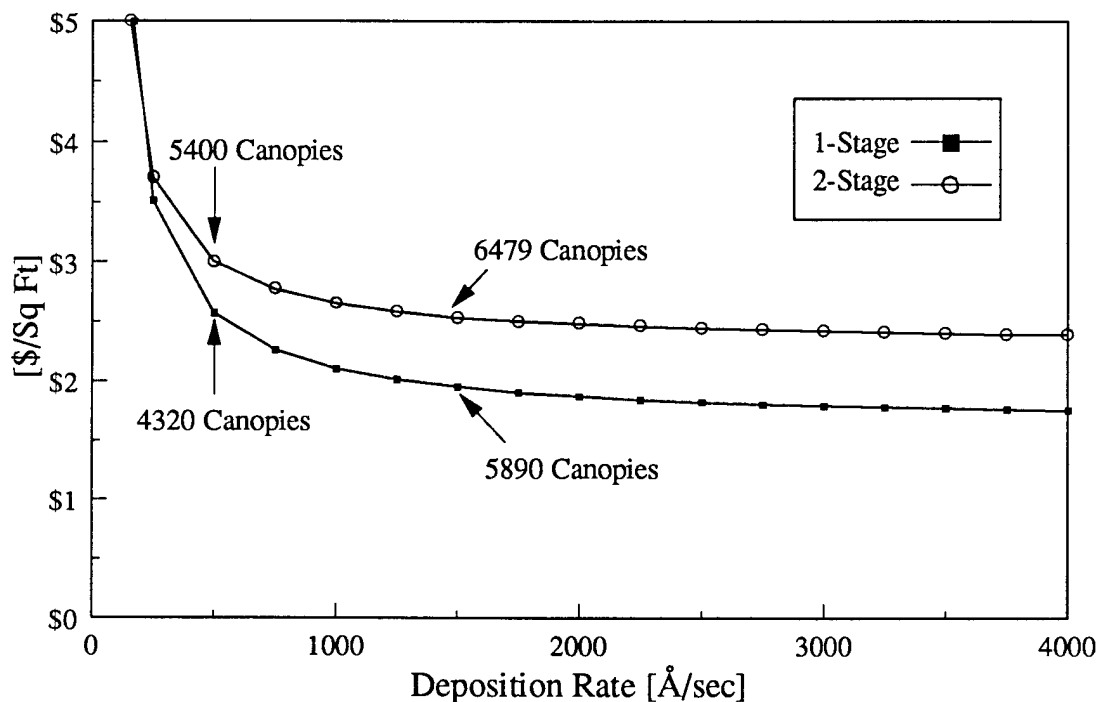
Figure 7: Equipment Design Shows Strong Effect on Manufacturing Cost

deposition rate increases, the production volume is not constant along each curve. The maximum number of coated canopies is given for deposition rates of 500 and 1500 Å/sec. As the cycle time decreases, more substrates can be coated, which decreases the fixed costs per canopy by spreading them over the higher output. Comparison of single-stage and double-stage equipment curves shows that the double-stage remains at a greater cost/ft^2 for nearly the entire deposition range, although at very low deposition rates the double-stage cost/ft^2 is lower than the single-stage. This crossover occurs at about 200 Å/sec. At 500 Å/sec, the cost differential is about $0.50/ft^2 due to increased capital costs of the two-stage equipment, but the production capacity of the two stage equipment is higher.

The deposition rate range explored in Figure 7 extends from currently achievable rates (below 100 Å/sec) to rates that are beyond the capability of the new cathode technology. In Figure 8, the feasible regions of IBAD deposition rates for single- and double-stage equipment are shown graphically with respect to ion gun current limitations. The upper portion of this graph indicates the increase in ion gun current with deposition rate for one- and two-stage equipment. Each cathode is limited to a current below 3 amps, hence deposition rates where the current becomes
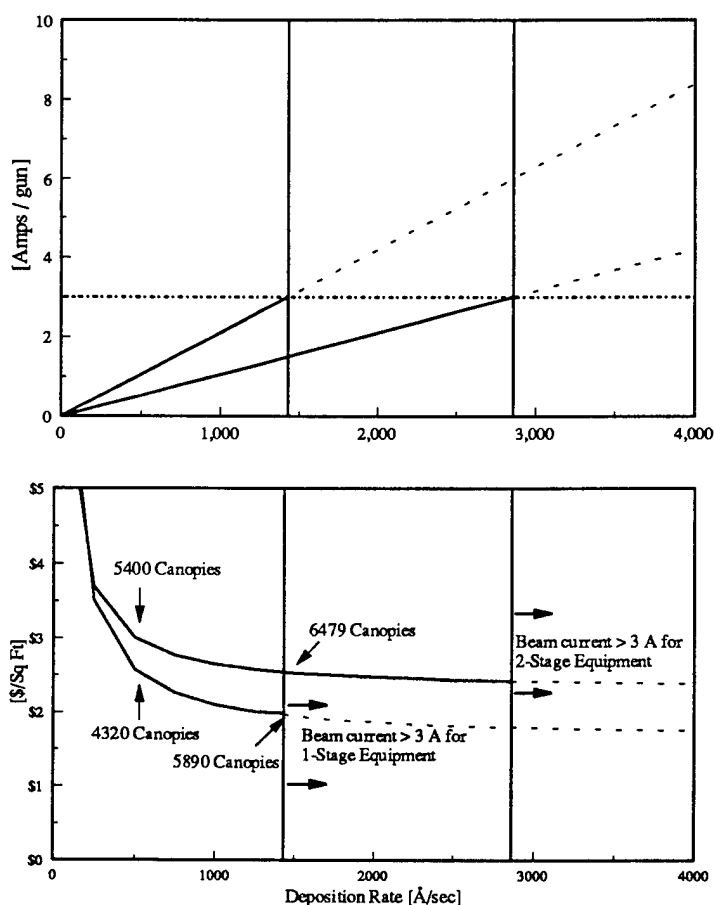
Figure 8: Ranges for Feasible Deposition of 1- and 2- Stage Equipment For Small Substrates

greater than 3 amps are unachievable, as indicated by the dotted lines. The lower portion of Figure 8 is a reiteration of Figure 7, which indicates the regions of feasible deposition rates by the solid curves. For deposition rates using single-stage equipment, coating is infeasible above 1430 Å/sec. For double-stage equipment, coating becomes infeasible above 2863 Å/sec.

A comparison of the economies of scale are shown for various deposition rates in Figure 9. Again, these results assume a 4 μm coating on polycarbonate canopies each with area of 105 ft² (9.75 m²) using one line of equipment at maximum capacity, with no downtime and 100% yield. For each of the four deposition rates (20, 60, 600 and 1000 Å/sec) the two-stage equipment incurs a higher manufacturing cost for a given production volume. The maximum annual production capacities for the one-stage equipment are shown in the graph in units of millions of

square feet (MSF) and translate to 236, 634, 2674 and 3120 total canopies for deposition rates of 20, 60, 600 and 1000 Å/sec, respectively.
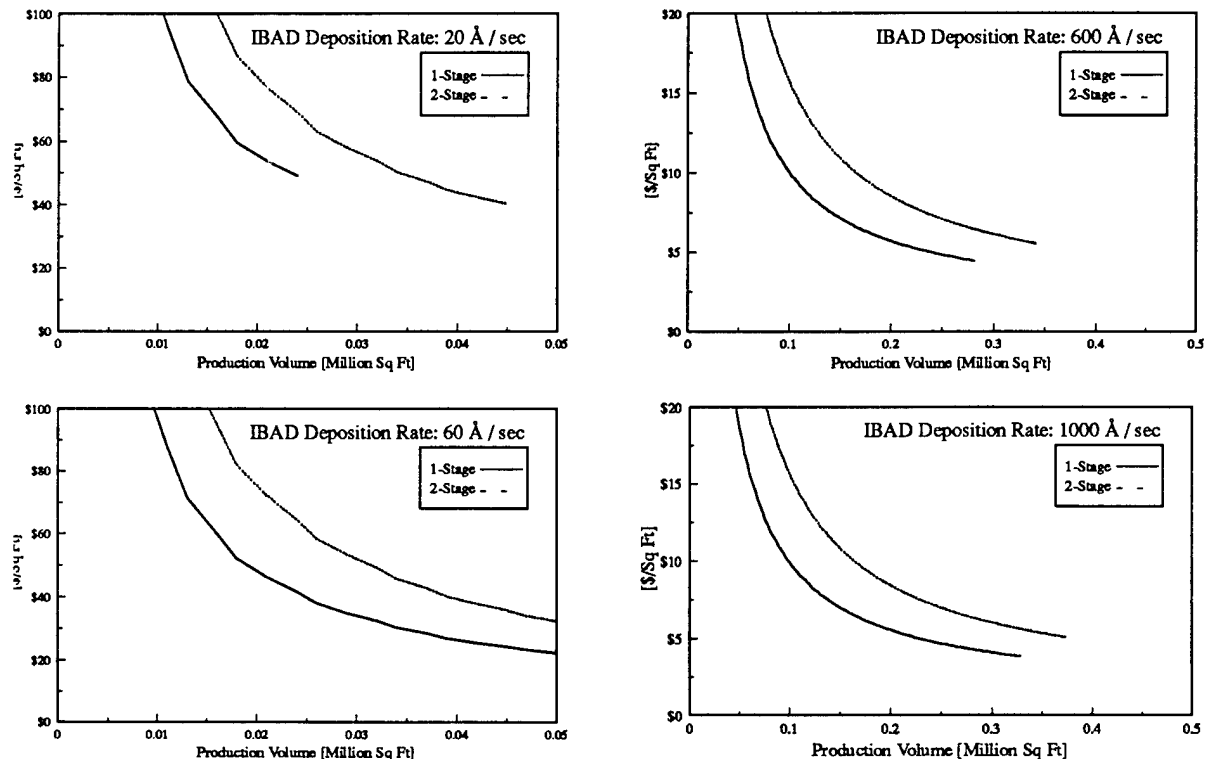

Figure 9: Economies of Scale at Various IBAD Deposition Rates For Small Substrates

Economic Analysis for Coated Solar Reflector Materials

The same technical cost model is used to simulate the deposition costs for manufacturing solar reflector films, which generally require a larger product area than the canopy. For this analysis, an assumed web width of 3.5 ft (1.067 m) is maintained, with a web length of 2400 ft (730 m). With all other parameters and assumptions unaltered, this change has a major effect on the cycle time per batch. The simulation at this point does not include the metallic evaporant coating as part of the manufacturing cost.

In Figure 10, the feasible regions of IBAD deposition rates for 1- and 2-stage equipment are shown graphically with respect to ion gun current limitations. The upper portion remains unchanged from Figure 8. The unachievable deposition rates remain unchanged and are shown by dotted lines. The two-stage curve remains at a greater cost/ft^2 for the most of the deposition
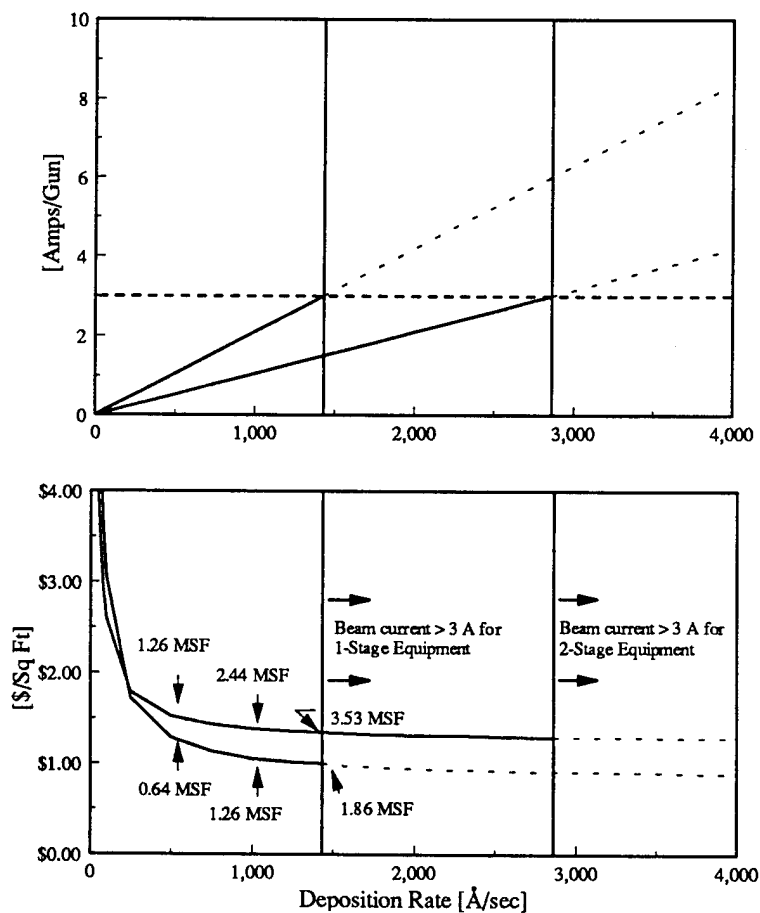
Figure 10: Ranges for Feasible Deposition of 1- and 2- Stage Equipment For Large Substrates

range, but at deposition rates less than 250 Å/sec, two-stage is less expensive. This implies that two-stage equipment could be cost effective at production volumes above a critical substrate roll length at a given deposition rate. This occurs because the percentage of cycle time dedicated to actual coating is increased, rather than breaking chamber vacuum and recharging. Under single-stage conditions, 0.64 MSF of coated material can be produced for less than $1.28/ft^2 if deposition rates of 500 Å/sec can be achieved.

As the deposition rate and, consequently, the production volume increase, the crossover point becomes apparent (Figure 11). These results assume a 4 μm coating on a PET substrate with a coated area of 8400 ft^2 (730 m^2) using one line of equipment at maximum capacity, with no downtime and 100% yield. For three of the deposition rates (20, 60, and 600 Å/sec) the two-stage equipment incurs a higher manufacturing cost for a given production volume. For the
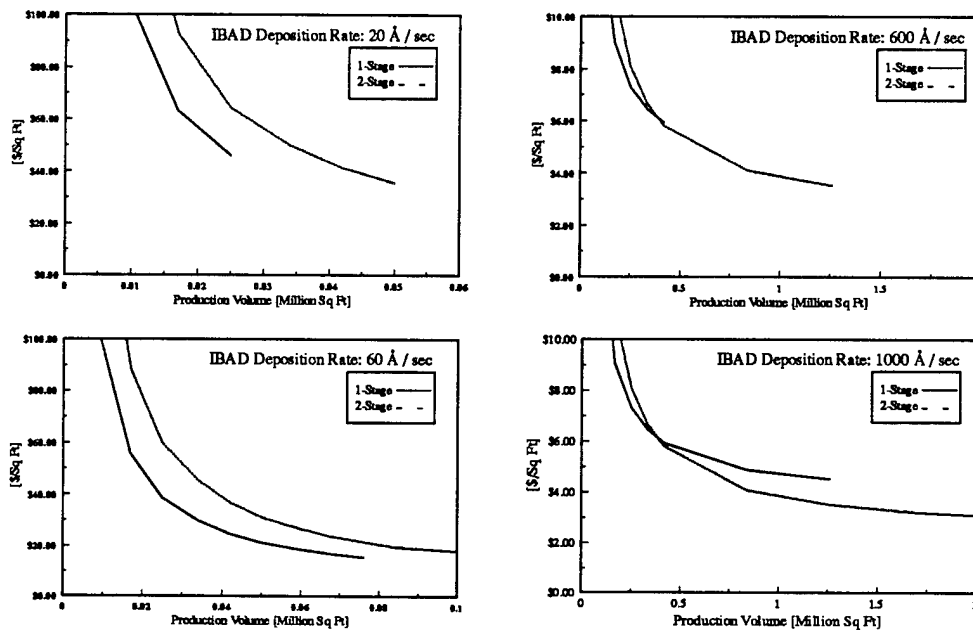
Figure 11: Economies of Scale at Various IBAD Deposition Rates For Large Substrates

1000 Å/sec rate, however, two-stage equipment becomes more cost effective. The maximum annual production capacities for the one-stage equipment in the graph, although substantial in MSF, are rather limited in the number of rolls processed. For the single-stage deposition rates of 20, 60, 600 and 1000 Å/sec, the number of rolls coated is 3, 9, 91 and 150, respectively. If the number of shifts is increased to allow 24 hour production, the production volumes and the equipment utilization would increase, and the cost/ft^2 would drop correspondingly.

A modified version of this technical cost model is used to simulate the deposition costs for manufacturing solar reflector films with metallic interlayers in addition to the protective alumina coating, as shown in Figure 12. This configuration is represented in text form as Al_2O_3/ Ag/ Cu/ PET. The manufacturing cost per square foot is calculated for this scenario based on varying the thickness of the aluminum oxide coating and changing the IBAD deposition rate. The substrate cost, though minimal, is included in these assumptions.

The cost results shown in Figure 13 are generated assuming for an annual production of approximately 1 MSF of a solar reflector material, which consists of a PET substrate coated with a 40 nm copper layer, then coated with 70 nm of silver, followed by the protective alumina of varying thicknesses. One line of equipment is in use with single-stage deposition at maximum

Front Surface Reflector
for Solar Reflector Applications
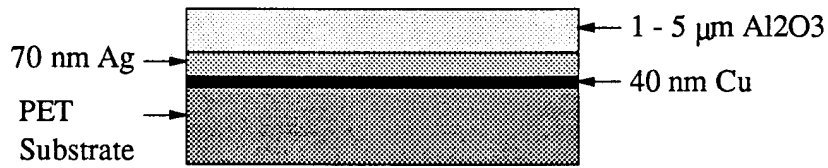
Figure 12: Schematic Diagram of the Solar Reflector Layered Structure Investigated

capacity, with no downtime and 100% yield. As the alumina coating thickness decreases from

5 μm to 1 μm, the cost per ft^2 decreases as expected, since a reduced amount of material is used.

As each curve approaches lower deposition rates, it ends abruptly, indicating that further

decreases to the deposition rates would require introduction of another line of equipment. At a

5 μm thickness, the rate must exceed 600 Å/sec to maintain a single line, while for a 1 μm

coating, rates as low as 200 Å/sec can still be accommodated by a single line. A second

phenomenon is observed as each curve approaches lower deposition rates - the capacity utilized
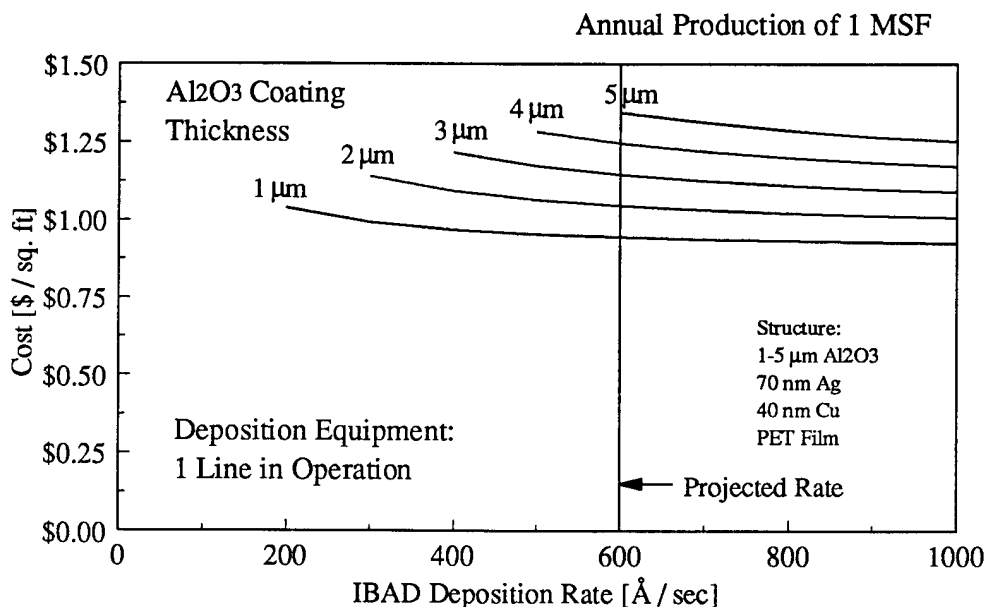
Figure 13: Sensitivity of Coating Thickness to Cost For Solar Reflectors Materials at 1 MSF

decreases with increasing deposition rates, since each curve represents a constant annual production of 1 MSF. As the deposition rate increases, it requires less time to finish the production cycle, and then the equipment lies idle. The cost/ft^2 of $0.89 at a deposition rate of 600 Å/sec for 1 MSF of coated material per year with a 1 μm coating actually reflects the price of underutilization. If the maximum production capacity of the equipment is achieved, the increased annual production volume of 5 MSF reduces the cost to $0.35/ft^2.

When more than one line of equipment is available, higher production volumes can be achieved for this set of assumptions. The manufacturing cost per square foot can now be assessed for annual production volumes of 5 MSF, based on varying thicknesses of the aluminum oxide coating and changes in the IBAD deposition rate. One line of equipment is in use with single-stage deposition at maximum capacity, with no downtime and 100% yield.

With reduced coating thickness, the manufacturing cost decreases, showing the same trend as found in Figure 13. The curves in Figure 14, however, show discontinuities, which increase the cost/ft^2 in small jumps as the deposition rate decreases. These jumps in cost occur when another line of equipment is required, which is implemented by the model to achieve the desired production volume. The discontinuity shows the difference in cost between 100% utilization at
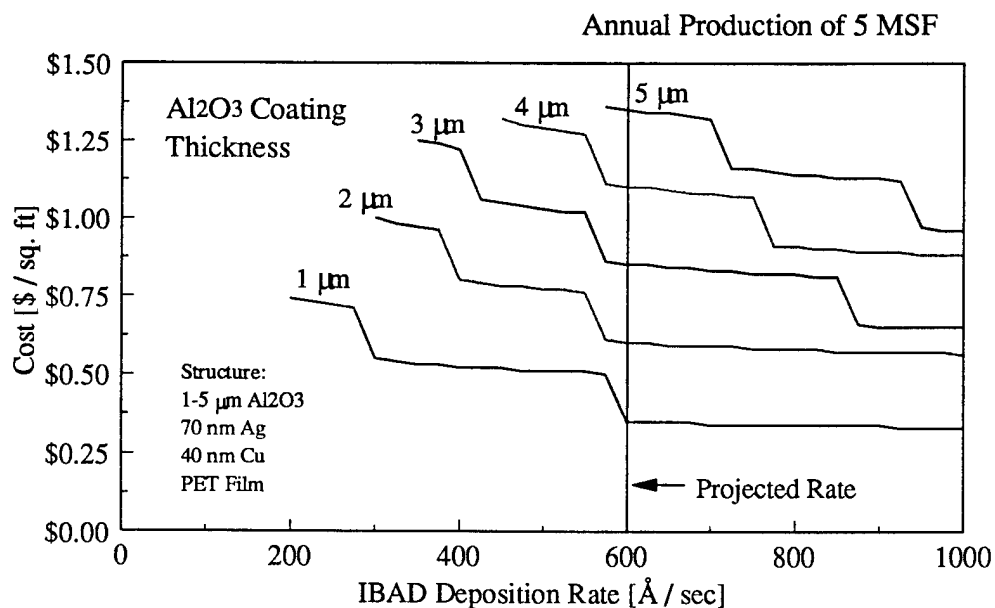
Figure 14: Sensitivity of Coating Thickness to Cost For Solar Reflectors Materials at 5 MSF

the lower cost side of the jump and the much lower initial utilization for an additional equipment line at the same production volume.

The curve for 1 μm coating thickness requires only one line at high deposition rates (600-1000 Å/sec), and at speeds lower than 600 Å/sec a second line is needed. For the 2 μm coating, two lines are necessary at high rates, and a third is needed below 600 Å/sec. The 3 and 4 μm coatings require three lines of equipment at high deposition rates, and the 5 μm coating uses four deposition lines at annual volumes of 5 MSF.

Summary & Conclusions

A technical cost model has been developed to simulate the manufacturing costs for an IBAD deposition system which implements a new cathode technology. The deposition of an aluminum oxide ceramic coating is explored for two equipment scenarios under various operating conditions. The dominant variables affecting the cost of the coated products include the IBAD deposition rate, the thickness of the ceramic coating and the desired annual production volume.

The assumptions behind these cost analyses are meant to reflect the processing conditions expected for high volume production scenarios. The range of production volumes are chosen as a result of discussions with potential customers for the technology. The coating thickness and deposition rates addressed in the cost analysis are currently being investigated on the technical side. The economic information generated here will be used in concert with the scientific analysis of film properties to indicate the configurations warranting further consideration for technological development.

Applications for both military and commercial end use were explored, specifically for ceramic coated polycarbonate aircraft canopies and solar reflector materials. The main objective in both economic analyses was to identify the processing conditions which minimize the manufacturing costs. The potential manufacturing process is based on modifications to standard roll coating equipment. This allowed the accurate calculation of a series of first order cost estimates for both applications under consideration.

A cost breakdown of materials, labor, energy and capital expenditures indicated that, based on the given assumptions, this process is highly capital and labor intensive. High utilization of the equipment is essential to the economic viability of this technology. Cost effective implementation may also require additional automation to reduce the labor costs. Single-stage and double-stage IBAD deposition equipment schemes show that, for canopies, the single-stage manufacturing costs are lower at most deposition rates, while, for solar reflector, double-stage manufacturing could be economically feasible under certain conditions.

A cost analysis for canopies is presented in which each canopy has an assumed area of 105 ft^2 (9.75 m^2), and is coated with an Al$_2$O$_3$ ceramic coating thickness of 4 μm, using one line of equipment at full capacity, with no downtime and no scrapped substrates. If the deposition rates

can achieve 600 Å/sec, the cost to coat 500 canopies would be around $2000 per unit. For low deposition rates of 20 Å/sec, the unit cost rises to about $3000. Since high production volumes of canopies are required to achieve lower cost, this technology, while perhaps technically superior, may not prove economically viable due to low fleet demands and the high specificity of other coating requirements for different aircraft canopies. The question remains as to whether investors or government agencies are willing to incur an additional cost to coat aircraft canopies for enhanced performance and lifetime.

A cost analysis for solar reflector layered structures which include metallic interlayers of copper and silver on a PET substrate is presented for larger web areas of 8400 ft^2 (730 m^2). Using one line of single-stage equipment at maximum capacity with no downtime and 100% yield, only the manufacturing cost of the 1 μm ceramic coating thickness falls below the desired $1/ft^2 goal at deposition rates greater than 600 Å/sec. At the higher annual production volume of 5 MSF, the cost of 1 μm coated materials is reduced to $0.35/ ft^2 for rates greater than 600 Å/sec. If the 1 μm and 2 μm coated reflector materials prove technically superior than the competition, the economic analysis indicates significant incentive for investment in the development of high volume production.

Attachment C

"Tribological Characterization of Durable,
Environmentally Friendly Coatings"

Tribological characterization of
durable, environmentally-friendly coatings

I.L. Singer and L.E. Seitzman
Code 6176
Naval Research Laboratory
Washington DC 20375

Tribological characterization of durable, environmentally-friendly coatings

ARPA order A680
Final Report, Naval Research Lab
13 September 1995

Authors: I.L. Singer and L.E. Seitzman

Abstract

This report summarizes the work performed at the Naval Research Lab (NRL) under ARPA order A680, an element of the Advanced Coatings Technology Program contract with SAIC (McLean VA). NRL's role was to evaluate the tribological properties of hard, transparent coatings on a variety of substrates, including plastics. We developed mechanical testing procedures that would predict performance of coatings under a variety of adverse conditions. The procedures enabled us to determine the hardness, adhesion, toughness and abrasion resistance of coatings on plastic substrates like polycarbonate and hard substrates like glass.

EXECUTIVE SUMMARY

Background.

Armstrong World Industries had developed a hard, transparent coating deposited by ion-beam-assisted deposition (IBAD) capable of protecting both metals and plastics from wear and corrosion. Based on potential environmental benefit, ARPA funded a program to scale up the coating process. SAIC would develop an ion source for scale-up and Armstrong would optimize the process for candidate DOD applications. NRL's task was to devise testing procedures for evaluating the mechanical properties of coated materials and provide feedback to Armstrong for process optimization.

Technical Approach.

NRL used three mechanical testing procedures for evaluating the mechanical properties of micron-thick hard-coatings. The procedures were **indentation, scratch,** and **abrasion** testing. **Instrumented indentation testing** was implemented during the last quarter of the project after it became clear that the a new methodology was needed to fully characterize the properties of thin hard-coatings on the softer plastics.

Summary of Accomplishments

Mechanical testing demonstrated that changes in Armstrong's processing parameters led to higher hardness, better adhesion and higher fracture resistance of IBAD Al_2O_3 coatings. The most significant processing changes included emphasizing N_2 gas over O_2 gas, optimizing ion-to-atom ratio, using a ion probe to monitor the ion current and pre-treating substrate surfaces with cleaning solutions or energetic ions (documented in the Armstrong final report). During this period, we identified the methodologies most suitable for measuring the mechanical properties of thin hard-coatings on plastics and glass (see Table 1). We also determined the stress state (both intrinsic and thermal-induced) of the coatings as well as the fracture toughness of coated substrates. The best coatings were shown to be very adherent, to have hardness values around 18GPa, and to be two to four times as abrasion resistant as polycarbonate.

MAIN REPORT

1. Introduction

Armstrong World Industries developed an environmentally-friendly, hard, transparent coating capable of protecting both metals and plastics from wear and corrosion. If the process to produce this coating could be scaled up, hazardous waste generated by the use of traditional paints and coatings could be significantly reduced. However, the mechanical properties of hard-coatings especially on soft substrates such as plastics were unknown. Therefore, NRL was tasked with evaluating the mechanical properties of micron-thick, transparent hard-coatings on a variety of substrates, including plastics. The purpose of the evaluation was twofold: 1) to assess methodologies for obtaining meaningful mechanical properties of thin hard-coatings on pliable substrates and 2) to provide timely feedback to program participants on the relationship between coating process conditions and mechanical properties.

NRL initially addressed the first goal by selecting three mechanical testing methods: **standard indentation testing, scratch testing, abrasion testing**. These three tests are conventionally used to evaluate hardness, adhesion, and wear resistance, respectively. In addition, indentation testing can be used to evaluate toughness and residual stress of the coating/substrate system such as. Part way through the program, it became clear that the standard hardness testing apparatus was unable to fully characterize the mechanical properties of thin hard-coatings on the elastically-softer plastics. Much more reliable data on plastic as well as elastic properties of coated substrates [Ref. 1] were obtained after an **instrumented indentation** machine was leased during the last quarter of the project. NRL also initiated, late in the program, stress testing and

an indentation toughness methodology to provide semi-quantitative measurements of the stress state and toughness of the coatings.

The coatings evaluated were primarily Al_2O_3 grown by Armstrong using ion-beam-assisted deposition (IBAD). Mechanical tests were also performed on magnetron-sputtered Al_2O_3 (produced by SAIC) and a few commercially-available coatings. Most of the testing was performed on coated polycarbonate and coated glass, with some testing done on bare reference substrates. Early in the program coatings on both plastic and glass were evaluated using all tests, except abrasion testing, in order to determine which test best characterized the durability and adherence of the hard-coating. These results were used to identify the most discriminatory tests for different substrates (see section 3). In the later stages of the program, only these discriminatory tests were performed.

In order to facilitate the second goal of the study, mechanical properties measured on Armstrong and SAIC coatings were correlated with processing parameters such as bombardment gas (N_2, O_2 and mixtures), ion bombardment level, coating thickness and substrate cleaning methods [See SAIC report for summary]. The results were reported at monthly meetings, which allowed rapid and orderly improvements in processing parameters and sample cleaning procedures.

2. Experimental

2.1 Apparatus

Four mechanical testing apparatus were used: the Wilson Tukon tester for **standard indentation testing**, the Fischerscope H100 for **instrumented indentation testing**, the CSEM Revetester for **scratch testing**, and a modified Buehler Ecomet III for **abrasion testing**.

The Tukon indentor has a load range of 0.1 to 500 N and can accommodate various indentor tips such as Knoop, Vickers, and Brale. The Knoop and Vickers indentors, shown in figs. 1 and 2, respectively, are sharp-tipped, while the Brale indentor is blunt (a 120° cone tipped with a sphere of 0.2mm radius). The indentor is driven into the sample to a preselected load, held for 15 sec, and retracted. The resultant indent must then be evaluated optically to measure impression geometries [Ref.2].

The Fischerscope H100, shown in fig. 3, has a load range of 1E-4 to 1N and can accommodate both Vickers and Knoop indentors. Unlike the standard indentation testers, the instrumented tester step-loads the indentor up to the preselected load, then step-unloads the indentor. The step

size and dwell time (time held at each step) for loading and unloading can be selected. The load and depth of each step is automatically recorded. The resultant indent can be evaluated optically, as well.

The CSEM Revetester has a load range of 1 to 100 N and typically uses blunt styli, such as diamond cones with spherical tips of 0.2, 0.5, and 0.8 mm radius. The stylus is driven into the sample at a linear loading rate up to a selected load. The sample is translated to produce a scratch either after the maximum load is achieved or during the ramping of the load. The loading rate and translation rate are adjustable. The normal force, tangential force, and acoustic emission of the stylus is continuously monitored (see fig 4). The scratch is also evaluated optically.

The modified Buehler Ecomet III is a metallographic polisher which rotates samples under a dead load against a rotating wheel. The speed, load, and polishing material can be selected. Up to nine samples, including three reference samples, can be polished at one time (see fig. 5). The samples are weighed, polished for a specified time, and re-weighed. This procedure is repeated until the coating is worn through. Weight loss is measured with μg precision using a Mettler UM3 microbalance.

2.2 Procedures

Properties measured were hardness, effective elastic modulus, critical load to fracture, toughness, residual stress, scratch adhesion, and abrasive wear. The definitions of and procedures for determining these properties are described below. It should be noted that multiple indentation, scratch and abrasion tests were performed per load per sample for verification of reproducibility.

Hardness is defined as the maximum indentation load divided by the area of permanent deformation in the sample (H=L/A). For standard indentation testing, the area A was determined by optically measuring the length d of the longest diagonal of the residual indent. For Knoop and Vickers, a simple geometric relation is used to relate d to A, as shown in figs. 2 and 3. For instrumented indentation, two values of hardness, Hp and Hu, are determined: Hp uses the depth h_r' which is extrapolated from the initial slope of the unloading curve and Hu which uses the maximum indentation depth h_t (see fig. 6). The area A is determined using geometric calculations similar to those for standard indentation; note that no optical measurement of the indentation is required.

The **effective elastic modulus** is defined as $E/(1-v^2)$, where E is Young's modulus and v is Poisson's ratio. This parameter is obtained from the initial unloading slope of d vs L in instrumented indentation[Ref. 3].

Critical load to fracture Lc is defined as the average load required to initiate cracking outside the indent. Cracks such as radial and circumferential are produced in brittle coatings using standard indentation with sharp and blunt indentors[Ref. 4 and 5], as indicated in fig. 7. In some cases, such as with glass substrates, care must be taken to distinguish between cracking and other forms of coating failure (see fig. 8). For the sharp indentors radial cracks normally appear at corners and project outward, as in fig. 8. This allows for uncomplicated determination of Lc by optical means. For blunt indentors the critical load to fracture is less readily identified due to the non-uniformity in crack location and type, as seen in fig. 9; therefore, determination of Lc usually requires the addition of graphical analysis. By plotting maximum crack diameter versus indentation load for both the coated and bare substrate, as shown in fig. 10, one can determine Lc as the load at which the slopes of the two curves begins to differ. Maximum crack diameter is the average in two orthogonal directions of the length between maximum circumferential or radial crack extremes.

Toughness Kc is defined as the resistance to crack propagation and is related to modulus, hardness, load, and crack size as shown in fig. 11. The load, hardness and crack length are determined from standard indentation, as noted above.

Residual stress is defined as the stress added to the system after deposition of the coating. It is determined by two techniques: 1) multiple indentation as developed by Gruninger, et. al[Ref. 6] and 2) curvature of a thin wafer[Ref. 7]. The Gruninger technique, fig. 12, is a three step method. First a Vickers indent is made at a load great enough to produce radial cracking in a brittle substrate, then the coating is deposited, and finally another indent is made at the same load. The toughness is measured at each step (see fig. 12). The residual stress in the coating is determined by the difference between state I and III toughness values, normalized by coating thickness (see Ref. 6). For the second technique, a flat, circular glass cover slip was coated, then the curvature was determined optically (see fig. 13) and by profilometry. Residual stress σ is determined by

$$\sigma = \frac{Et^2}{6(1-v)d} \frac{1}{R}$$

where E, v, and t are Young's modulus, Poisson's ratio, and thickness of the substrate, respectively, d is the coating thickness and R is the radius of curvature.

Scratch adhesion[Ref.8,9] is measured by a critical load, defined as the load at which the coating delaminates from the substrate. This is determined by ramped load scratch testing using a translation speed of 5mm/min and a ramp of 1 to 100N. Optical microscopy was used to determine the initial location on the scratch where the delamination occurred; this point was compared against friction coefficient and acoustic emission responses (see fig. 4b).

Abrasive wear is defined, in this case, as the loss of coating due to grinding by small hard particles. This is determined by comparative thickness reduction of coating and reference materials under identical abrasion test conditions. Thickness is determined from the weight loss, specimen geometry, and ideal density according to the formula shown in fig. 5. The ratio of coating loss to reference material loss is given as the relative wear resistance RWR[Ref. 10,11,12]. Reference materials used were single crystal sapphire, TiN coated Ni, Cr plated Ni, bare M2 steel and bare polycarbonate.

3. Results and Discussion

3.1 Methodologies

The methodologies evaluated in this study are summarized in Table 1.

3.1.1 Hardness

Initial tests were designed to determine the appropriate working load for hardness measurements using standard indentation. Armstrong IBAD Al_2O_3 on polycarbonate and glass substrates were evaluated over a load range of .1 to 50N. It was found that Vickers indentation led to excessive penetration at all loads and was, therefore, eliminated as a hardness test method. Knoop indentation at higher loads on both polycarbonate and glass led to excessive penetration into the substrate. At the lowest loads Knoop resulted in appreciable uncertainty in the measured hardness values. Therefore, 0.5N (50gf) was chosen to balance depth of penetration vs reproducibility. The 50gf Knoop hardness (HK 50) on polycarbonate and glass is reported in Tables 2 and 3.

As can be seen from Table 2, the depth of penetration on coated polycarbonate was typically 4μm, which is roughly identical to coating thickness. In order to minimize substrate contributions to coating hardness, the depth of penetration should be less than 0.2 of the thickness[Ref. 1]. Other difficulties with 50gf Knoop indentation on polycarbonate were distortion of the indentation shape (a 7:1 diagonal ratio was not maintained) and formation of

lateral cracks. Thus standard Knoop indentation, as defined above, was not an acceptable method for hardness determination of the coatings on polycarbonate.

The depth of penetration for the coatings on glass was usually about 0.25 the coating thickness, as seen in Table 3. Therefore, standard Knoop indentation gave reasonable hardness values for the coatings on glass. However, even at 50gf the hardness values were susceptible to low load measurement errors. To obtain hardness values on coated polycarbonate and to improve reliability of the values on coated glass, instrumented indentation tests were initiated.

Instrumented indentation was performed over a load range of 4 to 1000mN. The depth of penetration varied over this load range, and the transition from coating only to coating plus substrate hardness was observed. For coated polycarbonate and glass the measurement error, even at very low loads, was smaller than in standard indentation. Under comparable loads (0.1 to 1N) instrumented Knoop indentation gave similar hardness values as standard Knoop indentation, as shown for polycarbonate in fig. 14. Furthermore, it was found that instrumented indentation could be performed with Vickers indentors without unacceptable substrate contributions. Knoop and Vickers hardness on polycarbonate vs normalized depth (maximum indentation depth/thickness) are plotted in fig. 15. Vickers indentation was more reproducible and more clearly distinguished the point at which the substrate began to influence the hardness values (the drop at depth/thickness = 0.6). Also, Vickers indentation was able to effectively probe hardness over a greater range of depth/thickness. It is believed that Vickers was less susceptible to vibration and surface effects. In the range where Knoop and Vickers can be compared the hardness values are similar.

3.1.2 Effective elastic modulus

The effective elastic modulus was measured on coated polycarbonate and glass using Knoop and Vickers indentors. The effect of indentor type on the modulus vs normalized depth for coated polycarbonate is seen in fig. 16. As with hardness, the Vickers data cover a greater effective range and more clearly distinguish the onset of substrate influence. Again, the modulus values are similar for both indentor types.

3.1.3 Indentation fracture & adhesion

Standard Vickers indentation on coated polycarbonate and glass was first used to evaluate critical load to fracture. The critical load for radial crack formation of several coated polycarbonates is shown in fig. 17. Unfortunately, cracking could not be reliably induced at reasonable loads (1

to 50N); at higher loads (100 to 400N) the indents were too large. On coated glass, radial cracks were readily created at a reasonable load range. Also, Vickers indentation could discriminate between well and poorly adhering coatings on glass, as seen in fig. 8.

Standard Brale indentation of coated polycarbonate reliably produced radial and circumferential cracks under moderate loads (see fig. 9). Note that at 0.6kgf only circumferential cracks are produced, while at 1kgf one of the coatings (the commercial ITO/Au coating) has begun to exhibit radial cracks. In some cases, Brale indentation resulted in decohesion of the coating, but no systematic study of this phenomenon was performed. Brale indentation on glass was not studied.

3.1.4 Toughness and residual stress

Toughness and stress were evaluated on coated glass coupons only by Vickers indentation over a load range of 10 to 50N. As noted in 3.1.3 the vickers indentor does not produce fracture in coated polycarbonate.

Residual stress measurements on glass coverslips were easier to obtain and more reliable using profilometry to determine curvature than using optical means.

3.1.5 Scratch adhesion

Scratch adhesion tests were performed on coated polycarbonate and glass. While the scratch tracks on polycarbonate could be analyzed for delamination, those on glass could not due to substrate fracture. Three diamond styli (0.2, 0.5, and 0.8mm radius) were used to scratch on coated polycarbonate. Delamination occurred at very low loads (< 20N) over a limited range with the 0.2 and 0.5mm styli, which complicated data analysis. The 0.8mm radius stylus resulted in delamination over a range of 55 and 80N; failure over this larger range allowed easier discrimination of features due to fracture and decohesion.

Fig. 18 shows the friction coefficient and acoustic emission response during scratching of bare and coated polycarbonate, as well as an optical image of the scratch on coated polycarbonate. Unlike the bare polycarbonate which shows high friction and no acoustic emission, the coated sample shows a plateau in friction, followed by a small rise and small acoustic emission activity, then larger acoustic activity followed by another rise in friction. These plateaus can be correlated with: 1) tensile cracking of the coating at lowest loads, followed by 2) radial cracks outside the track then conformal cracking inside the track, followed by 3) decohesion of small pieces of the

coating inside the track. The large drop in acoustic emission at high loads in fig. 18, corresponds to complete removal of the coating. The fracture and decohesion behavior of hard-coatings on polycarbonate are consistent with similar effects seen on hard-coated metals and ceramics (see fig. 19). These observations were made but not fully utilized in the evaluation of coatings.

3.1.6 Abrasive wear

Abrasive wear was measured for coatings on polycarbonate, sapphire, and steel. Tests were performed at loads of 1, 2, and 4N (2.85 to 11.4kPa) in ambient atmosphere using 3 and 30μm diamond in paraffin oil on Texmet cloth. For coated polycarbonate, the RWR technique did not give satisfactory results because the polycarbonate absorbed moisture which complicated the weight loss measurements. For example, on going from vacuum storage to storage in an ambient of 50% RH a polycarbonate sample gained 500μg, which was 0.1% of its initial mass. Also, the coatings on polycarbonate occasionally chipped at the edges of the plastic, leading to accelerated wear. RWR measurements on coated sapphire and steel were straightforward and reliable. Neither diamond size nor load appeared to appreciably affect wear rate.

3.2 Coating performance

The most important results of the mechanical testing are summarized and discussed in this section.

3.2.1 IBAD Al$_2$O$_3$ coatings

Instrumented indentation showed that the Armstrong coatings increased the deformation resistance of the polycarbonate, as can be seen in fig. 20. For all four coating thicknesses shown, the coating reduced the indentor penetration depth in the early stages of loading. As coating thickness increased, the resistance to deformation increased, as would be expected. Note that the thickest coating nearly eliminated all plastic deformation of the system under the test conditions.

Over time, Armstrong altered processing parameters which resulted in increased hardness of the coatings on polycarbonate and glass, as seen in fig. 21 and Table 4. On polycarbonate, the best coatings had a hardness Hp up to 19GPa and effective elastic modulus between 30 and 40GPa. The coating hardness values on polycarbonate are a factor of two greater and the modulus values are a factor of 4 to 6 less than for IBAD and sputtered amorphous Al$_2$O$_3$ films on hard substrates

reported in the literature [Ref. 13,14]. The higher hardness may be due to optimization of the coating's mechanical properties; the lower modulus is likely due to the contribution from the underlying polycarbonate, whose modulus is about 2GPa. In fact, the modulus measurement may be interpreted as a measure of the increased surface stiffness of IBAD Al_2O_3-coated polycarbonate. Similar hardness values but higher elastic modulus values were measured on coated glass substrates.

A similar trend in critical load versus process history was observed. For example, coating adhesion to polycarbonate increased substantially after Armstrong began to monitor the ion beam current continuously during the deposition process (August 1994). Coatings prepared after August 1994 had critical load to fracture, Lc, values of 3 to 4kgf, more than double the highest Lc values ($\leq$ 1.5kgf) of coatings produced earlier in the program.

Table 4 shows the effect of changing bombardment gas species and current on coating properties while holding all other deposition conditions fixed (see SAIC report for deposition conditions). Overall, the coatings with the best performance in hardness and modulus on polycarbonate were grown under normal N_2 bombardment. It was also found that for both gas species normal bombardment produced the coatings with the best properties.

As mentioned above, the true hardness and modulus (normalized to depth over thickness) are independent of coating thickness. However, Lc generally increased as the coating thickness increased, as seen in fig. 22. The one exception, was for an 8μm thick coating which was a 4μm thick coating grown on a pre-existing 4μm coating.

The measured toughness and residual stress of the coatings on glass are summarized in Tables 5 and 6. In all cases the residual stress is compressive. The contribution to the residual stress due to differential cooling of the coating and substrate after deposition was calculated[Ref. 7]. Table 7 shows the thermal contribution to the residual stress at two different deposition temperatures; note that the thermal stress is tensile. The total residual stress is the sum of the thermal stress and the intrinsic stress (growth stress). As seen in fig. 23, the intrinsic stress of the coating is compressive and ranges between 150 and 210MPa. In general, a small compressive stress is beneficial to coating wear performance[Ref. 15].

The relative wear rates of the coatings are shown in fig. 24. The Armstrong coatings clearly wear more slowly than bare polycarbonate, but not as slowly as bare sapphire.

3.2.2 Magnetron sputtered Al_2O_3 coatings

Magnetron sputtered films on glass substrates were evaluated primarily for hardness, modulus, and critical load. The coatings grown without a good heat sink (hot) during deposition were harder and had higher Lc values than similar coatings prepared with a good heat sink (cool), as shown in Table 8. Also, the hot coatings had a ringed appearance; rings appeared directly beneath the sputter target. These regions had higher hardness and higher Lc than areas outside the ring, as seen in fig. 25. The hot coatings were harder than the Armstrong IBAD coatings (compare Table 2). Deposition at higher temperatures is expected to crystallize Al_2O_3 resulting in higher hardness and modulus [Ref. 16]; in fact, X-ray diffraction confirmed the existence of small Al_2O_3 crystallites in the hot coatings.

4. Conclusions

Methodologies were developed to evaluate mechanical properties of IBAD Al_2O_3 and other protective coatings on plastics and glass. These tests gave feedback to Armstrong that allowed them to improved processing parameters.

Table 1   Methodologies evaluated for mechanical property testing of thin (1 - 4 μm) Al$_2$O$_3$ coatings on various substrates. Comments given on limitations and important parameter.

Property tested	Method	Plastics	Glass and other stiff substrates
Hardness	Optical (Vickers)	poor; tip probes too deeply into coating	
	Optical (Knoop)	poor; distorted impressions and too deep	good; but errors at lowest loads
	Instrumented Indentation[1] (Vicker and Knoop)	good; to depths up to 30% of coating thickness on PC at depths > 0.2 μm (on polycarbonate)	
Elastic modulus	Optical (Vickers/ Knoop)	impossible	
	Instrumented Indentation (Vickers)	OK, but sensitive to elastically softer substrate at very low loads	good.
Indentation fracture and adhesion	Brale tip	good; circular and radial crack diameter	not evaluated
	Vickers	not useful in load range	good; radial cracks and decohesion
Toughness, Kc, and stress	Vickers	not used	from radial crack length
	Optical curvature	not evaluated	stress from curvature
Scratch adhesion	Spherical tip	excellent; 0.8 mm sphere better than Brale tip	poor; substrate cracked prematurely
Abrasion resistance	Polish with 3 μm and 30 μm diamond paste	unreliable; coating chips from plastic at edge; substrate absorbs moisture	excellent

[1] Fischerscope, Model H100.

TABLE 2

INDENTATION AND FRACTURE OF Al2O3 FILMS ON GLASS SUBSTRATES						
				Knoop (@ 50gf)		Vickers
Sample ID #	Deposition	Type	Thickness, (um)	Depth (um)	HK 50 (GPa)	Critical Load (kgf)
IBAD						
93-9-2 or 6	O2	Norm	1	N/A	N/A	< 0.1
93-93-9	O2	Norm	4	1.6	5.8*	< .1
93-9-14		No assist	4	N/A	N/A	< 0.1
93-9-19	O2	High	4	1.1	6.6	0.90
93-12-1	N2	Norm	2	1.5	6.3*	N/A
93-12-12	N2	Norm	4	1.2	5.4	0.70
94-1-10	O2	High	3	1.1	6.6	0.40
94-1-13	O2	High	3.8	1.1	6.5	0.50
94-2-3	N2	High	2.9	1.1	6.2	0.50
94-2-6	O2	Slow	3.6	1.2	5.5	0.05
94-3-6	N2	High	2.9	1.1	6.0	0.90
Treatments						
AR2405-Deta	N2	Normal	~4	0.9	8.7	0.70
AR2408-Deta	N2	Normal	~4	1.0	8.3	0.85
AR2415-13F	N2	Normal	~4	0.9	9.5	0.93
AR2416-13F	N2	Normal	~4	0.9	9.8	0.90
AR2423-CL	N2	Normal	~4	0.8	10.7	0.95
AR2424-CL	N2	Normal	~4	0.9	8.4	0.75
AR94-8-35-Deta	N2	Low	~4	1.1	5.7	0.40
AR94-8-36-Deta	N2	Low	~4	1.2	5.5	0.40
AR94-8-37-13F	N2	Low	~4	1.2	5.4	0.40
AR94-8-38-13F	N2	Low	~4	1.2	5.2	0.45
AR94-8-39-CL	N2	Low	~4	1.1	6.3	0.40
AR94-8-40--CL	N2	Low	~4	1.1	6.1	0.50
MAGNETRON						
AR-0104	O2		~1	1.6	5.8*	N/A
AR11-5	N2	13F	1	0.2	13.7	1.50
AR11-3	N2	clean	~1	0.9	9.0	1.20
AR052701-a	(Ar only)	13F	~1	1.1	6.1	0.30
AR052701-b	(Ar only)	clean	~1	1.0	7.0	1.00
AR052701-c	(Ar only)	Deta	~1	0.9	9.9	0.75
AR052702-a	N2	13F	~1	0.9	10.2	1.65
AR052702-b	N2	clean	~1	0.9	9.9	1.20
AR052702-c	N2	Deta	~1	0.9	9.0	1.25
AR052703-a	N2	clean	~1	0.9	8.8	1.25
AR052703-b	N2	13F	~1	0.9	9.4	1.3-1.4
AR052703-c	N2	Deta	~1	0.9	10.0	1.0-1.6
AR052704-a	N2	clean	~1	0.9	8.5	1.20
AR052704-b	N2	Deta	~1	0.9	8.8	1.60
AR052704-c	N2	13F	~1	0.9	8.4	1.40
AR2017	N2	Pulsed	2	1.0	7.5	0.70
AR0602A	N2	Pulsed	3.8	0.9	8.8	0.40

TABLE 2 cont.

INDENTATION AND FRACTURE OF Al2O3 FILMS ON GLASS SUBSTRATES						
Sample ID #	Deposition	Type	Thickness, (um)	Depth (um)	HK 50 (GPa)	Critical Load (kgf)
AR94-8-25	N2	Continuous	4			
	Inside magnet ring		4	0.6	21.2	0.6 ± 0.2
	On the magnet ring		4	0.8	12.0	0.6 ± 0.2
	Outside magnet ring		4	0.9	9.2	0.6 ± 0.2
High rate Magnetron						
13/7/94-1		"HR"	2 +	1.0	7.3	0.55
15/7/94-2		"HR"	3.2	0.9	8.7	0.65
5011307		"HR"	0.6	1.1	6.6	0.30
REFERENCE				Knoop (@ 50gf)		Vickers
SDC	Dip	primer + 123	Stand.	3.7	'0.5-1.0	< 0.1
	Dip	primer + 123	thinner	2.7	1.1	< 0.1
	Dip	primer + 123	thicker	3.0	0.8	< 0.1
	Dip	primer	- - - - - - - -	1.4	4.0	< 0.1
	Dip	123	- - - - - - - -	3.2	'0.7 - 1.0	< 0.1
Micrscope slide			- - - - - - - -	1.2	5.1	0.20
Single Crystal Sapphire			- - - - - - - -	0.8	24.2*	< 0.1

$ No Newton Rings

* Means 100gf

formulae: KHN = 14.101*L(kgf)/l^2(mm)

Depth = l/30

TABLE 3

INDENTATION AND FRACTURE OF Al2O3 FILMS ON POLYCARBONATE SUBSTRATES							
				Knoop (@ 50gf)		Brale " C "	
Sample ID #	Deposition	Type	Thickness, (um)	Depth (um)	HK 50 (GPa)	Critical Load (Kgf)	Cracking Type
IBAD							
93-9-8	O2	Normal	4	5.1	0.3	0.10	N/A
93-9-15	- - - -	No Assist	4	5.4	0.3	0.10	N/A
93-9-23	O2	High	4	3.9	0.5		N/A
93-9-13	N2	Normal	4		N/A		N/A
931213	N2	Normal	4			1.20	Jagged Lat.**
931218	N2	Normal	2.6	5.1	0.2	0.35	Jagged Lat.
940109	O2	High	3	5.3	0.3	0.25	Jagged Lat.
940301	N2	High	5.00	3.9	0.5	0.35	Jagged Lat.
940330	N2	Normal	3.6	3.9	0.5	0.65	Jagged Lat.
940413	N2	Standard	3.8	5.4	0.3	0.20	Jagged Lat.
940452	N2	Normal	3.2	5.0	0.3	0.20	Jagged Lat.
940604	N2	Normal	4	3.9	0.5	1.50	Jagged Lat.**
Treatments							
AR2312-O	N2	Normal	~4	2.8	0.9	3.50	Jagged Lat.**
AR2325-Cy	N2	Normal	~4	3.7	0.6	4.00	Jagged Lat.**
AR2348-DT-C	N2	Normal	~4	3.7	0.5	3.00	Jagged Lat.**
AR2351-MeH	N2	Normal	~4	3.4	0.6	3.75	Jagged Lat.**
AR2363-13F	N2	Normal	~4	4.0	0.5	3.00	Jagged Lat.**
940850-13F	N2	Normal	~4	4.0	0.5		Jagged Lat.**
940852-DETA	N2	Normal	~4	3.5	0.6		Jagged Lat.**
940855-NH	N2	Normal	~4	3.3	0.7		Jagged Lat.**
940857-O	N2	Normal	~4	3.6	0.6		Jagged Lat.**
940859-Cy	N2	Normal	~4	4.1	0.5		Jagged Lat.**
940860-CM2-OL	N2	Normal	~4	3.5	0.6		Jagged Lat.**
	N2	Normal	~4				Jagged Lat.**
	N2	Normal	~4				Jagged Lat.**
Face Shields							
94-7-4	N2	Norm	???	6.6	0.2		
94-7-6	N2	Norm	???	5.9	0.2		
Bare			???	8.2	0.1		
	MAGNETRON						
AR2014			2	4.5	0.4	0.80	Smooth/Jagg.
AR94-8-25			2	6.0	0.2		
AR94-8-25			2	4.7	0.3		
REFERENCE							
Tuffak	CM2 polysiloxane	STD	5	4.5	0.4	0.80	Smooth Lat.
SDC on PC	Silica	STD	app. 3.8	6.1	0.3	0.20	Radial
Back side	uncoated		???	7.3	0.1	'- - - - - - - - - - -	- - - - - - - - - - - -
SDC on Acrylic	Silica	STD	app. 3.8	4.7	0.3	0.80	Smooth/radial**
Bare Acrylic	uncoated		???	6.4	0.2	'- - - - - - - - - - -	- - - - - - - - - - - -
1/16" polycarbonate							
Vueguard			???	4.51	0.37		
Panel graphic			???	6.24	0.19		
Bare			???	7.62	0.13		
FIBERGLASS							
931215	N2	Normal	2.6	'- - - - - - - -	'- - - - - - - -	0.20	

#Run Date

formulae: KHN = 14.101*L(kgf)/l^2(mm)

** Different criteria

TABLE 4

t_f (μm)	L_c (kgf)	K_3 (MPa-m $^{1/2}$)		σ_f (MPa)	
		2 kgf	4 kgf	2 kgf	4 kgf
0	0.1	0.52 ± 0.04	0.49 ± 0.02	(no film, no stress)	
1.2	0.4	0.65 ± 0.01	0.61 ± 0.02	-33 ± 5	-24 ± 2
2.5	0.4	0.70 ± 0.02	0.67 ± 0.04	-28 ± 3	-32 ± 6
4.1	0.7	0.84 ± 0.04	0.88 ± 0.04	-80 ± 13	-94 ± 10
6.6	0.6	0.93 ± 0.06	0.83 ± 0.02	-90 ± 15	-82 ± 12
8.0	0.1	1.21 ± 0.2	0.92 ± 0.06	-136 ± 40	-84 ± 11

Critical load, toughness, K_3, and film stress, σ_f of IBAD Al_2O_3 coatings on annealed glass, from Vickers indentation measurements. Toughness and film stress calculated at 2 loads: 2 and 4 kfg. Method of Gruninger, et al.

M.F. Gruninger, B.R. Lawn, E.N. Farabaugh and J.B. Wachtman, Jr., J. Am. Ceram. Soc. 70 (1987) 344.

TABLE 5   HARDNESSES, ELASTIC MODULUS, & ELASTIC WORK VALUES FOR IBAD AL2O3-COATED POLYCARBONATE AND REFERENCE SAMPLES.   VICKERS DATA TAKEN AT L = 25 mN.

Bombardment	t (μm)	E (Gpa)	H_p (Gpa)	We%	H_u (Gpa)	d (μm)	t/d
None	5.5	39 ± 1.3	11.5 ± 0.7	74	2.0 ±	0.6	0.11
Norm O2	4	35.8 ± 1.2	12.3 ± 0.8	75	1.8 ±	0.6	0.16
Low O2	5	40.3 ± 1	10.5 ± 0.4	69	2.1 ±	0.6	0.12
High O2	3.5	22.9 ± 0.6	6.7 ± 0.4	72	1.2 ±	0.8	0.23
Norm N2	3.6	38 ± 3.1	18.6 ± 2.9	83	1.6 ±	0.7	0.18
Norm N2	3.6	33.7 ± 3.8	17.0 ± 3.7	84	1.4 ±	0.7	0.20
High N2	3	27.1 ± 1.2	16.4 ± 1.4	85	1.1 ±	0.8	0.28
Norm N2	4.1	39.9 ± 0.8	16.7 ± 0.6	82	1.8 ±	0.6	0.15
polycarbonate		2.95 ±	0.2 ±		0.1 ±	2.6	N/A
sapphire		370 ± 35	30.4 ± 2.4		13.4 ± 4	0.2	N/A

TABLE 6

Measured curvature, R, and coating stress, σ_f, of Armstrong IBAD Al_2O_3 films of glass coverslip.			
CSD#	Thickness, t_f (μm)	R (m)	Stress, σ_f (MPa)
95-1-22	1.2	-(4.9 ± 5)	-121 ± 120
95-1-39	2.5	-(4.5 ± 7)	-64 ± 100
94-12-2	4.1	-1.1	-163
94-12-7	6.6	-(0.78 ± 0.10)	-138 ± 20

using the following values:

$E_s^* = 74.5$ GPa; $\nu_s = 0.22$; $t_s = 0.21$ mm
* data supplied by Fisher Scientific, 95-01-27.

RESULT: COATINGS ARE COMPRESSIVE.

NOTE: Large errors in measured R due to assymetric "bulge" in glass: probably our fault for assuming glass was symmetrically flat before deposition.

TABLE 7

UPDATED CALCULATION:

Calculated thermal stresses in Al_2O_3 coatings on glass		
Thermal Coef. Expansion, α_s, (1 x 10^{-6})	Deposition Temperature, (°C)	
	80	120
7.4*	30 MPa	53 MPa

* data supplied by Fisher Scientific, 95-01-27.

using the following values for Al_2O_3:
$\alpha_f = 8.5$ x 10^{-6}; $E_f = 400$ GPa; $\nu_f = 0.24$; Final temperature: 23°C

RESULT: THERMAL EXPANSION LEAVES COATINGS IN TENSION.

Table 8 *Mechanical properties of aluminum oxynitride films deposited cool and hot are compared with reference materials*

	Hp (GPa)	Hu (GPa)	E (GPa)	Lc (gf)	% N*
Si(111)	19	7.8	190	<100	-
Sapphire	39	15	400	<100	-
Glass	9.2	3.7	83	200	-
Hot deposition#					
AR11-01	38	8.4	180	2500	5
AR11-05	30	7.4	160	1700	15
AR20-11	21	6.2	130	1400	10
AR20-13	24	6.2	140	na	10
AR20-08	19	5.5	110	1500	10
Cool deposition					
AR02-19	9	3.9	85	200	20
AR02-17	8.6	3.8	86	<100	20
AR02-21	8.9	4	89	<100	20
AR02-22	9.7	4.3	95	<100	20
AR02-20	8.5	3.8	87	<100	10
AR02-18	10	4	88	100	10

*Percent nitrogen in gas mixture during sputter deposition
#Measurements performed within ring

References

1. H.M. Pollock, D. Maugis and M. Barquins, in Microindentation Techniques in Materials Science and Engineering, (eds.) P.J. Blau and B.R. Lawn (ASTM, Philadelphia, PA, 1986) p. 47.

2. M.A. Meyers and K.K. Chawla, Mechanical Metallurgy (Prentice-Hall, New Jersey, 1984) Chapter 17.

3. J.L. Loubet, J.M. Georges, and G. Meille, in Microindentation Techniques in Materials Science and Engineering, (eds.) P.J. Blau and B.R. Lawn (ASTM, Philadelphia, PA, 1986) p. 72.

4. B. Lawn, Fracture of Brittle Solids, (Cambridge Univ. Press, Cambridge, 1993) Chapters 7 and 8.

5. P.C. Jindal, D.T. Quinto and G.J. Wolfe, Thin Solid Films, 154 (1987) 361.

6. M.F. Gruninger, B.R. Lawn, E.N. Farabaugh, and J.B. Wachtman Jr., J. Amer. Ceram. Soc., 70 (1987) 344.

7. K.L. Chopra, Thin Film Phenomena, (McGraw-Hill, New York, 1969) p. 269.

8. P.A. Steinmann, Y. Tardy and H.E. Hintermann, Thin Solid Films, 154 (1987) 333.

9. P.J. Burnett and D.S. Rickerby, Thin Solid Films, 154 (1987) 403.

10. R.N. Bolster and I.L. Singer, ASLE Trans., 24 (1981) 526.

11. R.N. Bolster and I.L. Singer, in Mechanical Properties, Performance, and Failure Modes of Coatings, (eds.) T.R. Shives and M.B. Peterson, (Cambridge University Press, Cambridge, 1984) p. 201.

12. I.L. Singer, R.N. Bolster, H.M. Pollock and J.D.J. Ross. Surf. Coat. Technol., 36 (1988) 531.

13. C.A. Ross and J.J. Barrese, in Mat. Res. Soc. Symp. Proc., 308, (eds.) P.H. Townsend, T.P. Weihs, J.E. Sanchez, Jr and P. Borgesen, (MRS, Pittsburgh, 1993) p. 595.

14. B.N. Lucas and W.C. Oliver, Mat. Res. Soc. Symp. Proc., 239, (MRS, Pittsburgh, 1992) 337.

15.   K. Holmberg and A. Matthews, <u>Coatings Tribology</u>, (Elsevier, Amsterdam, 1994) p. 86.

16.   R.V. Smilgys, E. Takamura, I.L. Singer, S.W. Robey, and D.A. Kirkpatrick, in Mat. Res. Soc. Symp. Proc. (MRS, Pittsburgh, 1995) in press.

The two most common microindentation tests are the Knoop and Vickers tests. The Knoop indenter is an elongated pyramid, shown in Fig. 1 The hardness is obtained from the surface area of the impression:

$$KHN = \frac{14.228P}{d^2}$$

where P is the load of kgf and d is the length of major diagonal, in mm. The ratio between the dimensions of the impression is

$$h/w/\ell = 1:4.29:30.53$$
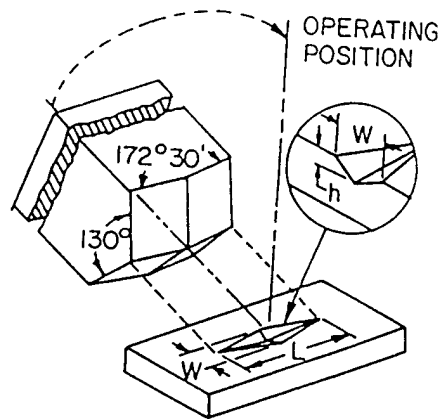
Figure 1 Some of the details of the Knoop indenter, together with its impression.

Feature	Vickers	Knoop
Factor for computing hardness number	1854 (Eq. 2)	14229 (Eq. 3)
Recommended g—f range, approx.	200–15000	25–1000
Depth of indentation, t in μm	$d_1/7$	L / 30
g—f ratio to obtain the same t $\approx$ 2/5, e.g.	200 g—f	500 g—f
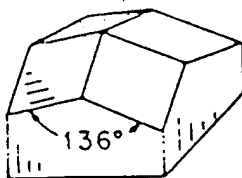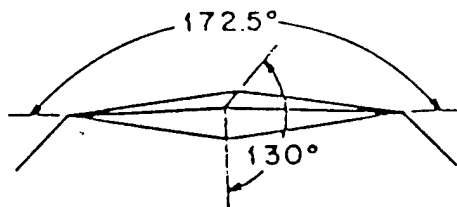
Fig. 2. (a) Vickers and (b) Knoop hardness indenters.
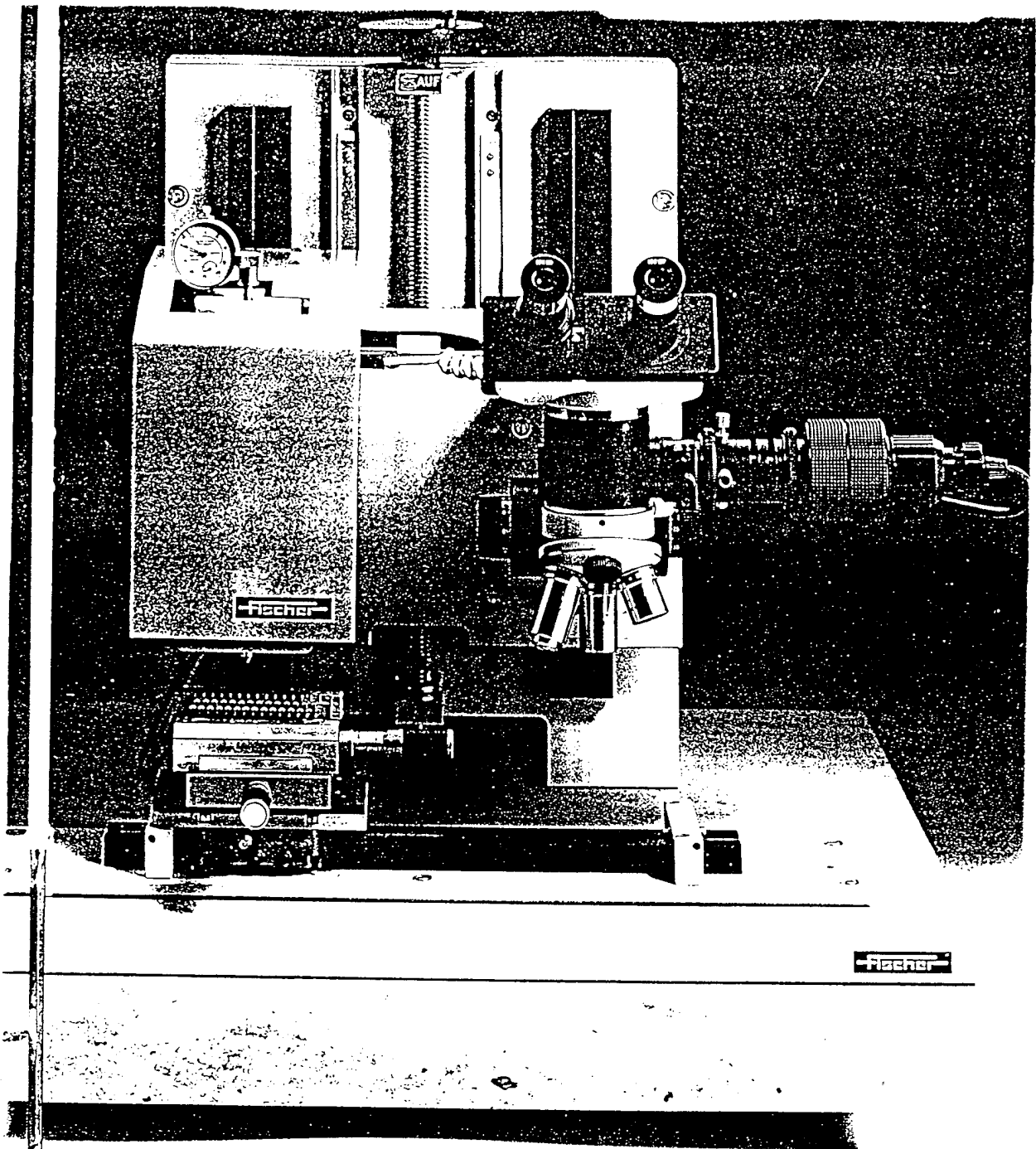
Fig. 3 Fischerscope H100

Fig. 4
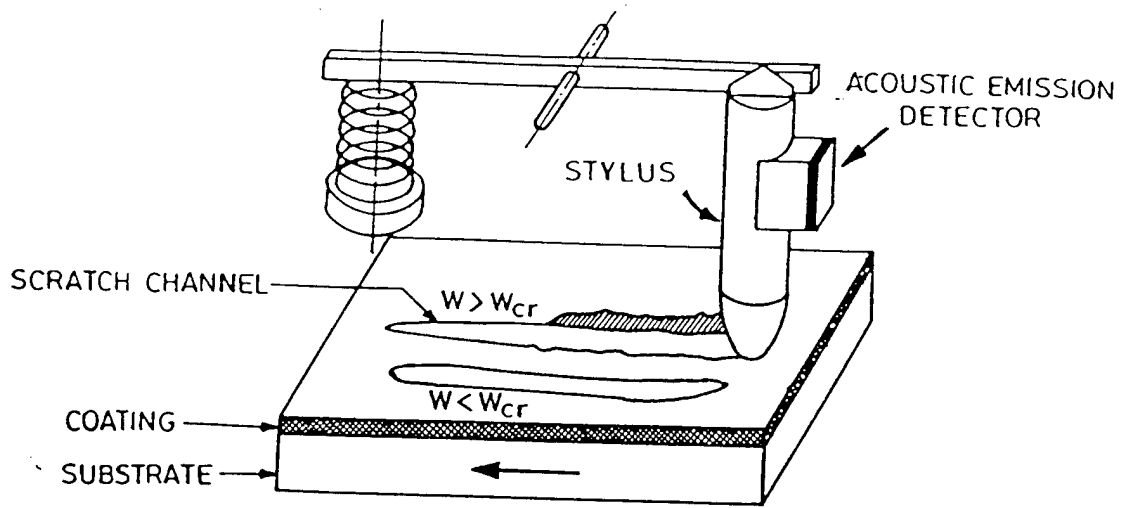
4a) Schematic illustration of the scratch method for adhesion
    measurement.

BHARAT BHUSHAN AND B.K. GUPTA,   HANDBOOK OF TRIBOLOGY
    Materials, Coatings, and Surface Treatments, 1991,
    p. 15.55
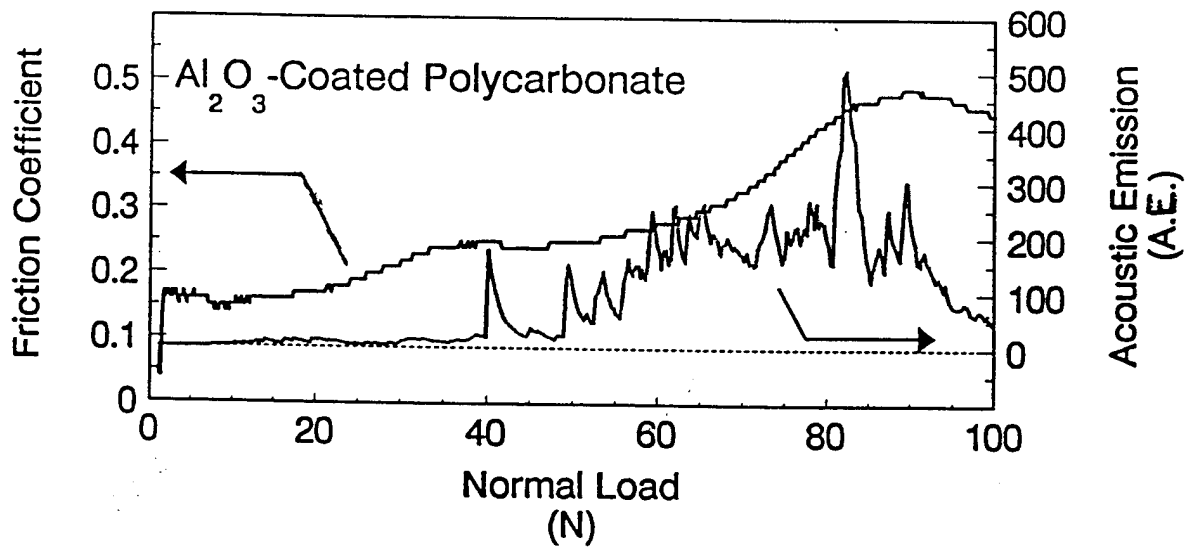
4b) Typical Acoustic Emission & Friction Coefficint load signal.

WEAR RATES OF THIN COATINGS ($<<\mu m$)
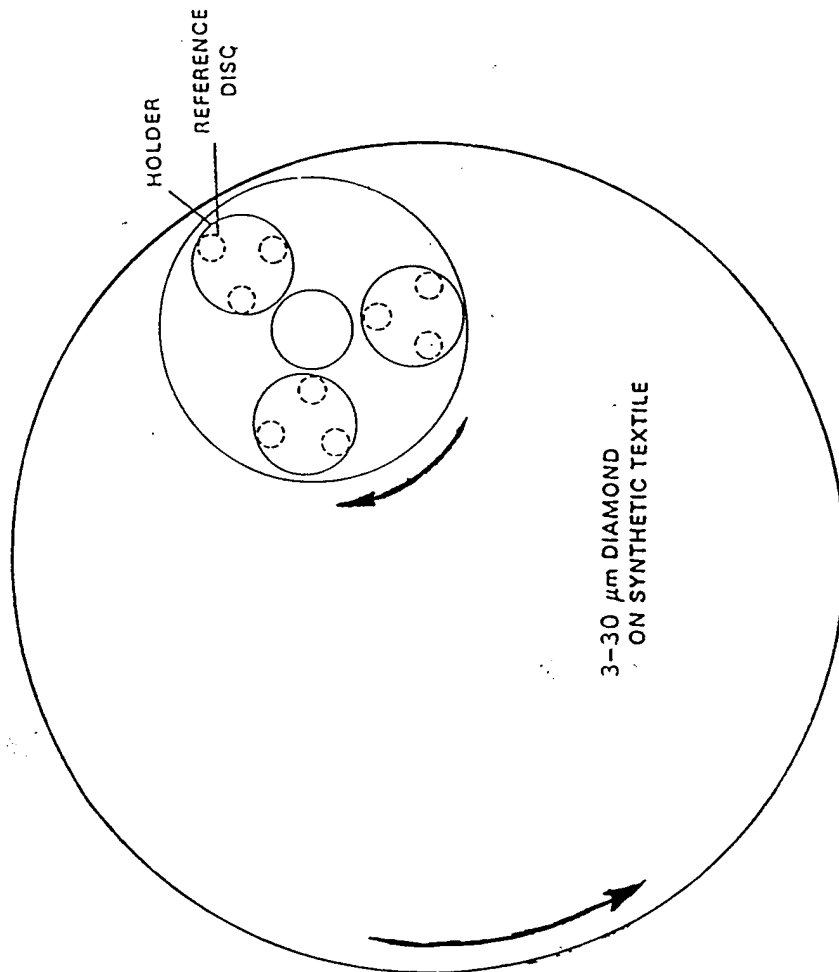
ABRASION RESISTANCE DURING POLISHING:

o weight loss $\longrightarrow \delta M$ (μg)

o depth $= \delta M/(\mathcal{S} A)$ (nm)
   $\mathcal{S}$ is density
   A is area

o wear resistance $(\rho A/\delta M)$

o Relative Wear Resistance (RWR)

$$\frac{(\rho A/\delta M)_{Coating}}{(\rho A/\delta M)^{Reference}} = (RWR)$$

HOLDER

REFERENCE DISC

3–30 μm DIAMOND
ON SYNTHETIC TEXTILE

Fig. 5   Abrasive wear apparatus

Fischerscope H100
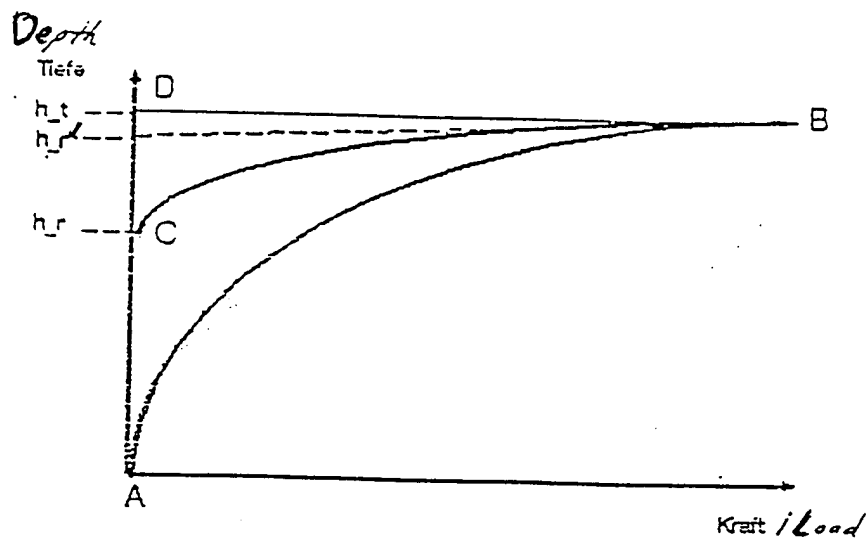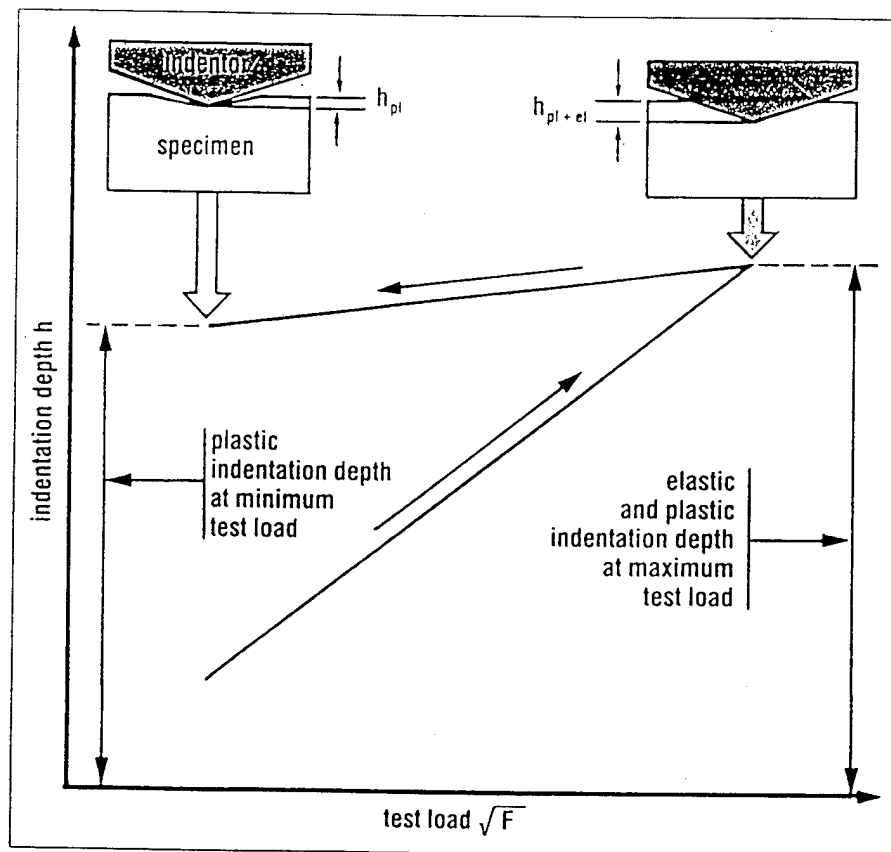
Fig. 6

CRITICAL LOAD FOR CRACKING
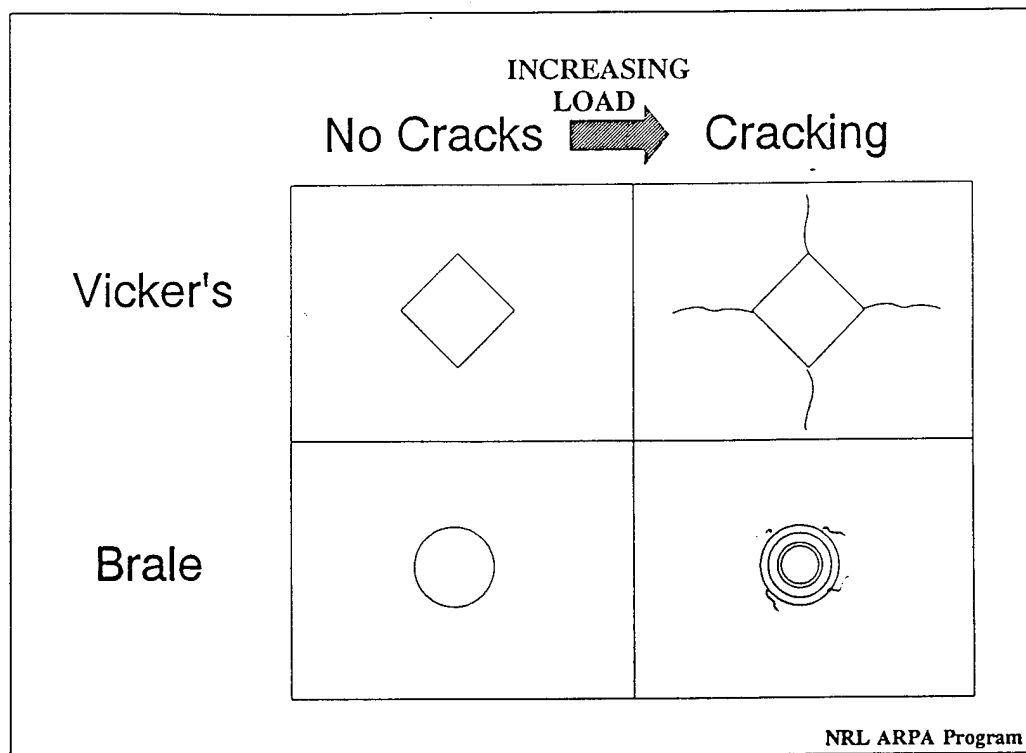
Fig. 7

VICKERS INDENTS IN IBAD Al$_2$O$_3$-COATED GLASS
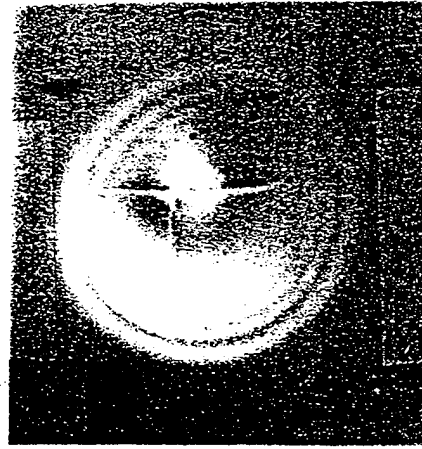
[40x]
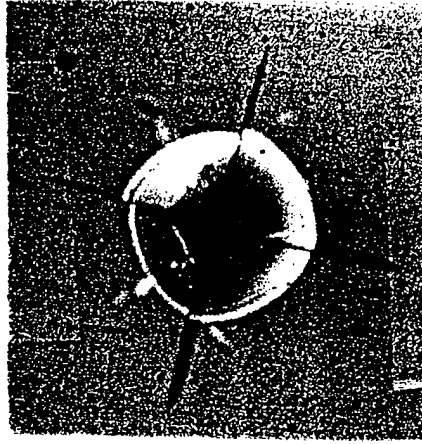
[10x]

Fig. 8

Newton's rings appear around indents at the first sign of radial cracks. The rings indicate "lift-off" of the coating from the glass. At L$_c$, radial crack lengths are less than the ring diameter. At higher loads, the radial cracks extend beyond the rings, i.e., into coated areas of the glass.

Fig. 9

CRACK PATTERNS ON COATED PC: NOMARSKI PHOTOS
Rockwell diamond (R_c = 0.2 mm) at Loads = 0.6 and 1.0 kgf

IBAD Al$_2$O$_3$

TEXSTAR ITO/Au

0.6 kgf

50 μm
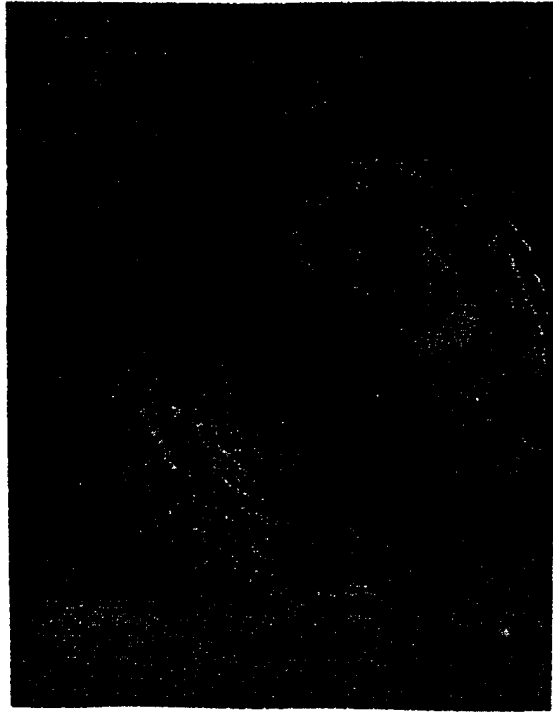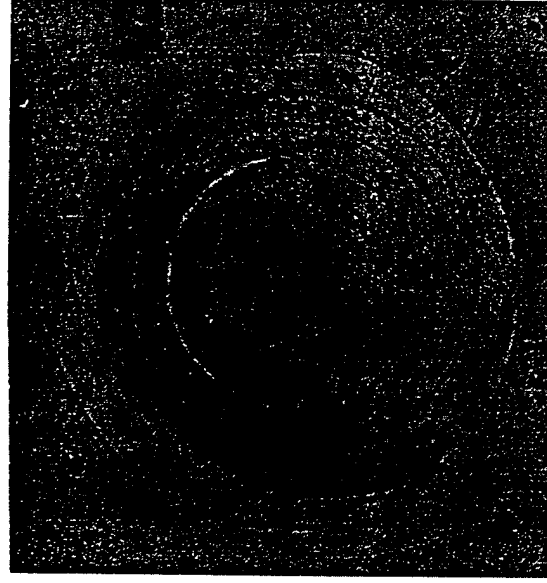
1.0 kgf

100 μm
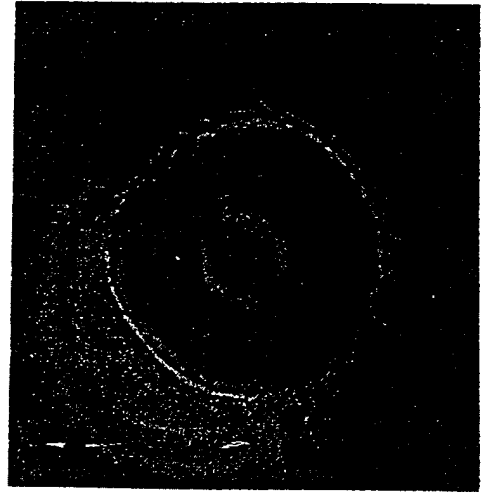
Fig. 10

Critical Load, Coated Polycarbonate Brale Indentor, (0.2mm)

Legend:
- ─X─ 6.6 um (94-12-16)
- ─□─ 4.1 um (94-12-15)
- ─◆─ pc solo
- ─●─ ITO-Au/PC
- ─■─ Al2O3/ITO-Au/PC (94-11-6)

Y-axis: Maximum Crack Diameter (um)

X-axis: Load (kgf)
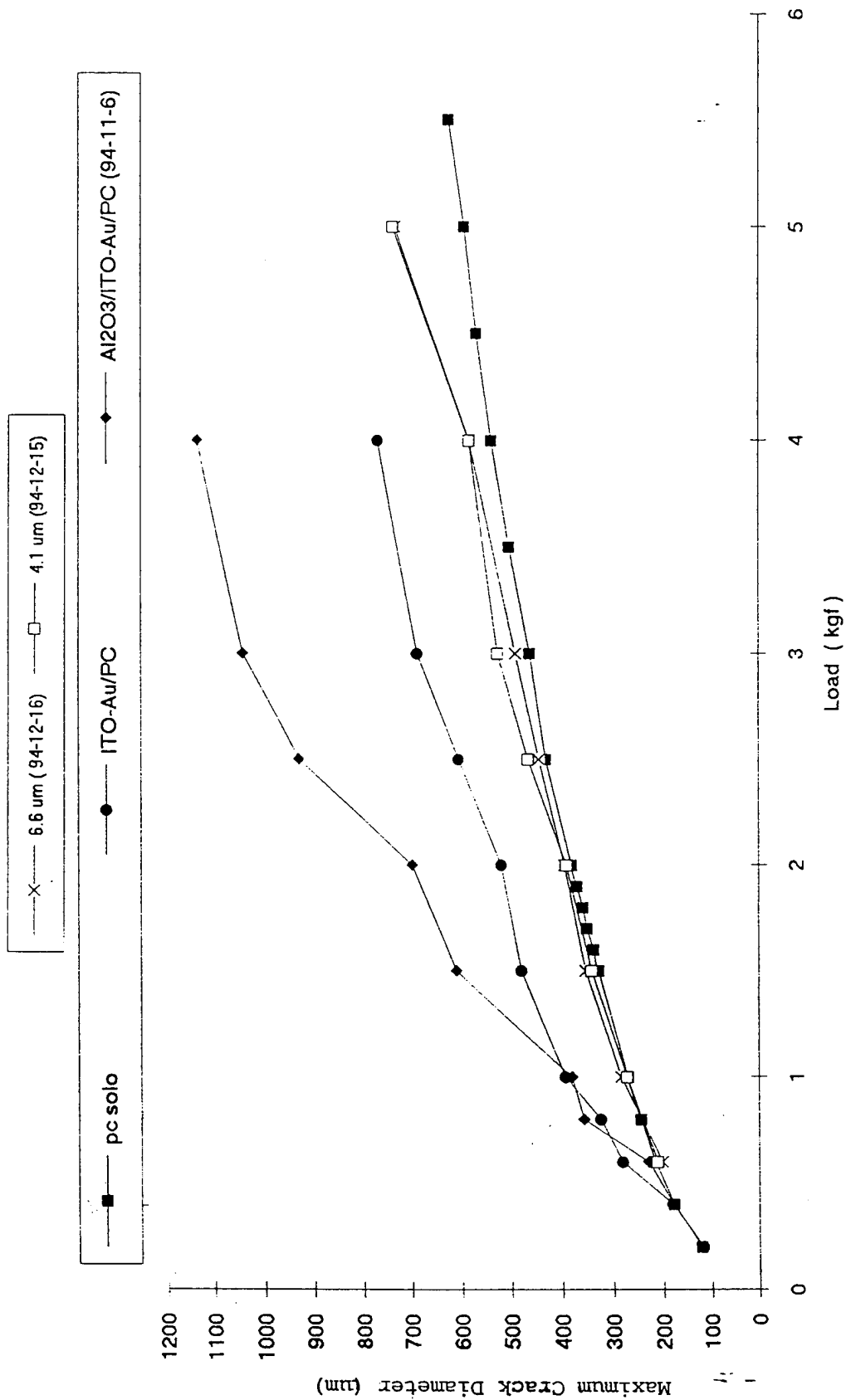
Fig. 11
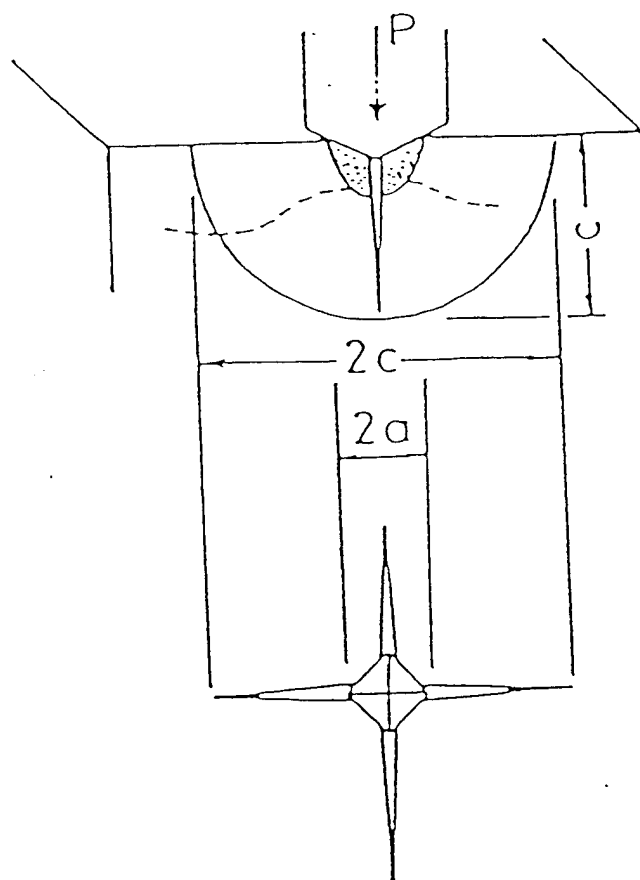
INDENTATION FRACTURE TOUGHNESS

$$K_C = 0.016 \times \left(\frac{E}{H}\right)^{1/2} * \left(\frac{P}{C}\right)^{3/2}$$

E — ELASTIC MODULUS
H — HARDNESS
P — LOAD
c — CRACK LENGTH

B.R. Lawn, A.G. Evans and D.B. Marshall, J. Amer. Ceram. Soc., 63 (1980) 574.
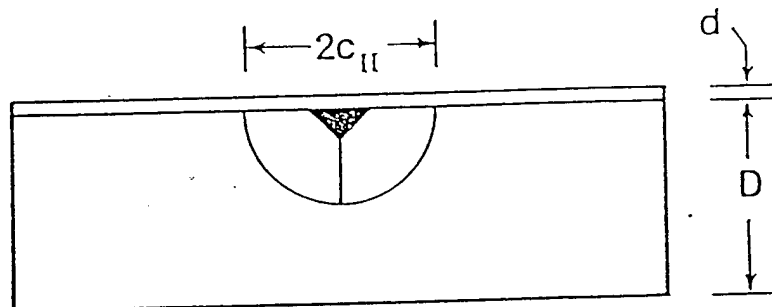
G.R. Antis, P. Chantikul, B.R. Lawn and D.B. Marshall, J. Amer. Ceram. Soc. 64 (1981) 533.

Fig. 12

(A) State I: Uncoated/Indented
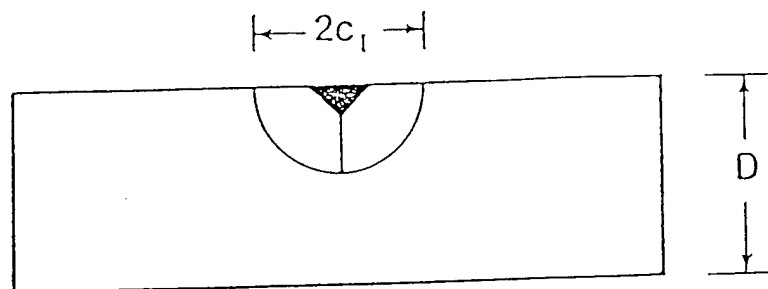
(B) State II: Indented/Coated
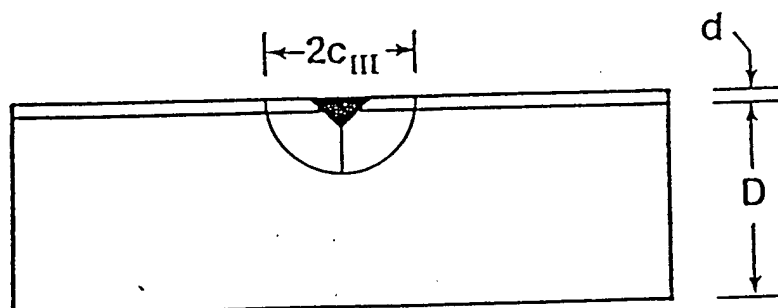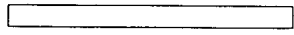

(C) State III: Coated/Indented

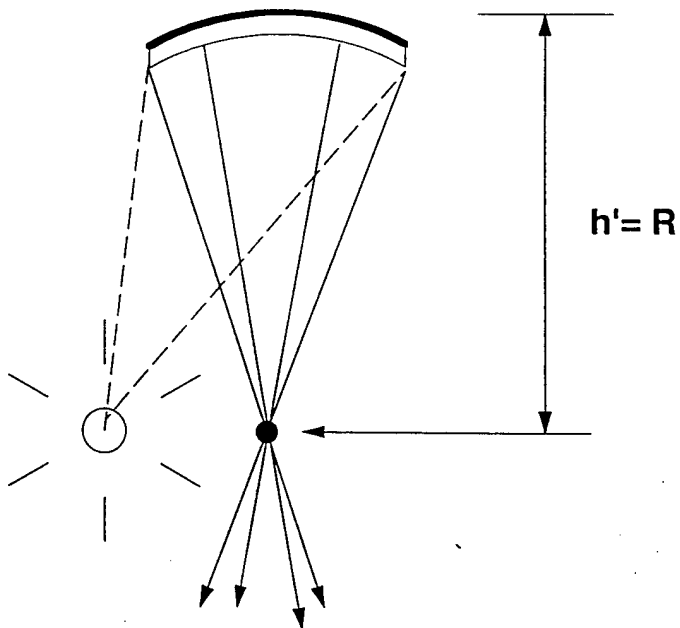M.F. Gruninger, B.R. Lawn, E.N. Farabaugh and J.B. Wachtman, Jr.,
J. Am. Ceram. Soc. : 70 (1987) 344.

Fig. 13

Stresses on Coated Wafer

Plain Wafer

Coating in Tension

Coating in Compression

Measurement of Curvature (R)

h'= R

3 Knoop Hardness Measurements
on 4.1 um IBAD film on glass

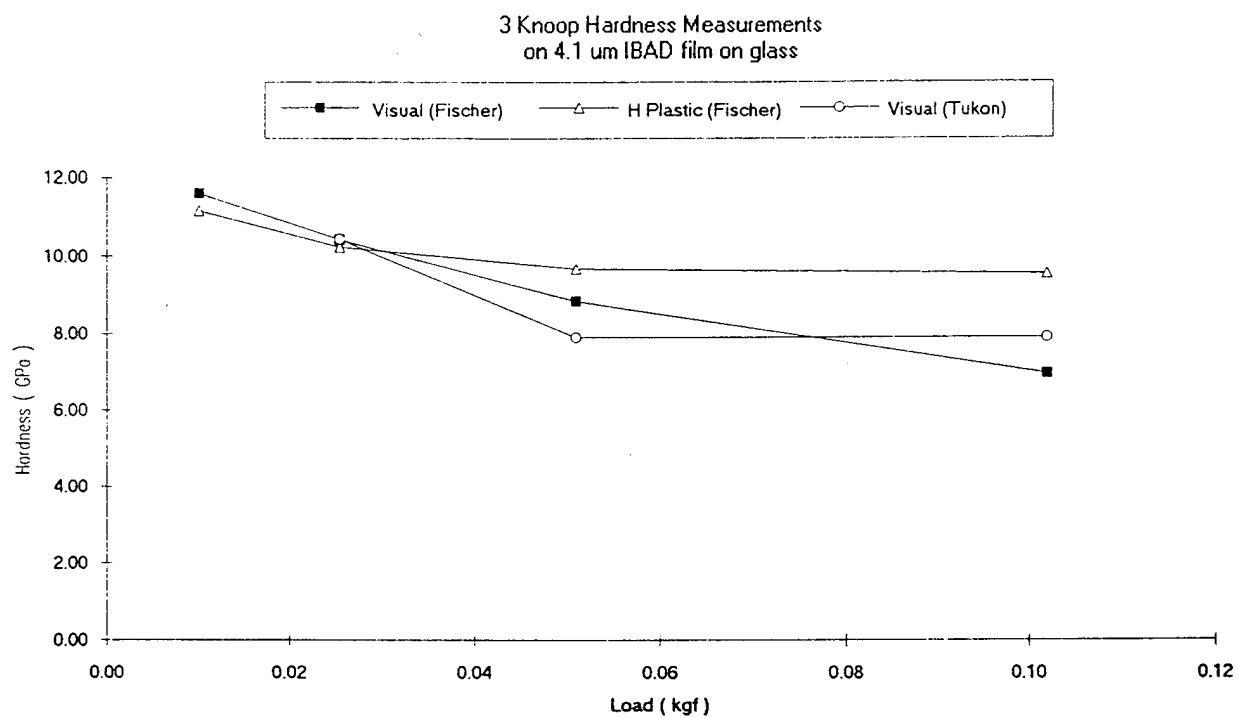| ■ Visual (Fischer) | △ H Plastic (Fischer) | ○ Visual (Tukon) |

Hardness (GPa)

Load (kgf)

Fig.14

Comparison between standard indentation and instrumented indentation

Fig. 15

Plastic Hardness vs Normalized Depth
IBAD Alumina on Polycarbonate, Vickers Indentor

Plastic Hardness vs Normalized Depth
IBAD Alumina on Polycarbonate, Knoop Indentor

Fig. 16

Elastic Modulus vs Normalized Depth
IBAD Alumina on Polycarbonate, Vickers Indentor

Film Thickness, μm
-×- 1.2   -▽- 2.5   -□- 4.1   -△- 6.6

Elastic Modulus vs Normalized Depth
IBAD Alumina on Polycarbonate, Knoop Indentor

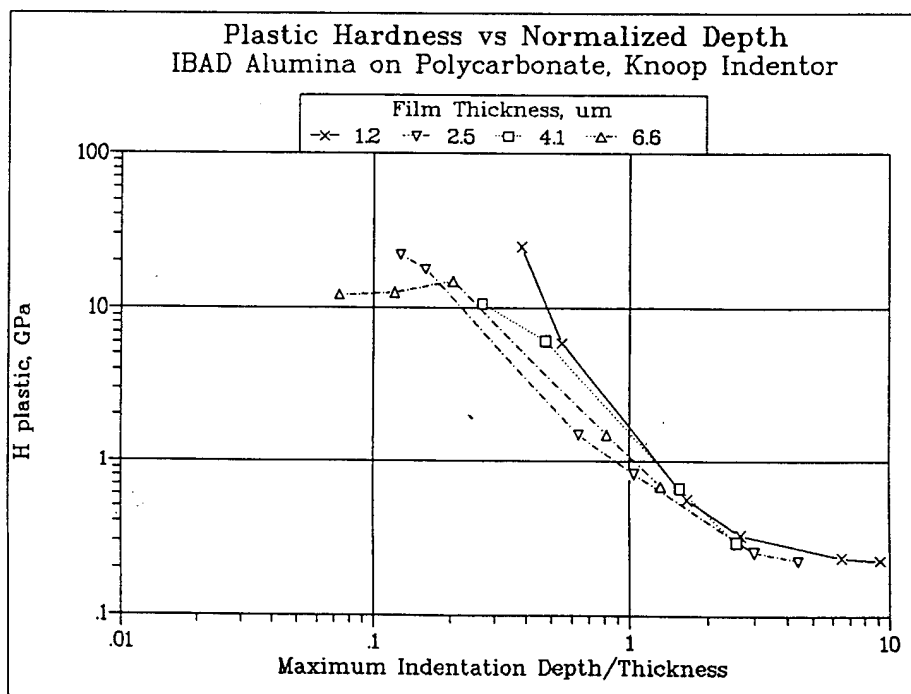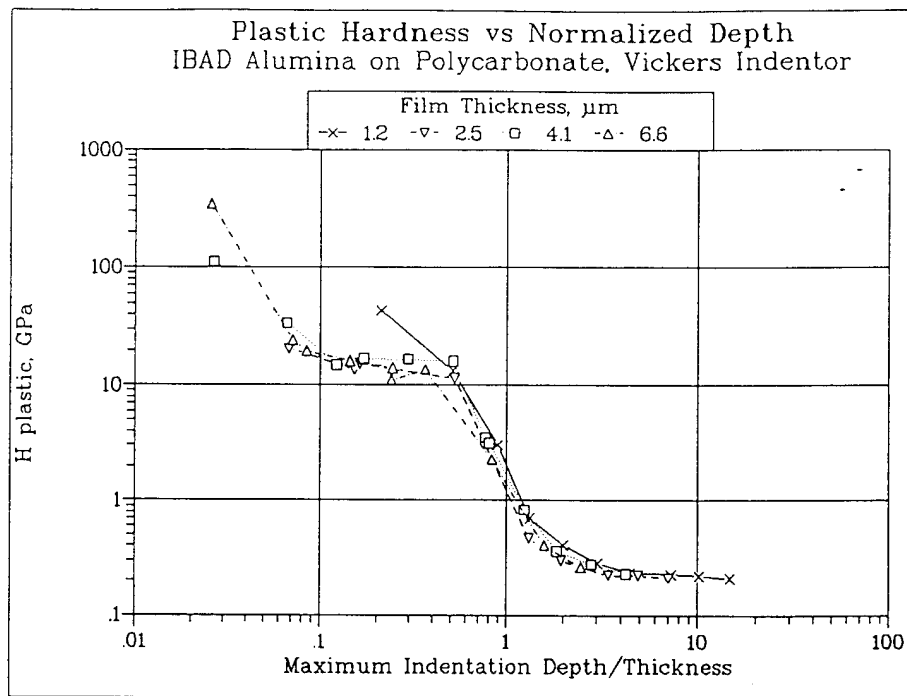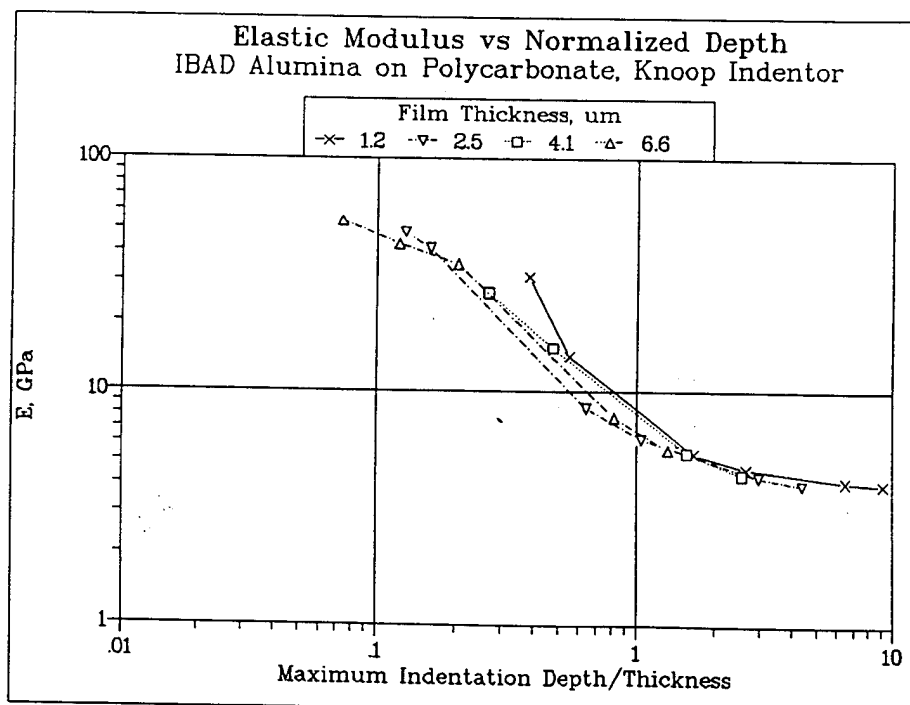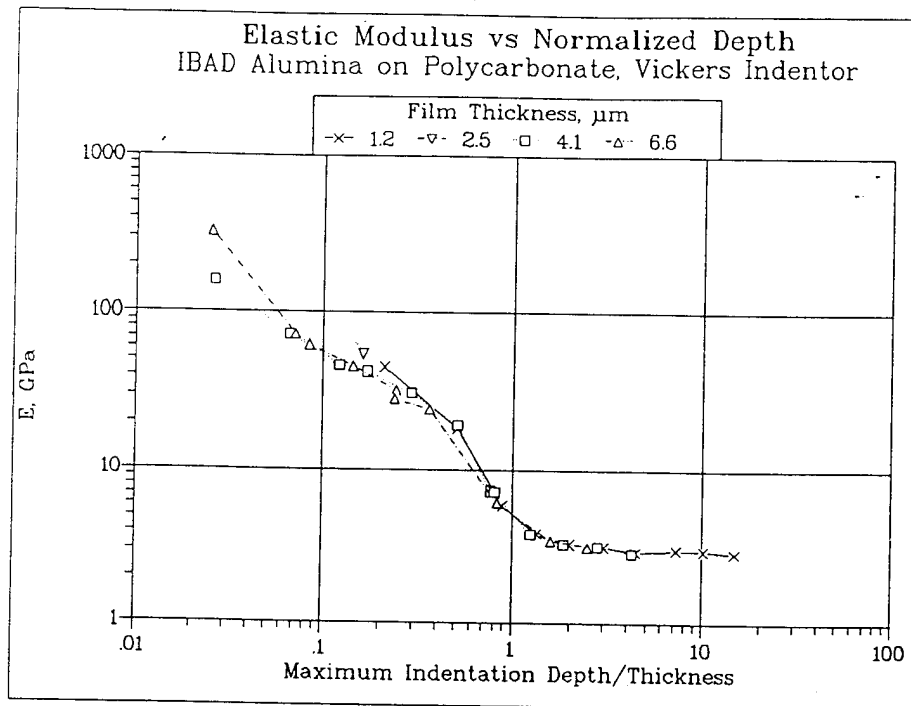Film Thickness, um
-×- 1.2   -▽- 2.5   -□- 4.1   -△- 6.6

Fig.17

Al$_2$O$_3$ ON POLYCARBONATE

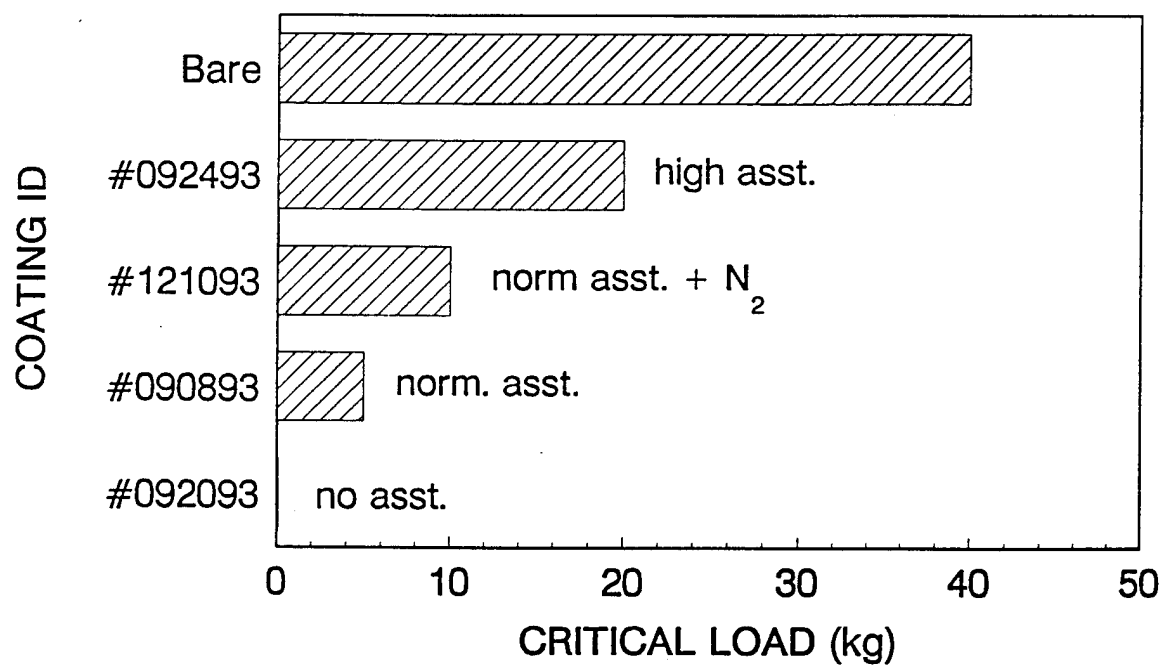## CRITICAL LOAD FOR CRACK FORMATION
(Vicker's Indentation)

Fig. 18

SCRATCH TEST RESULTS

Bare Polycarbonate

Al_2O_3-Coated Polycarbonate

Normal Load (N)

PHOTO OF SCRATCH TRACK

500 μm

Tensile Cracks

Radial Cracks

Decohesion

250 μm

250 μm
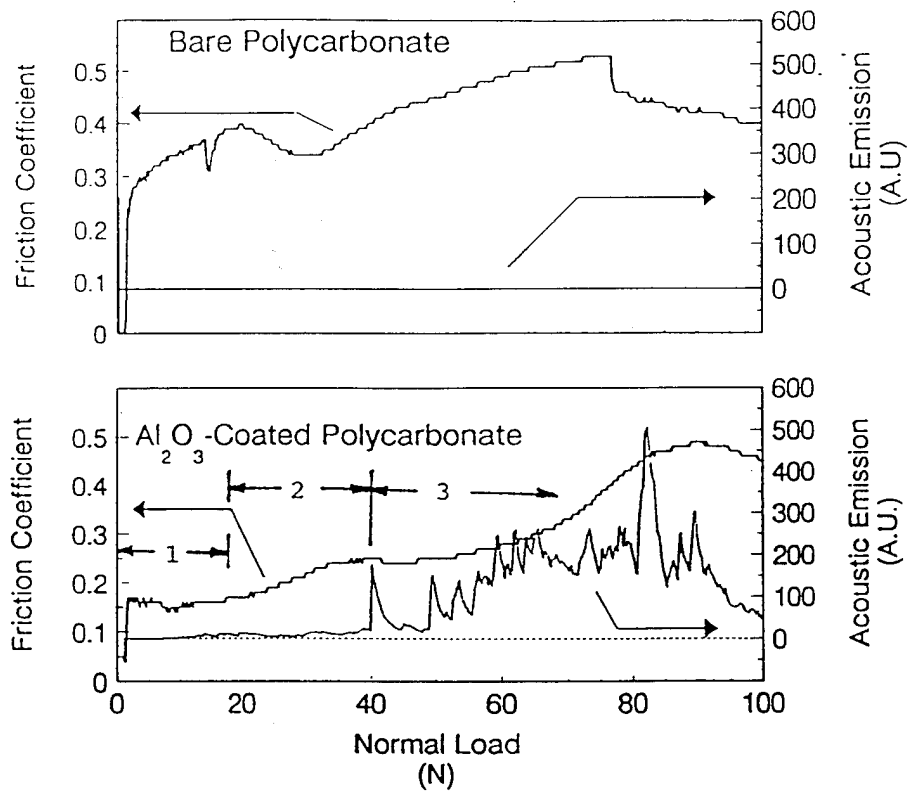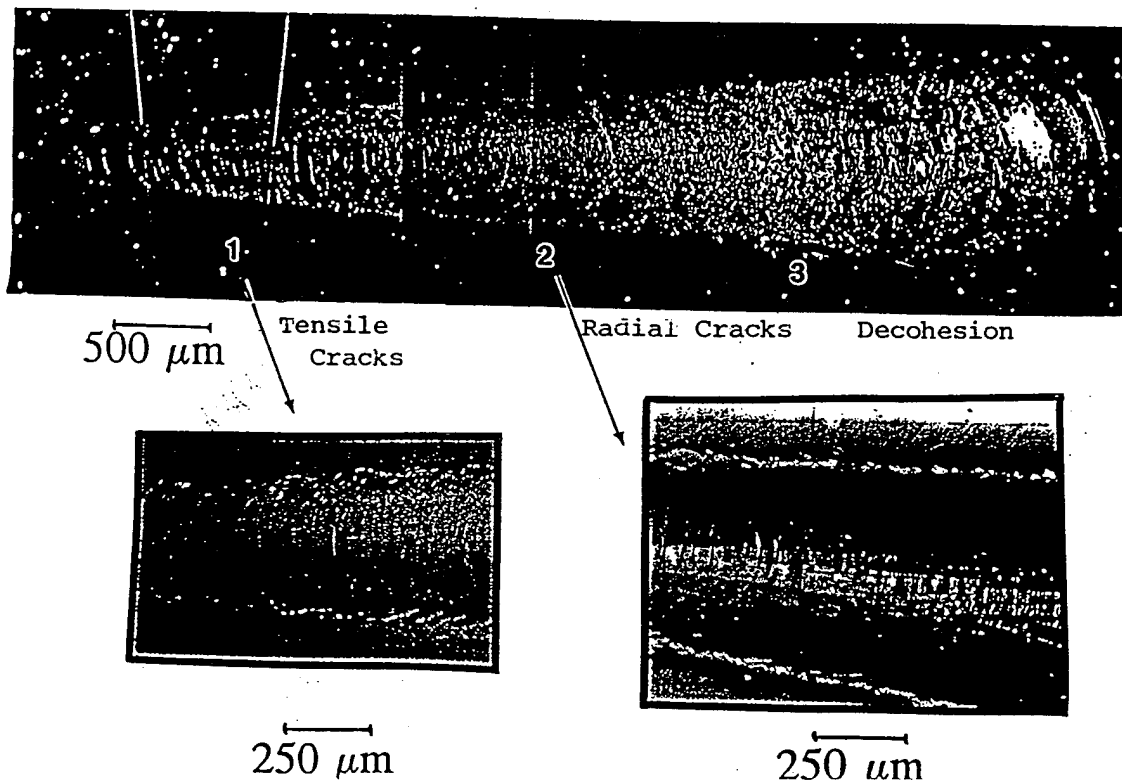
Fig. 19

THE RELATIONSHIP BETWEEN HARDNESS AND SCRATCH ADHESION

(a) — Complete adhesion failure

(b) — Local adhesion failure

(c) — Crack forms at slider contact

Adherent coatings:

(d) — P.D. substrate bending failure

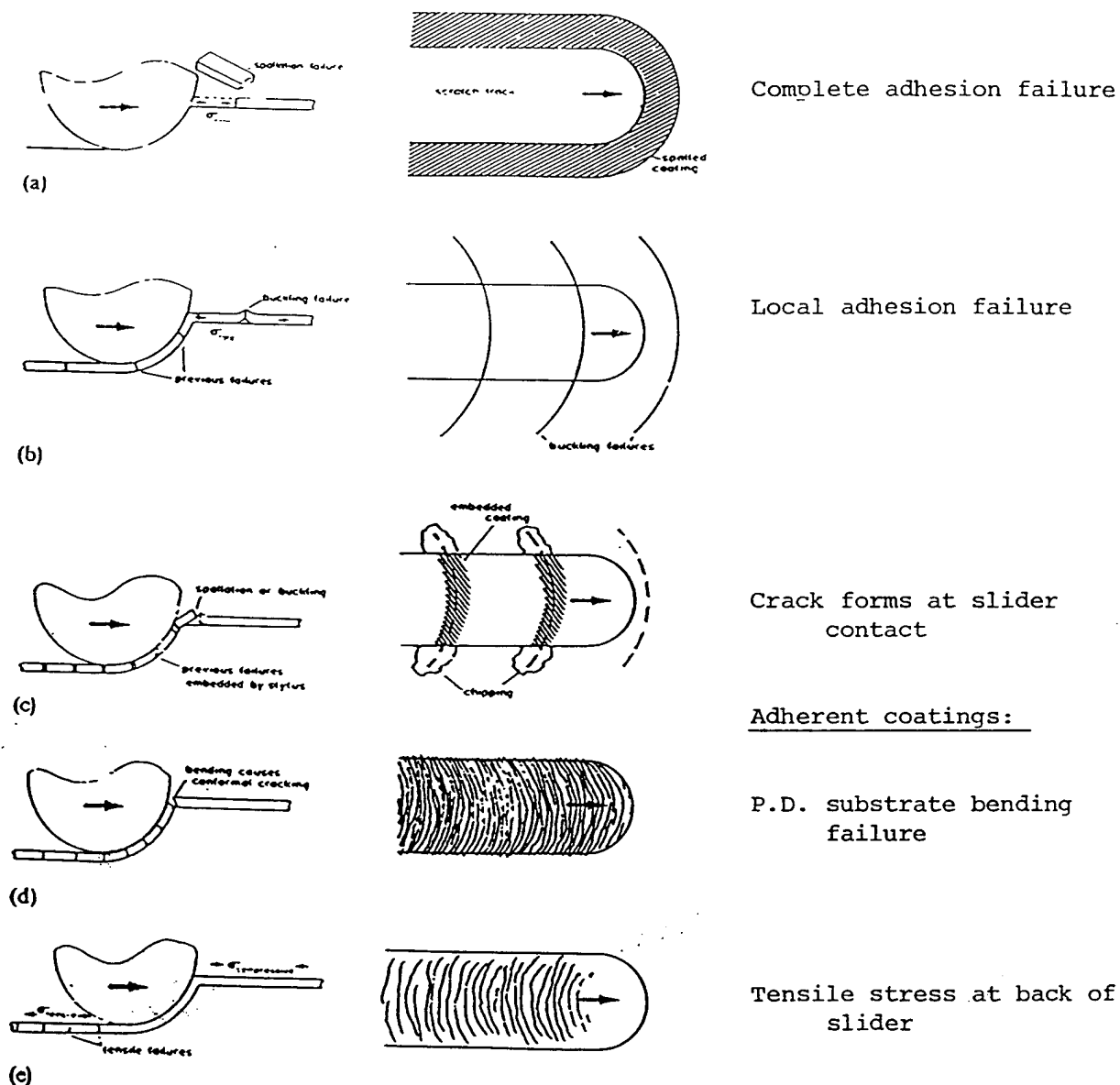(e) — Tensile stress at back of slider

Fig.   Schematic representation of coating failure modes in the scratch test in profile and plan views: (a) spalling failure; (b) buckling failure; (c) chipping failure; (d) conformal cracking; (e) tensile cracking.
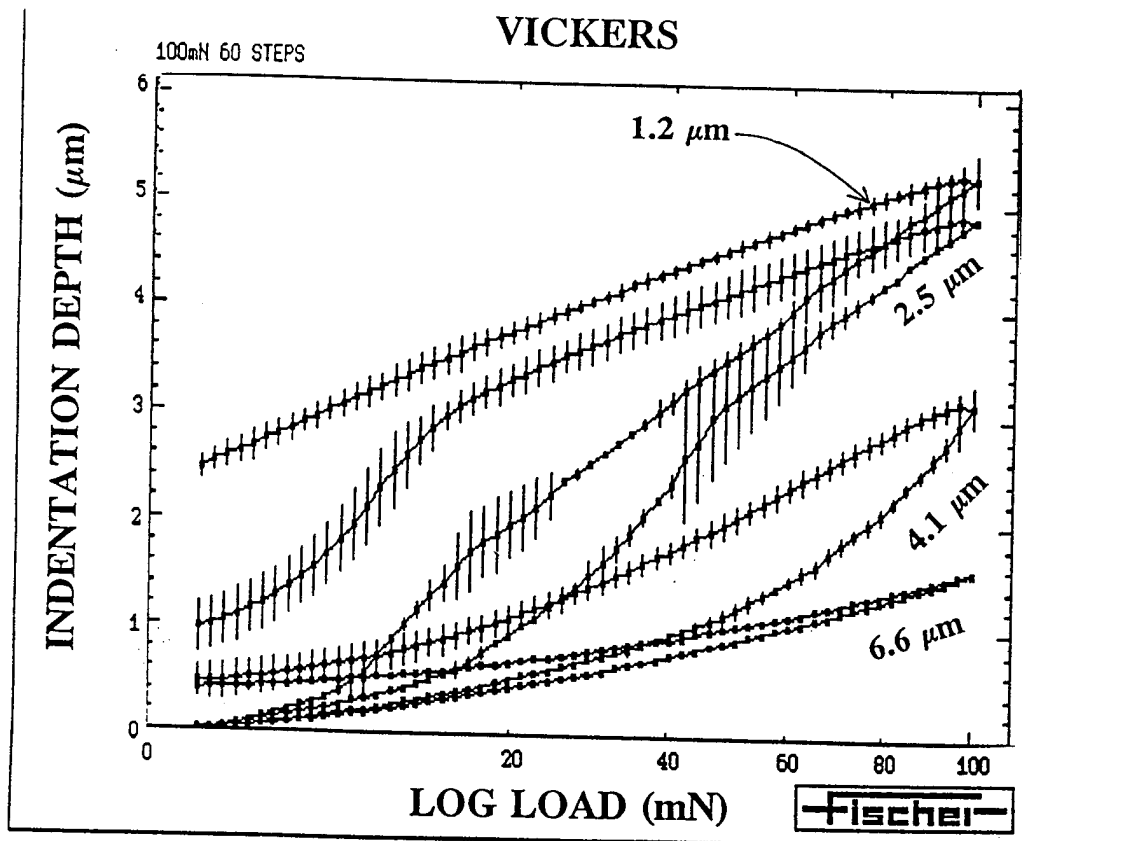
VICKERS

100mN 60 STEPS

INDENTATION DEPTH (μm)

polycarbonate

LOG LOAD (mN)

─Fischer─

VICKERS

100mN 60 STEPS

INDENTATION DEPTH (μm)

1.2 μm

2.5 μm

4.1 μm

6.6 μm

LOG LOAD (mN)

─Fischer─

Fig. 20

Fig. 21

Knoop Hardness vs. Load on IBAD Aluminum Oxide on PC
(Normal N2) HK ± 0.3 GPa

■ Oxygen treated	─□─ 94-6-4	◆ 94-4-13	◇ 94-4-52	▲ 94-3-30

Koop Hardness IBAD Aluminum Oxide Coatings on Glass
HK ± 0.3 GPa

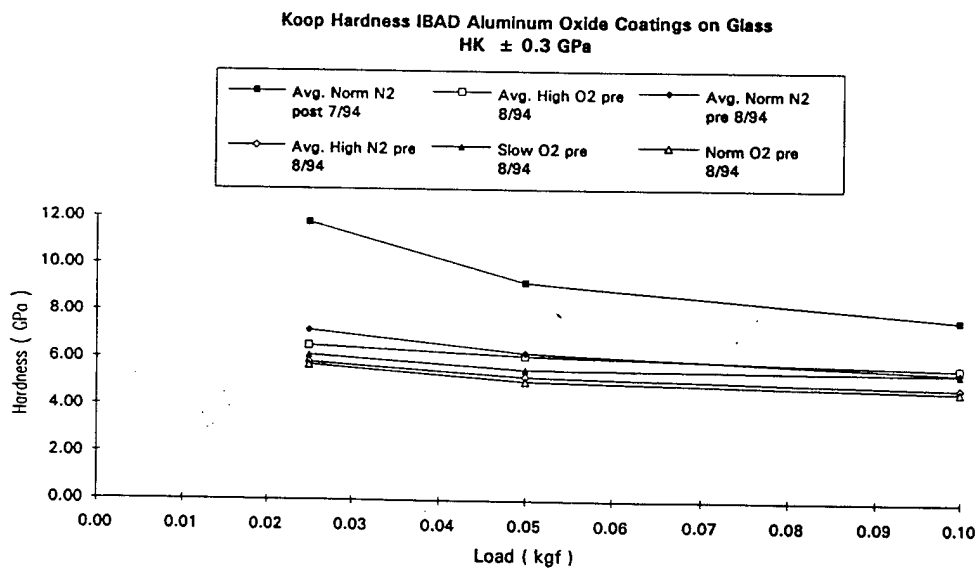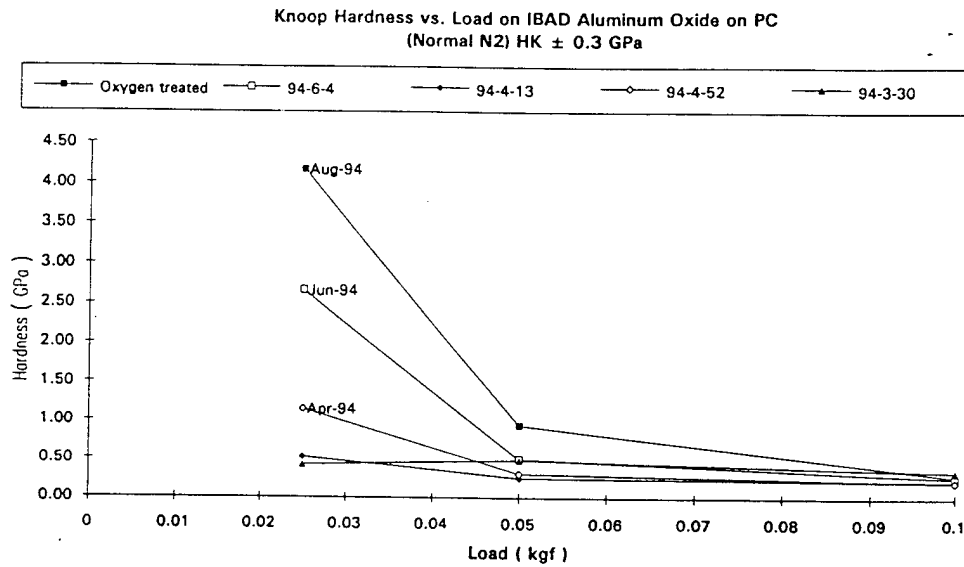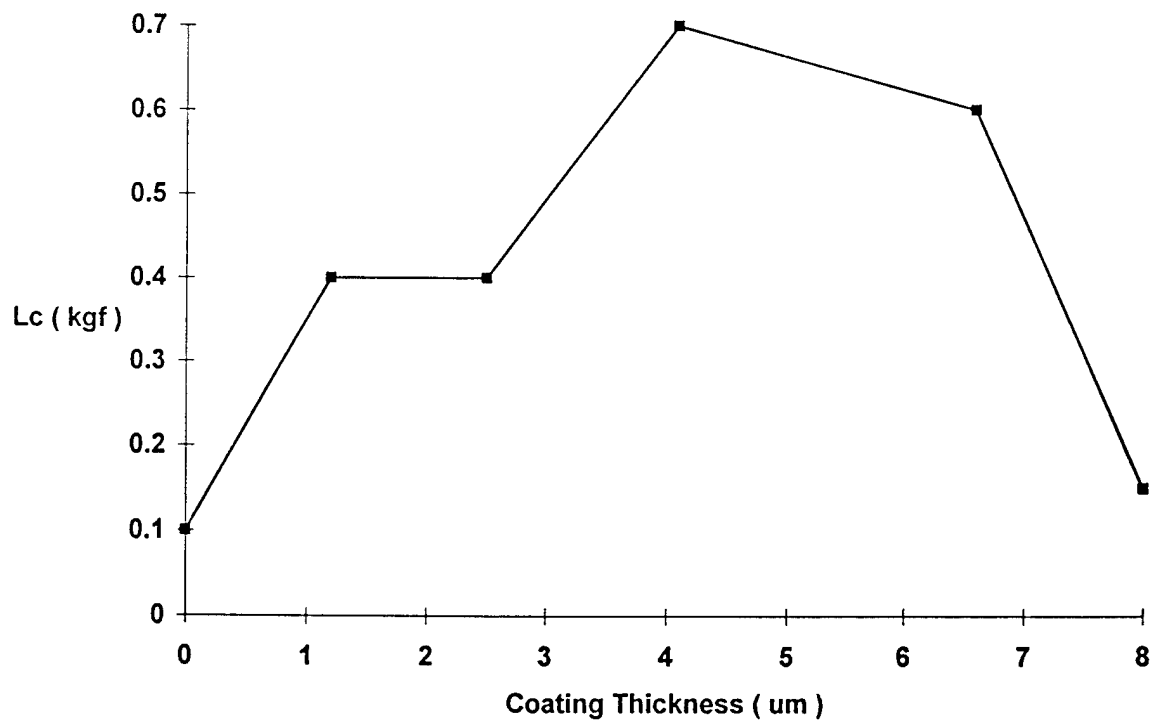|		
■ Avg. Norm N2 post 7/94	─□─ Avg. High O2 pre 8/94	◆ Avg. Norm N2 pre 8/94
◇ Avg. High N2 pre 8/94	▲ Slow O2 pre 8/94	△ Norm O2 pre 8/94

Fig. 22

Critical Load vs. Coating Thickness
IBAD Al2O3 on annealed glass

Fig. 23

SUMMARY: STRESSES OF IBAD Al$_2$O$_3$ FILMS

o   From curvature measurements, measured stresses are **compressive**, ranging in value from

$$120 < |\sigma_f| < 160$$

o   Thermal stresses place the coating in **tension**, estimated to be

$$30 < |\sigma_{th}| < 53$$

o   Intrinsic stress can be calculated as $\sigma_i = \sigma_m - \sigma_{th}$.

*   From curvature measurements and thermal calculations, intrinsic stresses of IBAD Al$_2$O$_3$ are **compressive**, ranging in value from

$$150 < |\sigma_f| < 210$$

Fig. 24

Polishing Wear Resistance

Relative to Sapphire, Diamond Abrasive

Legend: ▨ 3–μm ⊠ 30–μm

Relative Wear Resistance

Categories: Sapphire, IBAD Alumina, Polycarb., TiN, Cr Plate, M2 Steel

Y-axis: 10, 1, .1, .01

Hardness of Magnetron Aluminum Oxide on Glass
HK @ 50 gf
± 0.3 GPa
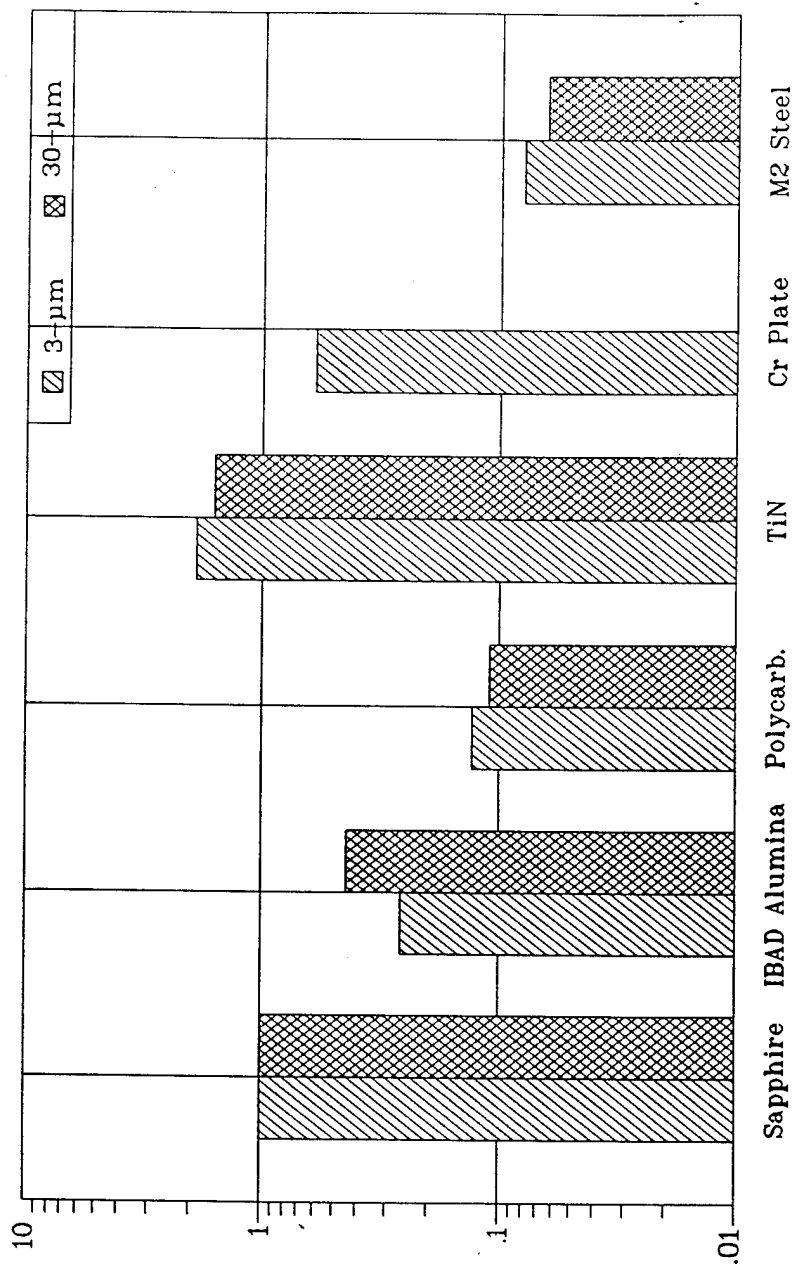
Fig. 25

Position dependence of "hot" Magnetron sputtering films

Attachment D

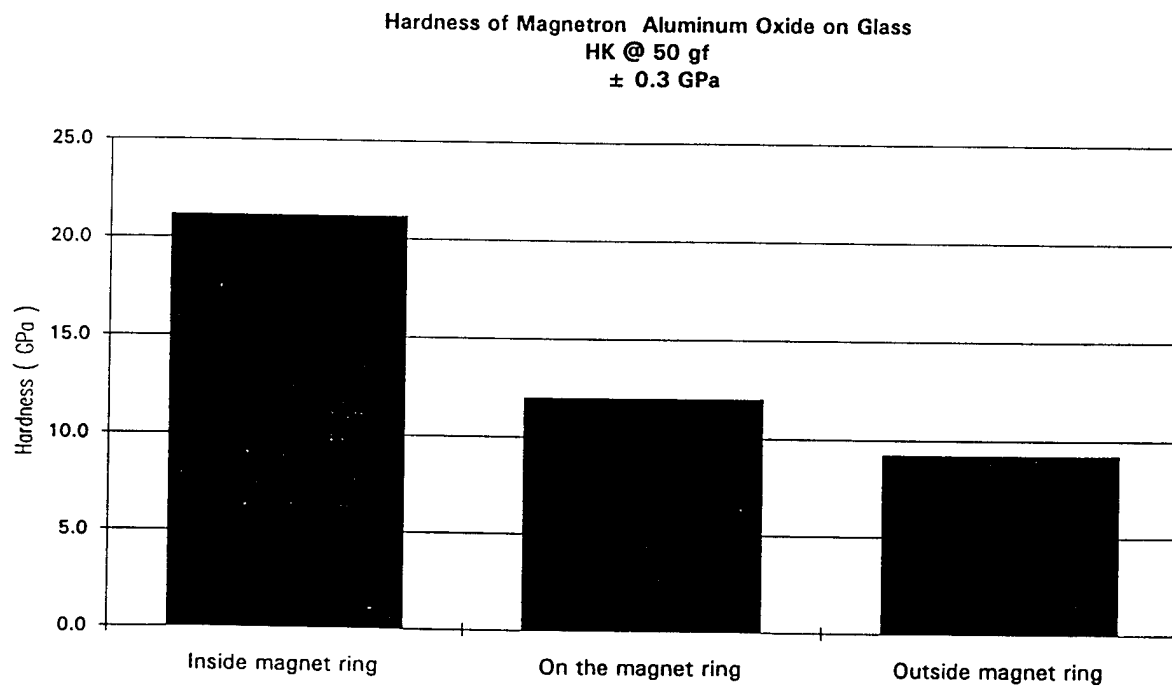"Deposition of Aluminum Oxynitride Films by Magnetron Sputtering: Effect of Bombardment and Substrate Heating on Structural and Mechanical Properties"

DEPOSITION OF ALUMINUM OXYNITRIDE FILMS BY MAGNETRON SPUTTERING: EFFECT OF BOMBARDMENT AND SUBSTRATE HEATING ON STRUCTURAL AND MECHANICAL PROPERTIES

RUSSELL V. SMILGYS*, ERIC TAKAMURA**, IRWIN L. SINGER+, STEVEN W. ROBEY++, AND DOUGLAS A. KIRKPATRICK*

*Science Applications International Corp., 1710 Goodridge Dr., McLean, VA 22102
**GeoCenters, 10903 Indian Head Highway, Fort Washington, MD 20744
+Naval Research Laboratory, Washington, D.C. 20375
++National Institute of Standards and Technology, Gaithersburg, MD 20899

ABSTRACT

Aluminum oxynitride films, 1 μm thick, are deposited onto glass substrates by planar magnetron sputtering from an alumina target in a mixture of nitrogen and argon. One set of films is deposited onto glass substrates that are heat sunk to a holder, whose temperature is held below 100°C. A second set of films is deposited onto glass substrates that are mechanically clamped to a holder, whose temperature is allowed to rise up to 250°C. Characterization by continuous indentation testing, secondary electron microscopy, and x-ray diffraction reveals significant differences in mechanical properties and surface structure between the two sets of films. Films deposited with holder cooling have a smooth surface and no evidence of crystallinity; films deposited without holder cooling have etch pits on their surface that vary with position across the substrate. The later films show crystallinity and have twice the hardness and a 60% greater elastic modulus.

INTRODUCTION

Alumina is a hard, inert, transparent ceramic. These properties are often desirable in a protective coating. Alumina films with bulk-like properties can be deposited by chemical vapor deposition (CVD) but high (>800°C) deposition temperatures are required [1]. Alumina films can also be produced at lower temperatures by physical vapor deposition (PVD) techniques such as sputtering. In general the properties of alumina films deposited by PVD techniques are inferior [1]. Many properties of films, such as hardness, adhesion to substrate and crystallinity depend critically on deposition conditions. One of the most difficult conditions to control is substrate temperature, especially when the substrate is a relatively poor conductor, such as glass.

In this study we examine the mechanical and structural properties of sputter-deposited aluminum oxynitride films subjected to two commonly used methods of thermal management: simple clamping of substrates to an uncooled holder and pasting down substrates to an intentionally cooled holder. Indentation testing is used to determine hardness, elastic modulus (defined as $E/(1-\upsilon^2)$, where E is Young's modulus and υ is Poisson's ratio) and indentation fracture toughness. Secondary electron microscopy (SEM) and x-ray diffraction (XRD) are used to characterize film morphology and crystallinity. Changes in the properties of the films are discussed in terms of bombardment and thermal effects.

FILM PREPARATION AND CHARACTERIZATION

Films are prepared by the technique of planar magnetron sputtering. The sputtering system is built around a stainless steel chamber approximately 15 liters in volume pumped by a 50 l/s turbomolecular pump backed by a mechanical pump. It achieves a base pressure of 4×10^{-5} Pa

A 2" diameter planar magnetron source is mounted in the chamber with the target horizontal. The magnetron is driven by a 500 W RF power supply (13.56 MHz) with a matching network. The target is alumina of purity 99.99%. Substrates are held horizontally facing the magnetron target at a distance about 4 cm. When the goal is to maintain a low substrate temperature, the substrate is mounted with silver paste to an aluminum block. The block is clamped with silver paste to a commercial cold finger (15 cm long, 2.5 cm in diameter). When compressed air is forced into the cold finger during deposition, the block temperature does not rise above 100°C. If neither silver paste nor compressed air are used, the block temperature rises to nearly 250°C over the course of an hour long deposition. These two conditions will be referred to as cool and hot deposition. The holder is electrically grounded.

A typical deposition begins by mounting a glass substrate (Erie Scientific microscope slide) 2-6 cm^2 in size on the holder. The glass is cleaned by rinsing in high purity alcohol. After loading, the chamber is pumped down below 1×10^{-2} Pa (8×10^{-5} torr) before beginning deposition. Substrates are not sputter cleaned prior to deposition. First nitrogen is leaked into the chamber to reach a pressure from 3.3×10^{-2} to 0.13 Pa (0.25-1 millitorr). Then argon is leaked to bring the total pressure up to 0.67 Pa (5 millitorr). In this way the percentage of nitrogen in the gas mixture is set from 5 to 20%. The RF generator is set to maintain a constant power, typically 400 W. Sputtering for one hour deposits a film about 1 μm thick. The film composition is not determined, but we refer to the films as being aluminum oxynitrides.

A SEM is used to view the films. Films are analyzed by XRD in the Seeman-Bohlin geometry.

Hardness and elastic modulus are measured by continuous microindentation [3] with a Fischerscope H100 using a Vickers indentor [4]. The shape function of the indentor (the area as a function of depth) was established by performing test indents on Si(111). In order to minimize the effect of the substrate on film tests, plastic indents are kept below 20% of the film thickness. In this study we report two hardness numbers. The first is the universal hardness (Hu), defined as the load divided by area of contact; Hu incorporates both elastic and plastic resistance to deformation. The second is the more traditional plastic hardness (Hp), which here is calculated as the load over the area of contact subtracting the elastic contributions to the area of contact. Elastic modulus is derived from the unloading portion of the load-displacement curves.

Another mechanical test based on indentation measures the ability of a film to resist fracture. Vickers indentation is performed with incrementally increasing maximum loads until radial cracks appear at the corners of the indent. This load is termed the critical load (Lc).

RESULTS

Surface morphology, structure, and mechanical properties are found to depend on substrate temperature. Films deposited cool appear smooth and uniform, whereas those films deposited hot have a roughly textured appearance. By eye the morphology manifests itself as a diffuse white ring approximately 2 mm in width and up to 2 cm in diameter. The center coincides with the axis of the magnetron. The remainder of the film, inside and outside of the ring, is clear and transparent.

SEM images show that films with a ring have a pitted surface morphology on a microscopic scale. Figure 1a-c shows that inside the ring the surface is completely peened, but with increasing distance from the center of the ring the density of pits drops. The ring seems to be an optical effect caused by light scattering from pitting of a certain density (see Figure 1b).
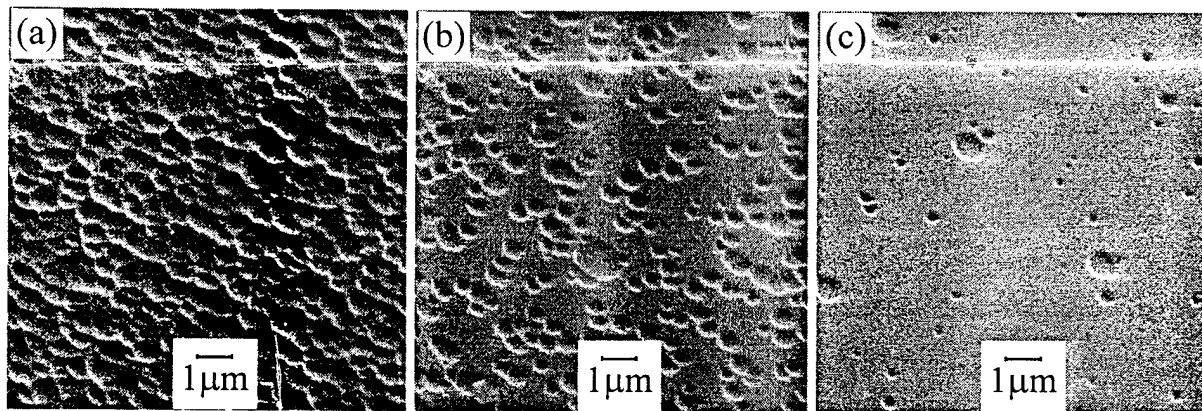
Figure 1. SEM images of surface of aluminum oxynitride film deposited hot. The density of pits varies with position across the film (a) position inside ring visible by eye, (b) position on ring, (c) position outside ring.

Figure 2 compares XRD spectra of representative films deposited cool and hot. Only the film deposited hot has features that indicate crystallinity. Line broadening prevents identification of the phase(s) present. Several aluminum oxide and aluminum nitride polymorphs are consistent with the features. Based on the width of the features we can conclude that either the crystallites are as small as 10 nm and/or are highly stressed.
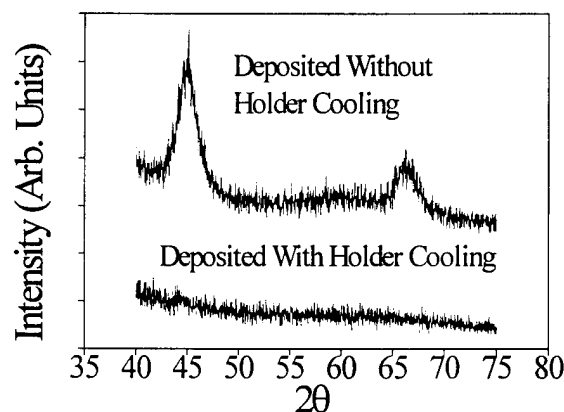

Figure 2. X-ray diffraction spectra shows crystallinity for film deposited without holder cooling.

Films deposited hot have mechanical properties that vary with position across the ring. Figure 3a shows that the hardness of the film increases as one moves closer to the center of the ring. The location and width of the ring is represented by gray bars at the bottom of the plot. Each data point represents the average of four continuous indentations, made in a row along a ring diameter; therefore the ring is crossed twice. The data points at the two ends of each plot correspond to regions of bare glass where clamps used for mounting the substrate mask the film. The same trends in film mechanical properties are observed in a row away from the clamps.

Figure 3b shows that the elastic modulus has less variation along the same row. We find that hardness and elastic modulus values across the ring have greater dispersion than outside the ring. This may be caused by the rough surface texture inside the ring. Films deposited cool have constant hardness and modulus values at all positions. They are also much softer and less stiff.
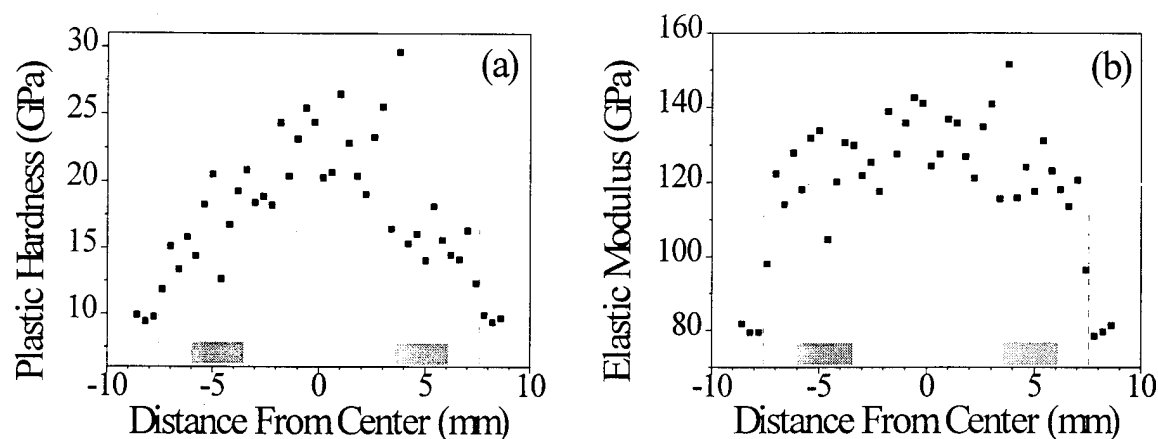
Figure 3. Microindentation measurements show that plastic hardness and elastic modulus are position dependent for films deposited without holder cooling. Measurements are made along a diameter of the ring. The position and width of the ring is identified by the gray bars at the bottom of each plot. The measurements farthest from the ring center correspond to masked regions of the glass substrate.

Films deposited hot also have a position dependent critical load. The critical load within the ring is above 1400g. Outside the ring the critical load drops to below 600g. Films deposited cool have critical loads below 200g. Table 1 compares Hp, Hu, E, and Lc for films, deposited cool and hot, with Si(111), glass and sapphire.

Table I. Mechanical properties of aluminum oxynitride films deposited cool and hot are compared with reference materials. 25 mN load used for hardness measurements.

	Hp (GPa)	Hu (GPa)	E (GPa)	Lc (gf)	% N*
Si(111)	19	7.8	190	<100	-
Sapphire	39	15	400	<100	-
Glass	9.2	3.7	83	200	-
Hot deposition#					
AR11-01	38	8.4	180	2500	5
AR11-05	30	7.4	160	1700	15
AR20-11	21	6.2	130	1400	10
AR20-13	24	6.2	140	na	10
AR20-08	19	5.5	110	1500	10
Cool deposition					
AR02-19	9	3.9	85	200	20
AR02-17	8.6	3.8	86	<100	20
AR02-21	8.9	4	89	<100	20
AR02-22	9.7	4.3	95	<100	20
AR02-20	8.5	3.8	87	<100	10
AR02-18	10	4	88	100	10

*Percent nitrogen in gas mixture during sputter deposition
#Measurements performed within ring

DISCUSSION

In this study we find that substrate temperature strongly influences the properties of aluminum oxynitride films deposited by sputtering. Films deposited cool are smooth with no evidence of crystallinity, whereas those deposited hot are pitted and have some crystallinity.

The development of surface morphology on films deposited by sputtering is well established in the literature. Depending on gas pressure, target to substrate distance, power, and total deposition time, surface features such as ripples, rods, cones, pyramids, and pits have been documented [5]. Energetic bombardment by ions and neutral particles activates the surface and causes resputtering. Etch pits, similar to those seen in Figure 1, are often initiated by preferential sputtering at dislocations or other heterogeneous features on an otherwise homogeneous material surface. Other researchers have also noted the development of a ring on films deposited by planar magnetron sputtering. Tominaga et al. observed a ring of discoloration concentric with the magnetron axis on their AlN films [6]. Based on time-of-flight measurements the authors identified bombardment by NO⁻ and O⁻ with development of the ring.

Films deposited either cool or hot are presumably subjected to the same bombardment conditions, yet a pitted surface morpology only forms when films are deposited hot. This suggests that pit formation is influenced by the substrate temperature. The connection may be crystallization that occurs at a higher temperature. Figure 2 shows that only the films deposited hot are crystalline. Bombardment can introduce defects into a crystalline film, and continued bombardment can lead to etch pits at the defects by preferential sputtering [7]. Pitting, similar to that shown in Figure 1, can be seen in ion bombarded natural alumina [8]. In contrast, the entire surface of a growing amorphous film is defective; therefore no selective etching can occur under the same bombardment conditions.

Films deposited at above 1/3 of the melting temperature are expected to be crystalline. Franze et al. reported that alumina films deposited by ion beam assisted deposition on glass show some crystallinity at 400°C [9]. This temperature is within the range possible for the unpasted substrate on an uncooled holder.

The mechanical properties can also be explained in terms of crystallinity. Studies of alumina films by continuous indentation testing indicate that the plastic hardness of amorphous films is about half that of crystalline films (about 7 to 10 GPa and 20 GPa, respectively [1]); elastic modulus values of amorphous films are from half to a third of crystalline films (140-250 GPa and 400 GPa, respectively [1,10]). While the absolute values for hardness of films studied in this experiment are somewhat higher, the ratios are consistent with literature values. The Vickers indentor and the machine used in this study were not designed to measure mechanical properties accurately at depths of 0.1μm; moreover, no special precautions were taken to minimize vibrations and thermal fluctuations during data acquisition. The increase in critical load can be attributed to a combination of increased compressive stress applied to the surface and improved adhesion of the film at higher temperatures. The thermal coefficient of alumina is greater than that of glass. Therefore, on cooling the film applies a compressive stress to the glass surface. The stress is proportional to the temperature drop and higher deposition temperatures apply a higher stress. Stress may also be introduced by energetic bombardment during deposition.

In summary, we find that the structural and mechanical properties of aluminum oxynitride films depend on the thermal behavior of glass substrates. We record the highest hardness and elastic modulus where resputtering, and by extension bombardment and substrate heating, is most intense.

ACKNOWLEDGMENTS

REFERENCES

1. J. -E. Sundgren and H. T. G. Hentzell, J. Vac. Sci. Technol. A **4**, 2259 (1986).
2. B. Lawn, Fracture of Brittle Solids (Cambridge University Press, Cambridge 1993) Chap 8.
3. W. C. Oliver and G. M. Pharr, J. Mat. Res. **7**, 1564 (1992).
4. W. W. Weiler, Amer. Soc. for Testing and Eval. **18**, 229 (1990).
5. D. J. Kester and R. Messier, J. Mater. Res. **8**, 1938 (1993).
6. K. Tominaga, S. Iwamura, Y. Shintani, and O. Tada, Jpn. J. Appl. Phys. **22**, 418 (1983).
7. O. Auciello, and R. Kelly, eds. Ion Beam Bombardment Modification of Surfaces (Elevier, New York, 1984).
8. B. A. Banks, NASA Tech. Memo. #81721 (NASA, 1981).
9. W. Franze, T. Tetreault, W. Kosik, W. Croft, and J. K. Hirvonen, Mat. Res. Soc. Proc. **279**, 825 (1993).
10. D. Dongfeng and K. Kato, Thin Solid Films **245**, 104 (1994).

Attachment E

"Effect of Plasma Pretreatment on Adhesion of Alumina Coating
to Polycarbonate and Poly(methyl methacrylate)"

To be submitted to the Journal of Adhesion Science and Technology:

Effect of plasma pretreatment on adhesion of alumina coatings to polycarbonate and poly(methyl methacrylate)

R. V. Smilgys, T. Long, D.A. Kirkpatrick, and J. Hickman

Science Applications International Corporation, 1710 Goodridge Dr, McLean, VA 22102

J. Ross, and D. Kester*

Armstrong World Industries, Lancaster, PA

J. Fu

National Institute of Standards and Technology, Gaithersburg, MD

I. Singer

Naval Research Laboratory, Washington, DC

* Present address: Advanced Refractory Technology, Buffalo, NY

Abstract- Alumina coatings, 2-8 μm thick, were deposited by ion beam assisted physical vapor deposition onto polycarbonate and poly(methyl methacrylate) substrates. Adhesion of the coatings to a polycarbonate substrate was typically excellent, whereas adhesion to a poly(methyl methacrylate) substrate was always poor, even under identical substrate preparation and deposition conditions. Poor adhesion was characterized by flaking under light abrasion. Treatment of the polymer substrates by either hydrogen plasma or oxygen ion bombardment prior to deposition was found to significantly affect adhesion. Oxygen ion bombardment of poly(methyl methacrylate) led to excellent adhesion, whereas hydrogen plasma treatment of polycarbonate reduced adhesion. Analysis by atomic force microscopy and x-ray photoelectron spectroscopy suggest that the treatments affected adhesion by forming either a strong or weak boundary layer at the surface.

Keywords: Alumina, plasma, physical vapor deposition, polycarbonate, acrylic, XPS, AFM.

1. INTRODUCTION

Polycarbonate (PC) and poly(methyl methacrylate) (PMMA) have many desirable properties, such as high transparency, low density, and great toughness. However, uncoated their use is limited by low resistance to surface maring, both by solvents and abrasion, that can quickly block transparency. A variety of commercial coatings have been developed to overcome this limitation [1-3]. Recently there has been renewed interest to develop harder, more abrasion resistant coatings for plastics based on vapor deposited glass or ceramic [4]. For good abrasion resistance, a coating should be at least 4 μm thick, but this can be difficult to achieve due to cracking or poor adhesion.

A great deal of work has shown that polymer activation by flame, corona, plasma, or ion bombardment can improve coating adhesion [5-7]. In most instances the coating was a metal or a thin ceramic. In the present work, the effect of polymer activation on adhesion of alumina coatings thick enough to offer abrasion protection have been studied. The coatings were deposited by ion beam assisted physical vapor deposition onto PC and PMMA. The work derived from several years of research into using vapor deposited coatings for surface protection [8,9].

2. EXPERIMENTAL

2.1 Coating Deposition System

Alumina coatings were deposited onto polymer substrates using an ion beam assisted physical vapor deposition (IBAD) system, which is shown schematically in Fig. 1. The IBAD system included: a 66 cm wide high-vacuum chamber assembly; a high speed pumping system (CTI Cryogenics CT-10 cryopump and Alcatel ZT 2033 mechanical pump); an electron-beam evaporation source (Temescal STIH-270-2MB four-hearth "Supersource," with an 8 kWatt Temescal CV-8 high-voltage controller and e-beam power supply, and Temescal XYS-8 sweep control); a cold cathode ionization source (Denton Vacuum model CC101 with CC101PS power supply); a residual gas analyzer (Inficon Quadrex 200); a quartz crystal type continuous deposition rate monitor/controller (Inficon IC6000); and an electric probe to periodically measure ion flux.

Four circular substrate holders (diameter 20.3 cm) were affixed to a planetary rotation subsystem. Samples (typically 2.5x2.5 cm to 10x10 cm) were mounted using stainless steel templates. The system was also equipped with a cooling shroud to prevent radiation from the electron-beam source from heating the substrates when they were not directly over the evaporation source. In this configuration substrates were exposed to deposition only 2 out of every 10 seconds. Substrate temperature could not be directly measured during a run. Instead it was estimated based on measurements from thermocouples mounted in the vicinity of the substrate holders.

2.2 Materials.

Vapor deposition grade alumina was obtained from either E. M. Industries as 99.9% 1-5 mm granules, or from Cerac, Inc. as 99.8% 3-12 mm pieces. Oxygen (Linde; welding grade) was passed through an in-line molecular sieve trap (Supelco, Inc.) to remove water vapor, and argon (Linde - welding grade) was purified by passage through an in-line cuprous oxide trap to remove oxygen, and by an in-line molecular sieve trap to remove water vapor. Hydrogen and oxygen (Air Products, ultra pure carrier grade) were used for RF plasma treatment without further purification. Special cleaning solutions included: 2% "MICRO" detergent solution (International Products Corp); and "Cyclone", a detergent solution with pH 13 (M. Buten & Sons Inc.).

2.3 Substrates

Fisher-brand "precleaned" glass microscope slides were used as "witness" coupons for thickness measurement. Polycarbonate (PC, "Hyzod" and "Tuffak") and Poly(methylmethacrylate) (PMMA, "Plexiglas") were obtained in sheet form (6.35 mm, 3.18 mm, and 1.59 mm PC; and 3.18 mm and 1.59 mm PMMA) from Sheffield Plastics and Atohaas.

2.4 Substrate Preparation and Pretreatment

Polymer substrates were cleaned with 'Cyclone', then rinsed with deionized water and alcohol (methanol or isopropanol). Glass witness coupons were cleaned by successive 5 minute ultrasonic treatments in, respectively, 2% "MICRO" detergent solution, deionized water, acetone and methanol, and then dried in a positive pressure hood immediately prior to use.

Some PC substrates were further treated with a hydrogen plasma in a commercial plasma cleaner (Harrick PDC-326). The plasma cleaner operated by inductively coupling the output of a 100 W RF generator (13.56 MHz) to a quartz gas cell about 1 liter in volume. The specific

treatment conditions were 2 and 6 minutes of exposure using 100% hydrogen at 39.9 Pa (300 mTorr). After treatment the substrates were stored in containers exposed to atmosphere. Treated substrates were used in four deposition runs performed from four to six weeks later. The coating thickness in these runs was nominally 4 μm. PC substrates not pretreated with hydrogen plasma were included as controls. Specific information about these coupons is contained in Table 1.

For three runs PMMA substrates were treated by oxygen ion bombardment *in situ* immediately before depositing the alumina coating. The ion source was set to 600 V and 660 mA. The first run used 5 minutes of argon ion bombardment (600 V and 300 mA), followed by either 0, 0.5, 2, or 10 minutes of oxygen ion bombardment (coupons 95-3-73, 95-3-66, 95-3-59, and 95-3-52, respectively). The second run used 5 minutes of argon ion bombardment followed by 10 minutes of oxygen ion bombardment (coupon 95-4-8). The third run followed the procedure: 1 minute argon ion bombardment, vent the chamber, pump down immediately, 2 minutes of argon ion bombardment, then 2 minutes of oxygen ion bombardment (coupon 95-4-16).

2.5 Coating Process.

A typical deposition run would begin by pumping overnight to reach a base pressure around 1.3×10^{-4} Pa (10^{-6} Torr). After performing pretreatments, if any, the alumina evaporation rate would be set corresponding to an instantaneous deposition rate around 1 nm/s. During this time the substrates would be blocked by a shutter. Once a stable rate was achieved, the shutter would be opened to begin deposition. After completion of the first micron, the electron beam and ion source would be turned off and a new crucible rotated into place. Only after the chamber had cooled down to at least 10°C would deposition begin on the next micron. By following these steps a coating up to four microns could be deposited. To deposit a thicker coating the chamber would be vented to reload the crucibles and continue the run.

2.6 Sample Testing

XPS was used to study the surface chemistry of PC and PMMA, and the effect of plasma or ion bombardment. Spectra were obtained on a Fisons EscaLab 220-IXL photoelectron spectrometer with a monochromatic Al Kα X-ray source (1486.6 eV) and a 600 μm spot size. The polymers were analyzed at ambient temperature and exhibited no sign of damage during

measurements. In order to minimize differential charging, photoelectrons were collected through a gold screen suspended a few mm above the sample surface [10]. The take-off angle was 90° for all spectra, which corresponds to a probe depth around 4 nm for C(1s). Spectra were referenced to the C(1s) peak for aliphatic carbon in the polymer, which was assigned the value 284.6 eV. Chemical state information was deconvolved by a nonlinear least squares routine using Gaussian peaks.

Atomic force microscopy (AFM) was used to image surface morpholgy. A Nanoscope II atomic force microscope (AFM) set to aquire images in contact mode.

Coating thickness was calculated by the interference fringe method from Uv-Vis spectra taken on a Perkin Elmer Lambda 3A spectrometer. The calculations assumed the index of refraction for alumina was 1.65. Occasionally, thickness calculations were verified by scanning electron microscopy of a cross sectional fracture of a coated sample, or by profilometry of a step created by masking the substrate during deposition.

Contact angles were measured with a Rame-Hart contact angle goniometer using the sessile drop method with water. At least three spots were measured and averaged for each sample.

In this study coupons were judged to have 'good' adhesion if the coating resisted removal by rubbing with steel wool. Those with 'poor' adhesion showed flakes or worm tracks without rubbing. Two coupons judged as good were scratch tested using a CSEM Revetester in order to quantify adhesion. The tests were performed with a load range of 1 to 100 N using a sapphire ball (3.18 mm diameter). The results are reported in terms of the normal and tangent forces necessary to cause delamination. Also the critical load to form radial cracks was determined using a Tukon indentor with a Brale indentor (sphere 0.2 mm radius).

3. RESULTS

The coating process described here routinely gave alumina coatings on untreated PC that were transparent, strongly adherent, and crack-free up to 8 μm thick. The coatings effectively protected PC against scratching by steel wool. Identical process conditions consistently gave alumina coatings on untreated PMMA that completly failed to adhere. Without rubbing, intact flakes several millimeters in size could be lifted off easily. The amount of flaking correlated to the coating thickness, with coatings under 2 μm showing more worm tracks than flakes.

Plasma and ion bombardment treatments were found to significantly affect adhesion. Pretreatment of PC with a hydrogen plasma led to reduced adhesion. The coating appeared coarse because of a dense pattern of worm tracks with flaking along the edges of the tracks, however, the coating continued to adhere between tracks. A tape pull removed flakes up to a few hundred microns in size.

Flaking from PMMA was prevented by performing oxygen ion bombardment *in situ* prior to alumina deposition. For specific ion source settings, 2 minutes or more of bombardment lead to an adherent coating, while 30 seconds gave no benefit.

3.1 Poly(methyl methacrylate)

3.1.1 XPS

XPS spectra were acquired on PMMA substrates, both treated by oxygen ion bombardment and untreated, in an attempt to correlate surface chemistry to coating adhesion. Spectra were also acquired from the interface side of an alumina flake removed from a PMMA substrate.

Survey spectra of untreated PMMA revealed only carbon and oxygen. Figure 2 shows high resolution spectra of the C(1s) and O(1s) photolines for untreated PMMA. The C(1s) spectrum has been deconvolved into four components, following the work of Beamson, Bunn, and Briggs [11]. The components correspond to the chemical composition shown in the figure inset: the aliphatic bonded C1, the aliphatic bonding state C2, which is shifted to higher binding energy due to the next nearest oxygen influence (so-called β-shift), the state C3, corresponding to the carboxyl group, and finally the state C4 corresponding to the carbonyl carbon. Based on the stoichiometry of PMMA, these states should be present in the ratio 2:1:1:1, respectively, whereas 2.0:1.1:1.0:1 was recorded. The O(1s) spectrum was fit by two components, O1 corresponding to carbonyl and O2 to ester. These two states should be present in the ratio 1:1, whereas 1.1:1 was recorded. This deviation from ideal stoichiometry has been reported, but not fully explained [12-14].

The survey spectrum from the interface side of an alumina flake removed from a PMMA substrate revealed carbon, oxygen, and aluminum. Figure 3 compares the C(1s) and O(1s) spectra of the flake interface to untreated PMMA. It reveals that the characteristic C(1s) states

associated PMMA are also present on the flake interface, which suggests that a layer of PMMA remained adhered to the flake. The layer could not be thicker than the XPS probe depth, otherwise aluminum would not have been visible in the survey spectum. This places an upper bound around 5 nm on the thickness of the layer. The O(1s) spectra could not be used to corroborate the C(1s) analysis because states of oxygen bound to aluminum contributed to the photoline.

Figure 4 compares C(1s) and O(1s) spectra of PMMA treated by oxygen ion bombardment. The substrates went through the same initial treatment as coupons 95-3-73, 95-3-66, 95-3-59, and 95-3-52 listed in Table 1, except for deposition of the alumina coating. We note that these spectra were acquired from samples exposed to atmosphere for several weeks after treatment, whereas the coupons were immediately coated after treatment. The effect of ageing and atmospheric exposure on adhesion was not investigated.

The C(1s) spectra of treated PMMA showed significant broadening compared to untreated PMMA. The spectra could not be adequately represented by only four components. This suggests that a range of oxygen functionalities were formed, which is supported by the broad O(1s) spectra. In spite of this, the basic lineshape of PMMA was still evident, which is evidence that the surface was not totally degraded.

The oxygen to carbon ratios were calculated from the integrated area of each element scaled by the Schofield factors (C: 1; O: 2.85). Treatment for 30 seconds increased the ratio by 20% compared to untreated PMMA. But then over 9 more minutes of treatment did not lead to further incorporation of oxygen. This was supported by the C(1s) lineshape, which also did not show significant change with increasing treatment.

3.1.2 Atomic Force Microscopy

Masked and unmasked regions of PMMA bombarded by an oxygen ion beam for at least 2 minutes could be distinguished by eye. The masked regions had slightly better surface reflectivity. In order to quantify this effect we attempted to image the samples using a SEM, but the electron beam rapidly induced damage. Nevertheless, a step about 1 μm was visible at the boundary between masked and unmasked regions on a sample bombarded 10 minutes. This corresponds to a 100 nm/min etch rate.

To image the surface morphology nondestructively an AFM was used. Figure 5 compares both masked and unmasked regions of a sample bombarded 10 minutes. It reveals that etching during bombardment left the surface roughened. Table 2 lists the root mean square (rms) roughness of bombarded samples.

3.1.3 Contact Angle

Table 2 lists the contact angles for PMMA samples. The contact angle dropped for treatment up to 2 minutes, but then reversed. The measurements were performed a week after treatment.

3.1.4 Mechanical Tests

Scratch tests and Brale indentation were performed on coupons 95-3-59 and 95-3-52 to correlate coating adhesion to treatment by oxygen ion bombardment. Table 3 indicates that neither mechanical test revealed any significant difference in adhesion between the two coupons.

3.2 Polycarbonate

3.2.1 XPS

XPS spectra of PC were acquired both before and after treatment by hydrogen plasma. The survey spectra revealed only carbon and oxygen. Figure 6 overlays $C(1s)$ and $O(1s)$ spectra of treated and untreated (wet cleaned only) PC. The plasma treatment was identical to that for coupons 94-8-7, 94-8-56, and 94-8-91 (i.e. 6 minutes of exposure to hydrogen RF plasma).

The $C(1s)$ spectrum of untreated PC was fit to the aliphatic bonded C1, the state C2, corresponding to the carboxyl group, and a composite feature corresponding to carbonate and a $C(1s)$ shake-up satellite[15]. The intensity of the composite feature was 13% of C1, but the relative contribution of carbonate and the satellite to the overall intensity could not be resolved. The expected ratio of C2 to C1 in stoichiometric PC is 15:1, whereas 17.6:1 was recorded. The $O(1s)$ spectrum was fit by two components, O1 and O2, corresponding to carbonyl and ester states, respectively. The recorded 2:1 ratio of ester to carbonyl states is characteristic of carbonate.

Plasma treatment of PC caused severe changes to the XPS spectra. The carbonate signature disappeared (2:1 ratio of ester to carbonyl states). The best fit showed a 1:2 ratio instead. This effect was mirrored in the $C(1s)$ line where there was a large loss in the composite carbonate-satellite feature. Also the main lineshape was transformed into a broad band extending

8

from C1 toward the carbonate-satellite feature, suggesting the presence of hydroxyl, carbonyl, ester, and carboxyl functionalities. Finally, the ratio of oxygen to carbon dropped by over 25% compared to untreated PC.

3.2.2 Contact Angle

Contact angle measurements were performed on PC, before and after treatment with the hydrogen plasma. Treatment lowered the contact angle by over 20° (Table 4).

4. DISCUSSION

Adhesion can be approached at three levels: molecular adhesion, thermodynamic adhesion, and practical or experimental adhesion [16]. Molecular adhesion describes the intermolecular interactions between the adherend and adherate. In general, the interactions can be ionic, covalent, van der Waals, or electrostatic. Thermodynamic adhesion describes the change in free energy when a unit area of surface is disrupted. Practical adhesion is the experimentally determined force per unit area, commonly known as 'bond strength'.

Theoretical studies have reported on the expected molecular interactions between alumina and organic monomers, such as methyl methacrylate [17,18]. They found covalent interactions, based on Al-C and C-O-Al type bonding geometries, with bond strengths over 21 eV. These studies suggest that molecular adhesion of alumina to both PC and PMMA should be excellent. Furthermore, strong bonding between alumina and polymer should be promoted by the deposition process itself, which includes energetic bombardment by ions.

In this work we judged the practical adhesion of a coupon to be either 'good' or 'poor' depending on whether or not the coating flaked. The highly adherent coatings on untreated PC observed here indicate that molecular adhesion was good to this substrate. Similarly, XPS spectra of the interface of an alumina flake removed from a PMMA substrate support the contention that molecular adhesion of alumina to PMMA was also good. If molecular adhesion were poor, the spectra would not have revealed a layer of PMMA still bound to the flake. The issue to address is why practical adhesion was poor to untreated PMMA.

Good molecular adhesion is essential for practical adhesion, but it is not sufficient. Factors such as mechanical interlocking, electrostatics, and a boundary layer can increase or decrease practical adhesion. In particular, residual coating stress can impose significant forces at an interface that may exceed the cohesive strength of a boundary layer [19].

Stress develops in vapor deposited coatings from extrinsic and intrinsic sources [20]. For example, extrinsic stress is present when deposition and measurement occur at different temperatures, and the coefficient of thermal expansion (CTE) of substrate and coating are mismatched. The extrinsic strain can be calculated for an alumina coating deposited on PC. The CTE for the coating has not been measured, but the CTE for alumina ceramic is probably valid $(6-7 \times 10^{-6} /°C)$ [21]. The CTE for PC below its glass transition temperature $(T_g = 150°C)$ is an order of magnitude greater, $6.8 \times 10^{-5}/°C$ [22]. Using standard formula [20], one finds that if the interface were stress-free at 110°C, a 0.4% strain would be present at ambient.

Stress also develops intrinsically in vapor deposited coatings for reasons that are not completely understood. In general, the level of stress increases with coating thickness. In this work the net stress in coatings on PC was regulated by the level of ion bombardment used during deposition. Without ion bombardment, alumina coatings on PC formed tensile cracks. Experimentally, ion bombardment was increased until tensile cracks were prevented. This was presumably the point where intrinsic and extrinsic stresses just canceled, and practical adhesion was optimal.

Stress at the interface between alumina and PMMA could not be similarly managed because the glass transition temperature of PMMA is much lower $(T_g = 105°C)$ [23]. The deposition process followed here formed the interface between alumina and PMMA while the substrates were cold (T<20°C). But before completion of a coating 1 μm thick, the chamber temperature approached 110°C. This temperature is too low to significantly change the CTE of PC, but a PMMA coupon would be transformed into a gel-like solid with a quickly increasing CTE. The manufacturer could not quote the CTE of PMMA near T_g, so the strain could not be calculated. However, these considerations do suggest that interfacial stress plays a significant role in limiting practical adhesion to PMMA.

The next issue to address is how plasma (or ion bombardment) treatment altered practical adhesion of alumina to PC and PMMA. Plasma treatment is believed to affect adhesion to plastic substrates by four major mechanisms [6]: removal of organic contaminates at the surface; sputtering or etching of substrate material to remove a weak boundary layer or to increase surface area; cross-linking (chain scission) to increase (decrease) cohesive strength of a boundary layer;

and surface chemistry modification to increase or decrease chemical interactions at the interface (molecular adhesion). The relative importance of each mechanism depends on substrate chemistry, gas chemistry, and other processing conditions.

The reduction in practical adhesion observed for PC treated by hydrogen plasma is probably not due to poor molecular adhesion. Coupon 95-3-28 had 2 minutes of treatment without flaking, while coupons with 6 minutes of treatment showed flaking. This indicates that at least several minutes of treatment were necessary to affect adhesion. Yet under the conditions used for RF plasma treatment, chemical changes to the top few monolayers of surface were probably completed quickly. This suggests that another mechanism was more important.

XPS spectra offer insight into chemical changes that occur several nanometers deep (XPS probe depth). After plasma treatment the C(1s) shake-up satellite and carbonate peak (Fig. 5b) were reduced by 80%. This indicates saturation or break-up of the aromatic rings and loss of the carbonate functionality. The later effect is further substantiated by the large drop in the O2 state compared to O1 state. At the same time the total oxygen content at the surface was reduced by 25%. These changes describe hydrogenation, deoxidation, and scission of the polymer within a thin boundary layer near the surface [15]. This boundary layer would be weakened compared to bulk PC, and susceptible to cohesive failure.

The discussion above proposes that practical adhesion to PMMA was poor because of cohesive failure in a thin boundary layer Nevertheless, certain conditions of oxygen ion bombardment were found to prevent flaking.

One factor to consider is surface roughness. Some researchers have suggested that roughness can improve adhesion by a mechanical interlocking mechanism [16]. AFM measurements clearly showed that ion bombardment caused profound morphological changes to PMMA. Surface roughness increased from 0.4 nm to over 11 nm after 10 minutes of treatment. This increase in roughness probably led to the rise in contact angle. At the same time upwards of a micron of material was etched. Based on the interlocking mechanism one might predict that increasing roughness should have led to increased adhesion. However, scratch tests showed no difference in adhesion between coupons 95-3-59 and 95-3-52 (i.e. 2 minutes versus 10 minutes of bombardment), even though roughness increased by over a factor of four. Furthermore, the difference in roughness between samples with 30 seconds and 2 minutes of treatment was only

1.3 nm, yet adhesion was still poor after 30 seconds. Based on these considerations, increased surface roughness alone is probably not sufficient to account for the differences in practical adhesion.

Another factor to consider is development of a boundary layer with increased cohesive strength and a higher effective glass transition temperature. The mechanism of formation would be implantation of oxygen ions into the substrate that cross-link polymer chains. The cold cathode ion source used in this work could drive multiple physical processes at the surface due to its broad energy distribution. Ions with energies on the low side of the distribution (<400 eV) would effectively etch weakly bound material. Ions with energies on the high side of the distribution would penetrate deeper to effect chemical modifications, such as cross-linking.

We hesitate to interpret the XPS spectra for treated PMMA samples because the surfaces may have been altered by atmospheric exposure or ageing before analysis. Given this caveat, the XPS spectra do not show great changes for treatment beyond 30 seconds. And those changes are probably influenced by the drastic increase in surface roughness. This suggests that by 30 seconds a boundary layer at least as deep as the XPS probe depth was already formed. Based on XPS spectra alone, it is not possible to determine if the boundary layer has improved cohesive strength. If it does, the dramatic improvement in adhesion after 2 minutes of bombardment, but not after 30 seconds, may be explained by an increase in thickness of the boundary layer beyond the XPS probe depth. After 30 seconds the boundary layer may have been still too shallow and/or insufficiently cross-linked to effect good practical adhesion. Measurements are needed by an instrument with greater probe depth to test this mechanism.

The importance of coating stress is implied by comparing coupons 95-3-59 and 95-4-16. The two coupons were treated by identical oxygen ion bombardment, yet only 95-3-59 showed good practical adhesion. The difference was that the coating on 95-4-16 was twice as thick, the major effect of which would have been a higher level of residual stress applied to the interface. The extra stress apparently exceeded the cohesive strength of the boundary layer.

5. CONCLUSIONS

We used ion beam assisted physical vapor deposition to deposit alumina coatings onto PC and PMMA substrates. The coatings on PC were transparent, strongly adherent, and crack-

12

free up to 8 μm thick. Treatment of PC with hydrogen plasma prior to deposition led to coatings that flaked. XPS analysis of treated PC indicated severe polymer degredation. This suggests that the plasma treatment formed a weak boundary layer that blocked adhesion.

Coatings on untreated PMMA completely failed to adhere. XPS analysis of a coating flake showed that a thin layer of PMMA remained adhered. This suggests that adhesion failed because of cohesive failure in a near surface boundary layer within the PMMA. Adhesion was made more difficult to PMMA because during deposition the chamber temperature exceeded the glass transition temperature of PMMA. This could cause significant interfacial stress to develop between the polymer and coating due to a large mismatch in thermal expansion.

In situ treatment of PMMA with oxygen ion beam bombardment prior to deposition was found to prevent flaking of coatings up to 4 μm thick. AFM and SEM images of treated PMMA surfaces revealed extensive etching and roughening. XPS analysis showed oxygen enrichment, and the formation of new oxygen functionalities at the surface. Roughening could improve adhesion by mechanical interlocking and increasing surface area. Another possibility is that oxygen bombardment etched weakly bound material, and cross-linked the remaining polymer. In this way a boundary layer with increased toughness and cohesive strength could have been formed.

REFERENCES

1. S. J. Razad, D. J. Conley, C. W. Reed U.S. 5156882 (1992).

2. Y. Kisma U.S. 4668588 (1987).

3. A. Revis and C.W. Evans U.S. 50753348 (1991).

4. Symposium J, Mat. Res. Soc. Spring Meeting 1995.

5. E.M. Liston, L. Martinu, and M.R. Wertheimer, J. Adhesion Sci. Technol. 7, 1091-1127 (1993).

6. E. M. Liston, J. Adhesion 30, 199-218 (1989).

7. J.G. Dillard and I.M. Spinu, J. Adhesion 31, 137-159 (1990).

8. D. Hensel, L.N. Ray, Jr. J. F. Reuwer, Jr., J. D. Wisnosky U.S. 5077112 (1991).

9. D. Hensel, L.N. Ray, Jr. J. F. Reuwer, Jr., J. S. Ross, J. D. Wisnosky U.S. 5188876 (1993).

10. C. E. Bryson, Surf. Sci., 189/190, 50-58 (1987).

11. G. Beamson, A. Bunn, and D. Briggs, Surf. Interface Anal. 17, 105-115 (1991).

12. D.G. Castner and B.D. Ratner, Surf. Interface Anal. 15, 479 (1990).

13. A. Naves de Brito, M.P. Keane, N. Correia. S. Svensson, U. Gelius, and B.J. Lindberg, Surf. Interface Anal. 17, 94 (1991).

14. G. Beamson, A. Bunn, and D. Briggs, Surf. Interface Anal. 17, 105-115 (1991).

15. L.J. Gerenser, J. Adhesion Sci. Technol. 7, 1019-1040 (1993).

16. K. L. Mittal, J. Vac. Sci. Technol. 13, 19-25 (1976).

17. J.W. Holubka, R.A. Dickie, and J.C. Cassatta, J. Adhesion Sci. Technol. 6, 243-252 (1992).

18. D.A. Drabold, J.B. Adams, D.C. Anderson, and J. Kieffer, J. Adhesion 42, 55-63 (1993).

19. J.J. Bickerman, The Science of Adhesive Joints (Academic New York, 1968), 2nd ed.

20. M. Ohring, The Materials Science of Thin Films Academic Press Inc., San Diego, CA (1992).

21. C. T. Lynch (Ed.), Handbook of Materials Science, vol. 3, CRC Press Inc. Boca Raton, FL 1988.

22. AtoHaas North America Inc., technical brochure on 'Tuffak A', (1992).

23. AtoHaas North America Inc., technical brochure on 'Plexiglas G', (1995).

Table 1. Identification of coupons with alumina coating in this study. Coupons are grouped by deposition run.

Substrate Material	ID #	Treatment	Coating Thickness (μm)	Coating Appearance
PC	94-8-10	none	4.3	adhered
PC	94-8-7	6 min H_2 RF plasma	4.3	flaking
PC	94-8-59	none	4.4	adhered
PC	94-8-56	6 min H_2 RF plasma	4.4	flaking
PC	94-8-94	none	4.2	adhered
PC	94-8-91	6 min H_2 RF plasma	4.2	flaking
PC	95-3-28	none	4.4	adhered
PC	95-3-29	2 min H_2 RF plasma	4.4	adhered
PMMA	95-3-22	none	4.4	flaking
PMMA	95-1-30	none	2.5	flaking
PMMA	95-3-73	none	4.5	flaking
PMMA	95-3-66	30 sec O_2 ion bombard	4.5	flaking
PMMA	95-3-59	2 min O_2 ion bombard	4.5	adhered
PMMA	95-3-52	10 min O_2 ion bombard	4.5	adhered
PMMA	95-4-8	10 min O_2 ion bombard	2.8	adhered
PMMA	95-4-16	12 min O_2 ion bombard	8.2	flaking

Table 2. Experimental measurements of surface chemistry, roughness,
and contact angle of PMMA samples treated by oxygen ion bombardment.

Duration	AFM Results rms roughness (nm)	Contact Angle	XPS Results O(1s)/C(1s)
none	0.4	60	0.35
30 sec	1.3	36	0.42
2 min	2.6	22	0.40
10 min	11.2	48	0.38

Table 3. Scratch tests and Brale indentation measurements of alumina coatings on PMMA.

Coupon #	Scratch Test Results Tangent Critical Force (N)	Brale Indentation Results Critical Load (Kg)
95-3-59	45	4
95-3-52	43	5

Table 4. Experimental measurements of surface chemistry and roughness of polycarbonate.

Treatment	Duration	XPS Results O(1s)/C(1s)	Contact Angle
	none	0.19	76
Hydrogen RF plasma	6 min	0.15	51

Figure Captions:

Figure 1. Schematic of ion beam assisted physical vapor deposition system.

Figure 2. High resolution XPS spectra of C(1s) and O(1s) states acquired from PMMA. The insert identifies the fitted peaks with the chemical states in the polymer structure.

Figure 3. High resolution XPS spectra of C(1s) and O(1s) states acquired from interface side of an alumina flake removed from a PMMA substrate.

Figure 4. High resolution XPS spectra of C(1s) and O(1s) states acquired from PMMA exposed to varying duration of oxygen ion bombardment.

Figure 5. Atomic Force Microscope images of PMMA both untreated, and exposed to oxygen ion bombardment for 10 minutes.

Figure 6. High resolution XPS spectra of C(1s) and O(1s) states acquired from polycarbonate both untreated and exposed for 6 minutes to a hydrogen RF plasma.

Figure 1.

SUBSTRATE
HOLDERS

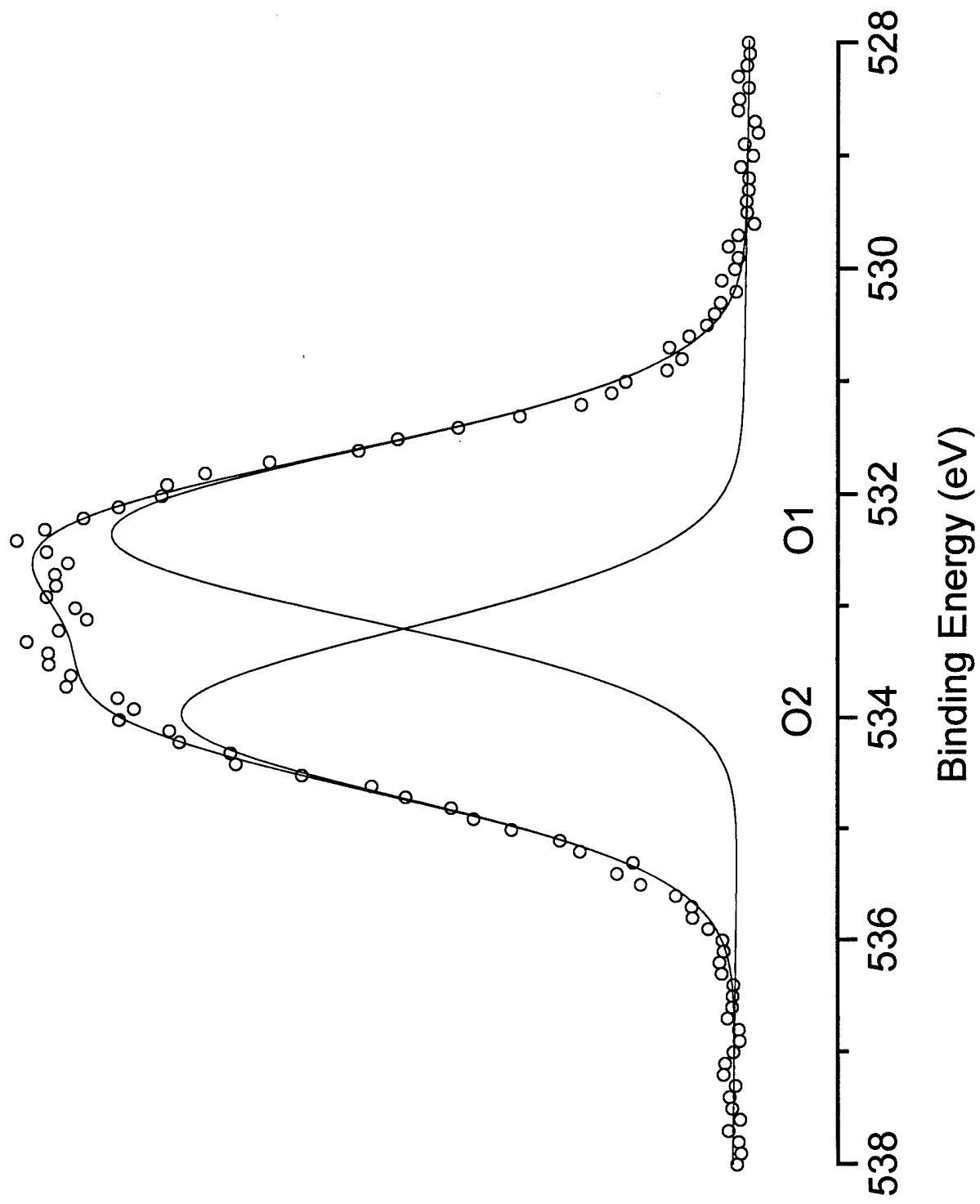ELECTRIC
PROBE

SHROUD

SHUTTER

RATE
MONITOR

COLD
CATHODE
·ION SOURCE

E-BEAM
SOURCE

CRYOPUMP

Fig. 2 C(1s)

Binding Energy (eV)

C4   C3   C2 C1

Fig. 2 O(1s)

O1

O2

Binding Energy (eV)

Fig. 3 C(1s)

—— PMMA Control

········ Flake Interface

Binding Energy

Fig. 3 O(1s)

—— PMMA Control

········ Flake Interface

Binding Energy (eV)

Fig. 4 C(1s)

10 min.

2 min.

30 sec.

untreated

Binding Energy (eV)

Fig. 4 O(1s)
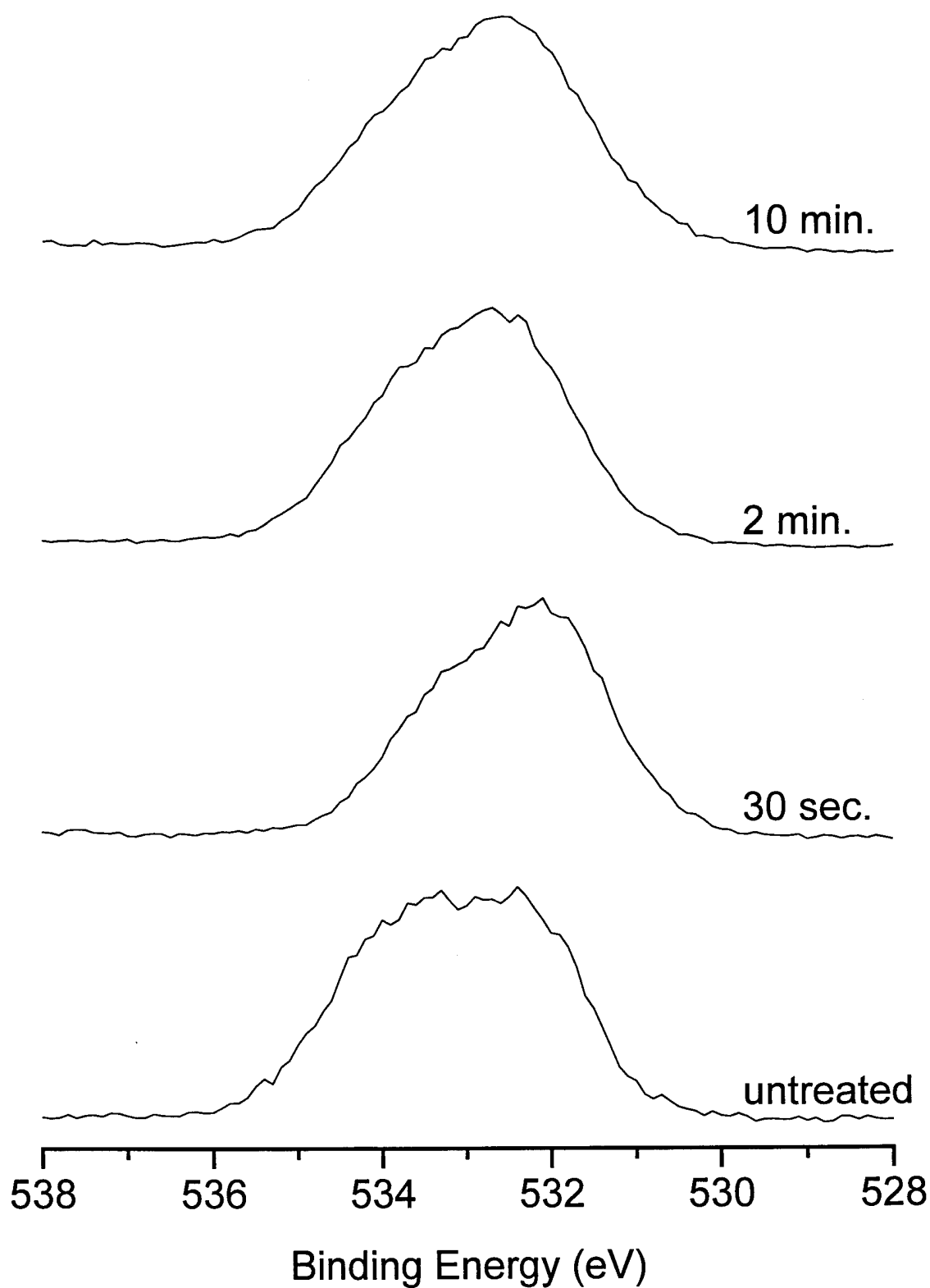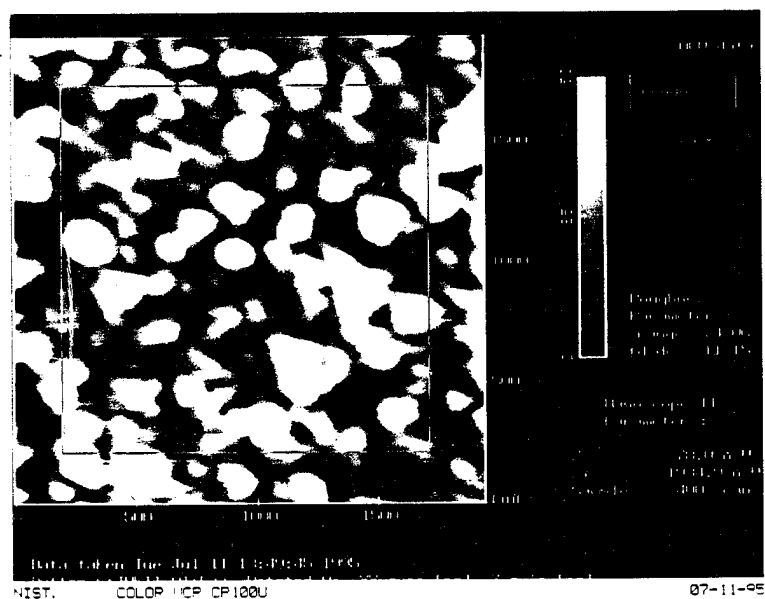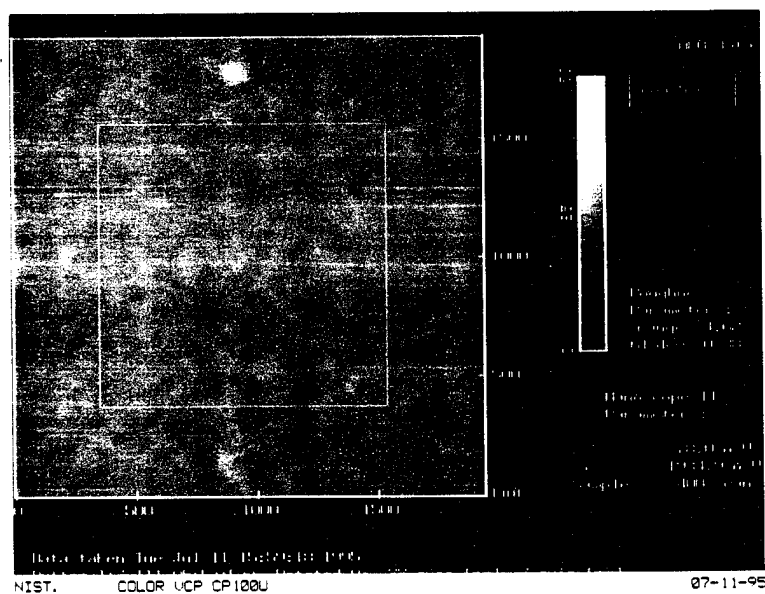
10 min.

2 min.

30 sec.

untreated

Binding Energy (eV)
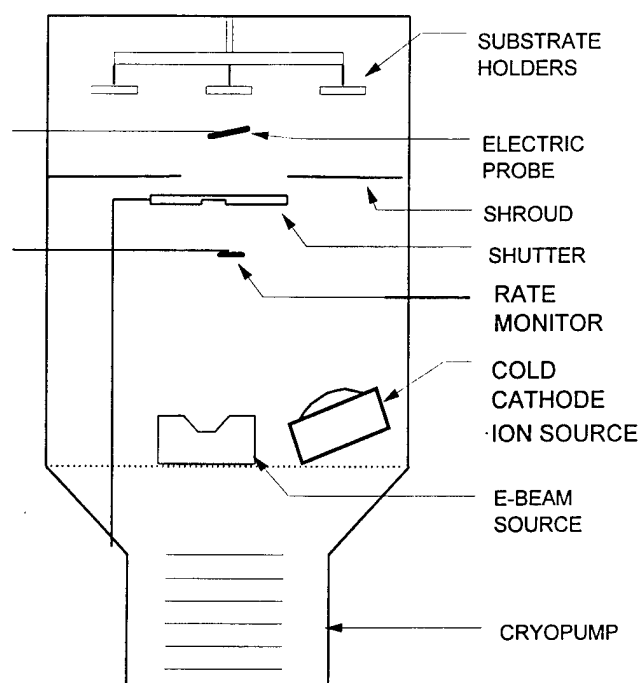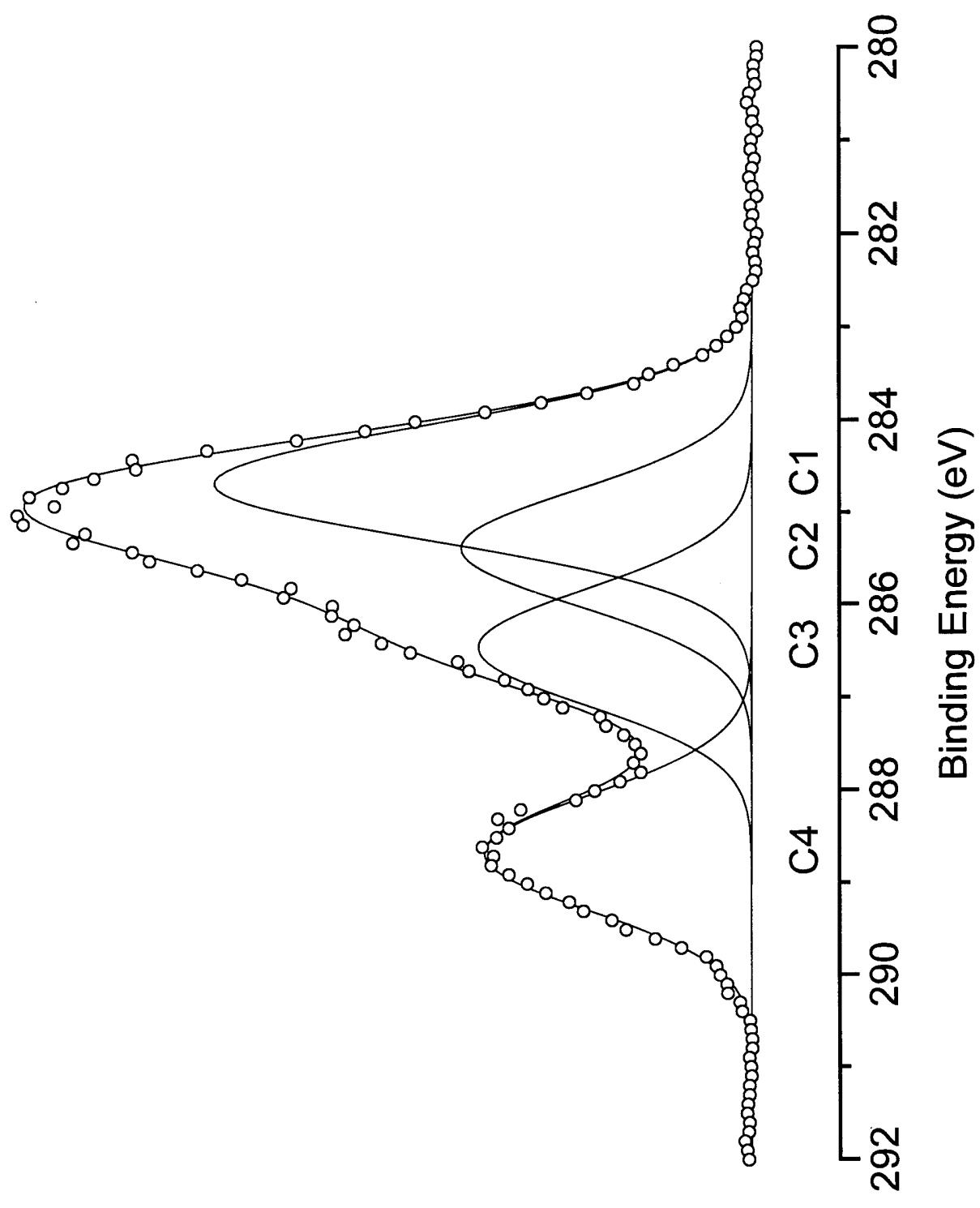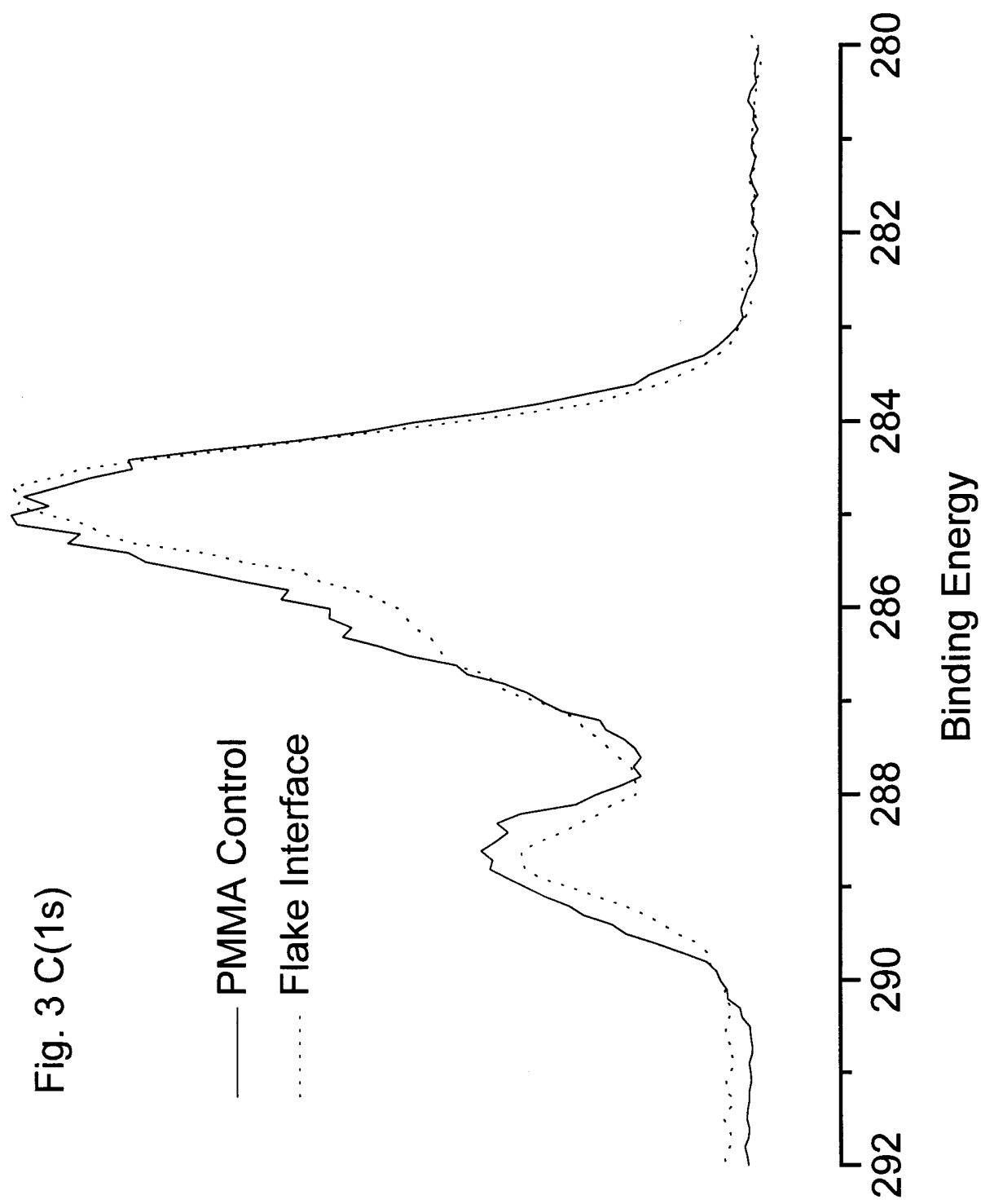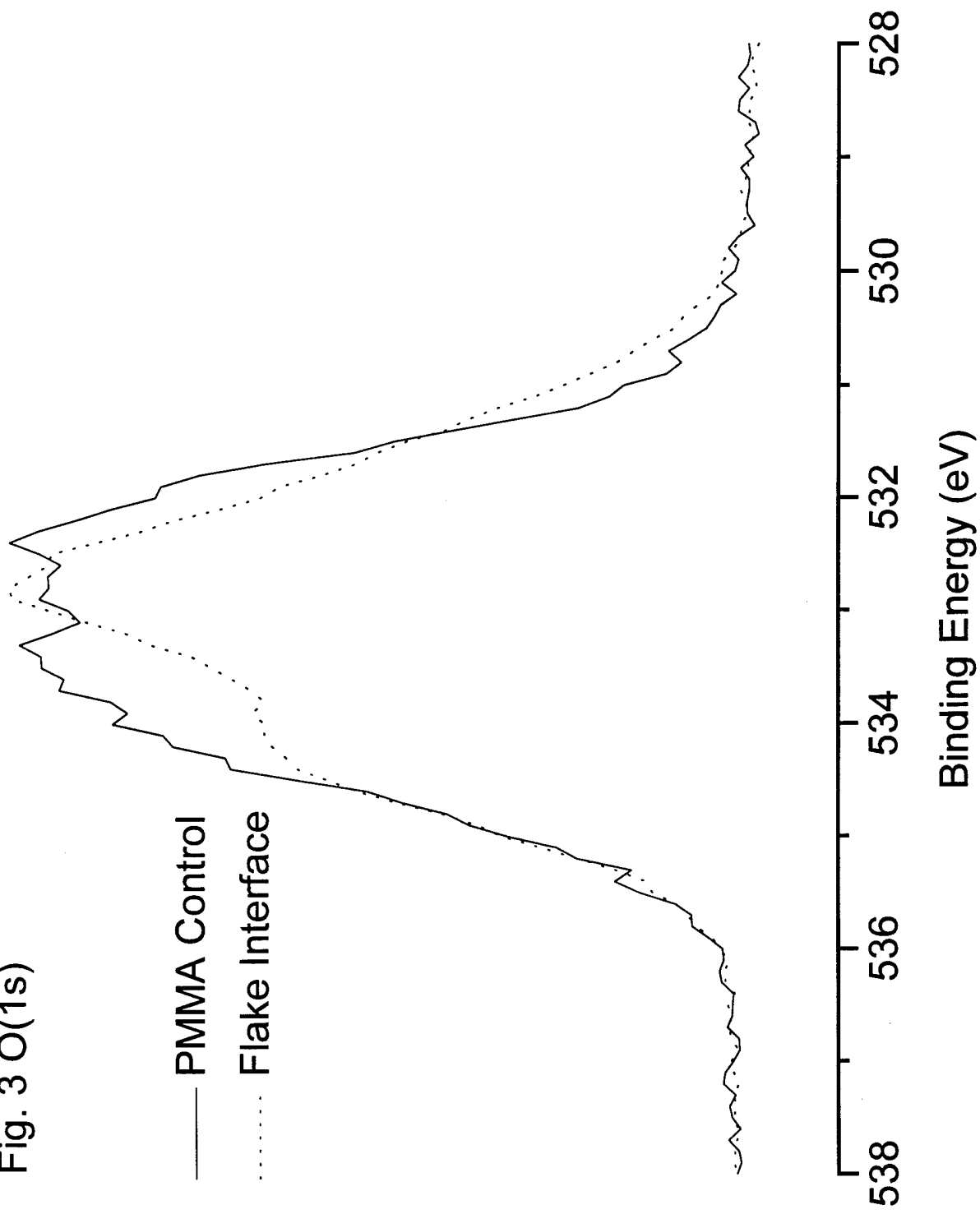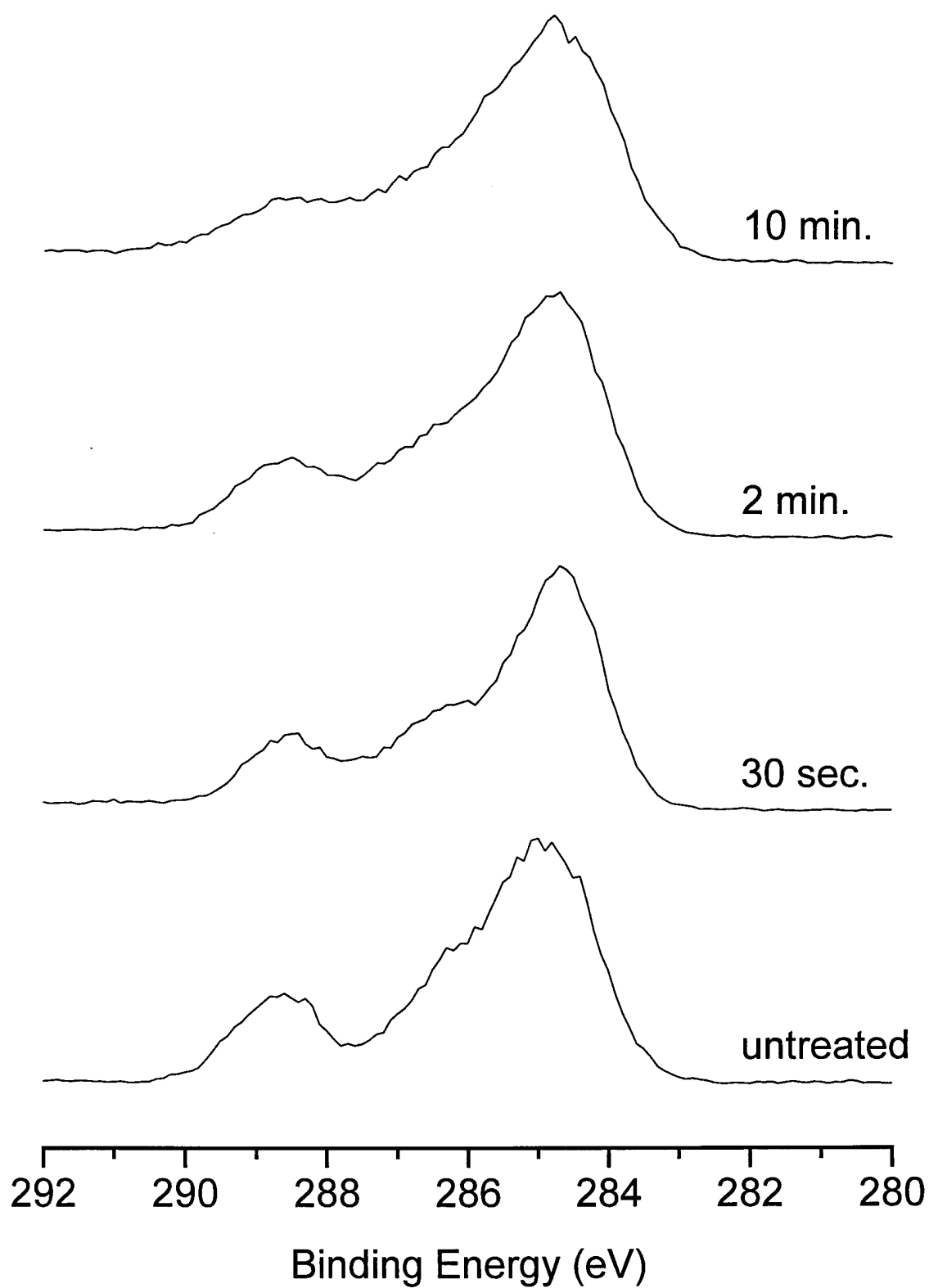
Fig. 5

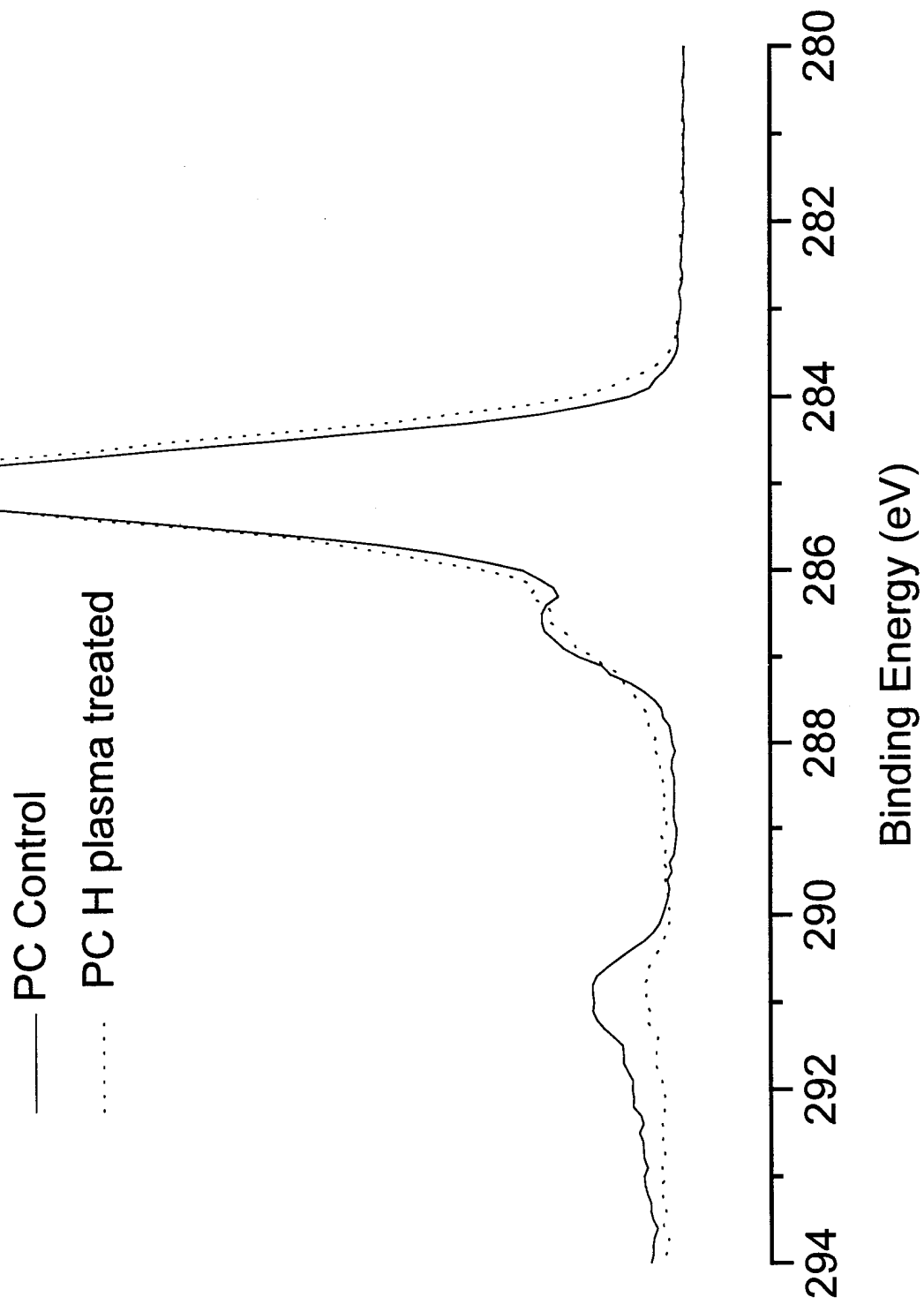

10 Minute O_2 Pretreatment

No Treatment

Fig. 6 C(1s)

PC Control
PC H plasma treated

Binding Energy (eV)

Fig. 6 O(1s)

— PC Control
...... PC H plasma treated

Binding Energy (eV)